H2020-LC-SC3-2018-2019-2020
Solar Energy in Industrial Processes

FRIENDSHIP
Forthcoming Research and Industry for European and National Development of SHIP
Starting date of the project: 01/05/2020
Duration: 48 months

= Deliverable: D3.1 =

Initial heat pump concepts and integration principles for SHIP200 targeting heat delivery up to 200 °C (steam cycle) and 250 °C (e.g. CO2 cycle)

Due date of deliverable: 30/06/2021
Actual submission date: 15/07/2021

Responsible WP: Heat pump for solar thermal boost, WP3, SINTEF
Responsible TL: Ole Marius Moen, SINTEF Energy Research
Revision: V2.0

Dissemination level		
PU	Public	x
PP	Restricted to other programme participants (including the Commission Services)	
RE	Restricted to a group specified by the consortium (including the Commission Services)	
CO	Confidential, only for members of the consortium (including the Commission Services)	

This project has received funding from the European Union's Horizon 2020 research and innovation programme under grant agreement No 884213.

AUTHOR

Author	Institution	Contact (e-mail, phone)
Ole Marius Moen	SINTEF Energy Research	Ole.moen@sintef.no
Tarjei Heggset	SINTEF Energy Research	Tarjei.Heggset@sintef.no

DOCUMENT CONTROL

Document version	Date	Change
V1.0	02/07/2021	Initial version
V2.0	08/07/2021	Comments from project coordinator incorporated

VALIDATION

Reviewers		Validation date
Work Package Leader	Ole Marius Moen	08/07/2021
Project Manager	Loïs Wittersheim	15/07/2021
Exploitation Manager	Anna Paraboschi	15/07/2021
Coordinator	Valéry Vuillerme	15/07/2021

DOCUMENT DATA

Keywords	SHIP200, heat pump
Point of Contact	Name: Ole Marius Moen Partner: SINTEF Address: Sem Saelands vei 11, TRONDHEIM 7465, Norway Phone: +47 45 45 05 16 E-mail: ole.moen@sintef.no
Delivery date	15/07/2021

DISTRIBUTION LIST

Date	Issue	Recipients
15/07/2021	V2.0	All partners + P.O.

Executive Summary

This report presents an evaluation of initial heat pump concepts and integration principles for SHIP200. Two main concepts have been developed: a high-temperature concept based on water/steam (R718) for short term heat delivery up to 200°C and a reversed Brayton heat pump concept based on CO_2 (R-744) for long-term heat delivery up to 250°C.

Evaluations of different heat pump concepts, component and system TRL level and cost have been performed. Both heat pump concepts were modelled in Modelica for detailed investigation of both design and off-design (part load) operational performance and stability in order to assess operability and integrability of the heat pump.

The steam heat pump achieved a COP of 4.97 at design conditions, while the reversed Brayton cycle heat pump achieved a COP of 2.44. Model improvements to both concepts can be made to improve simulation accuracy and performance.

Table of Contents

List of acronyms

ACRONYM	*MEANING*
AIT	Austrian Institute of Technology
CEA	Alternative Energies and Atomic Energy Commission
COP	Coefficient of Performance
DLR	German Aerospace Center
DSH	De-superheating
EXV	Electronic Expansion Valve
GHG	Green House Gas
GWP	Global Warming Potential
HFC	Hydrofluorocarbons
HFO	Hydrofluoroolefins
HTF	Heat Transfer Fluid
HTHP	High Temperature Heat Pump
HX	Heat Exchanger
IEA	International Energy Agency
IHX	Internal Heat Exchanger
LMTD	Logarithmic Mean Temperature Difference
MVR	Mechanical Vapor Recompression
NIST	National Institute of Standards and Technology
NTNU	Norwegian University of Science and Technology
PCHE	Printed Circuit Heat Exchanger
PI	Proportional Integral
PID	Process and Instrumentation Diagram
PTC	Parabolic Through Collector
R&D	Research and Development
SC	Subcooling
SCO2	Supercritical Carbon Dioxide
SHIP	Solar Heat in Industrial Processes
TRL	Technical Readiness Level
TVR	Thermal Vapor Recompression
TXV	Thermal Expansion Valve
VCRC	Vapor Compression Refrigeration Cycle
VHTHP	Very High Temperature Heat Pump
WP	Work Package

1 Introduction

This task (WP3.1) investigates high-temperature heat pump concepts for FRIENDSHIP SHIP200. Two main concepts are developed; a high-temperature concept based on water (R-718) for short term heat delivery up to 200°C and a reversed Brayton heat pump concept based on CO_2 (R-744) for long-term heat delivery up to 250°C.

The purpose of the heat pump in SHIP200 is to interact with the PTC solar field and combined heat storage and provide the required temperature lift from the PTC to the final process consumers.

This report is outlined as follows: first a general overview of industrial heat pumps is presented in chapter 2, which includes a classification and categorization of heat pumps, market overview, current research and development status, and known barriers. In addition, the key performance indicators for how heat pump performance is evaluated are presented.

The main concepts are presented in chapter 3 and 4, with a more detailed investigation of research and development status for steam heat pumps and reversed Brayton cycles based on CO2 in particular. Here, a review of working fluid properties, heat pump components and research projects for high-temperature heat pumps based for steam and CO_2 is presented. Based on this review, an estimation of the TRL-level of the components and systems is presented.

Evaluations of the main concepts are performed in chapter 5, which are based on the mapped boundary conditions for the heat pump systems. Various concepts of steam heat pump and reversed Brayton heat pump for SHIP200 are investigated and evaluated in terms of performance at both design and off-design conditions. Sizing and cost estimations of the most promising concepts are performed. In chapter 6, the developed Modelica models and simulation results of the concepts are presented. Here, a more detailed analysis of the expected performance is given, including operational performance, behaviour and integrability on off-design and part load conditions.

The overall objective of the deliverable 3.1 is to develop high-temperature **heat pump concepts** based on water (R718) and CO_2 (R744) as working medium.

This deliverable is linked to task 3.1: Developing high temperature heat pump concept and integrability. The task includes:

- T3.1.1 Specification of heat pump boundary conditions based on input from WP1
- T3.1.2 Development of modelling tools for heat pump design, total system integration, and performance evaluation
- T3.1.3 Development of initial system concepts for SHIP200 short term (200°C) and long term (250°C)
- T3.1.4 Development of final system concepts for SHIP200 short term (200°C) and long term (250°C)

The delivery includes the results from all subtasks with the exception of T3.1.4, which is to be commenced later in the project.

2 Overview of Industrial Heat Pumps

2.1 Introduction to Heat Pumps

Heat pumps are devices that are capable of elevating a heat source at a certain temperature to a higher temperature, through providing work, typically from electrical energy. Compared to other heating technologies for industrial processes, such as gas or electrically fired boilers heat pumps are typically very effective and can enable significant energy savings. A heat pump uses a working fluid, which acts as the heat carrier between the heat source and the heat sink.

A wide range of working fluids exist, and their suitability depends on the operating conditions of the heat pump. Heat pumps can operate at various temperature levels, and with different forms of heat sources and heat sinks such as air, water, thermal heat transfer fluids and steam to name a few.

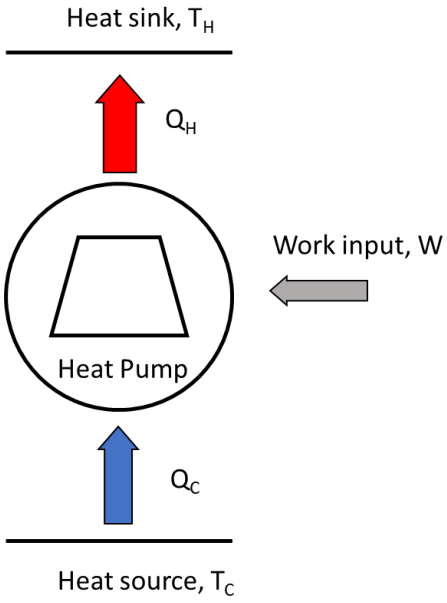

Figure 1: Heat pump principle.

2.2 Temperature Classification

In terms of heat delivery temperature, various attempts of categorizing heat pumps according to the temperature have been made. The term High-Temperature Heat Pump (HTHP) has for example been used to described heat pumps capable of delivering high-temperature heat with various definitions of the required temperature. For example, Bauder described applications of HTHP capable of delivering temperature above 100°C [1], while Arpagaus et al. used the term for systems above 90°C [2].

The International Energy Agency (IEA) proposed a classification where HTHPs were defined with heat delivery temperatures between 80 and 100°C, while the term Very High Temperature Heat Pump (VHTHP) was used for delivery temperatures above 100°C, as illustrated in Figure 2. SINTEF generally uses a definition that HTHP delivers heat above 100°C. For a long time, all high-temperature heat pumps were state-of-the art, and commercially underdeveloped. However, in the last 20 years the heat pump technology has progressed significantly along with the market suppliers in terms of delivery temperatures.

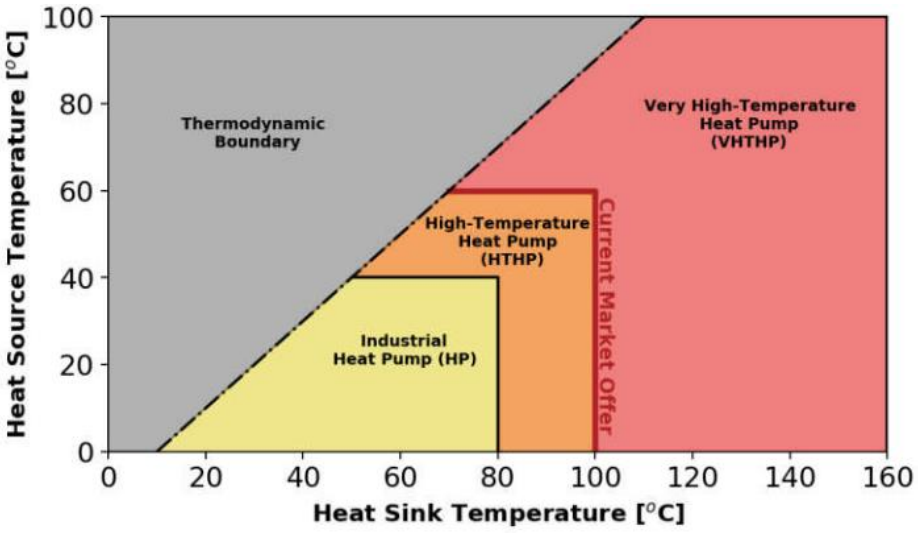

Figure 2: IEA classification of heat pumps according to temperatures [3].

2.3 Heat Pump Categorization

Heat pumps can be divided into different categories, and although the term heat pump is typically synonymous with electrically driven vapor compression, many variations of heat pumps exist.

A way to separate between different heat pump systems is to distinguish between open and closed systems, as shown in Figure 3. Closed systems are the most common, here the refrigerant is only circulated within the heat pump and heat exchangers are used to transfer the heat. In open systems the refrigerant in the heat pump is used directly in the industrial process. The refrigerant in these cycles is usually steam (R-718), as this is used for a range of different applications in the industry, such as drying, evaporation and distillation [4].

Closed-cycle compression heat pumps are the most widely adopted heat pump systems. They are compressor driven system, typically operating according to the vapor compression refrigeration cycle, where the working fluid is heated by the heat source and evaporates. It is then compressed to higher temperature and pressures. This allows the refrigerant to reject heat to the heat sink through condensation at a higher temperature level, before it is expanded through a valve and enters the evaporator again. In some heat pumps, the refrigerant does not undergo phase change and operates in gas phase during the entire cycle. These cycles are known as reversed Brayton cycle heat pumps.

Mechanical Vapor Recompression (MVR) systems are related to traditional compression heat pumps. In these systems, excess steam from a thermal process is applied directly in the heat pump, therefore there is no need for an additional evaporator. This also reduces exergy losses during the heat transfer, which makes MVR systems highly efficient. The steam is then compressed to higher pressures and temperatures and is used to reheat the main thermal process [5]. Other systems are Thermal Vapor Recompression (TVR), and different variants of sorption-based heat pump systems. However, these will not be covered in detail as they are not relevant in this aspect.

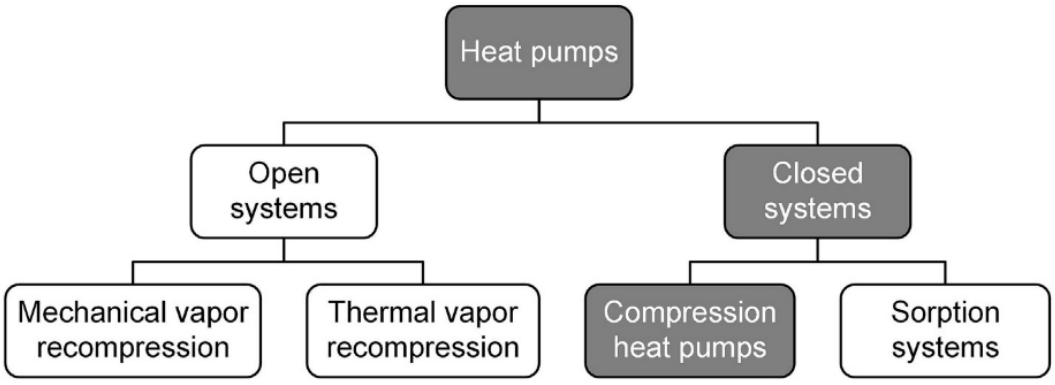

Figure 3: Categorization of heat pump systems [2].

2.4 Industrial Heat Demand – Market Potential for High Temperature Heat Pumps

According to the International Energy Agency (IEA) the final energy demand for heating and cooling was 6350 TWh in 2015. The industry accounts for almost 2500 TWh, almost 40%, of which nearly 2000 TWh is related to the need for process heating.

Figure 4 lists the industrial process heating and cooling demands according to the temperature levels. The diagram shows that the process heating demands in the range from 100 to 200°C accounts for 21 %, while the requirement from 200 to 500°C accounts for 9%. About 75% of this final energy demand is covered by fossil fuels such as gas, oil and coal [6].

In this aspect HTHPs have been recognized as a promising solution to supply heat at elevated temperatures, as they can achieve Coefficient of Performance (COP) values well above 1, which leads to increased system efficiencies compared to fossil fired or electrical boilers for processes heating supply. Furthermore, it leads to reduced Green House Gas (GHG) emissions, using potentially emission-free electricity.

However, commercially available industrial heat pumps are limited by their temperature, which currently stands at around 100°C for fully developed commercial systems (TRL 9) [2]. A development of heat pumps to enable higher supply temperatures will therefore contribute to higher energy efficiencies and electrification of process heating and is thus a vital contribution to the transition towards a sustainable and renewable-based energy system.

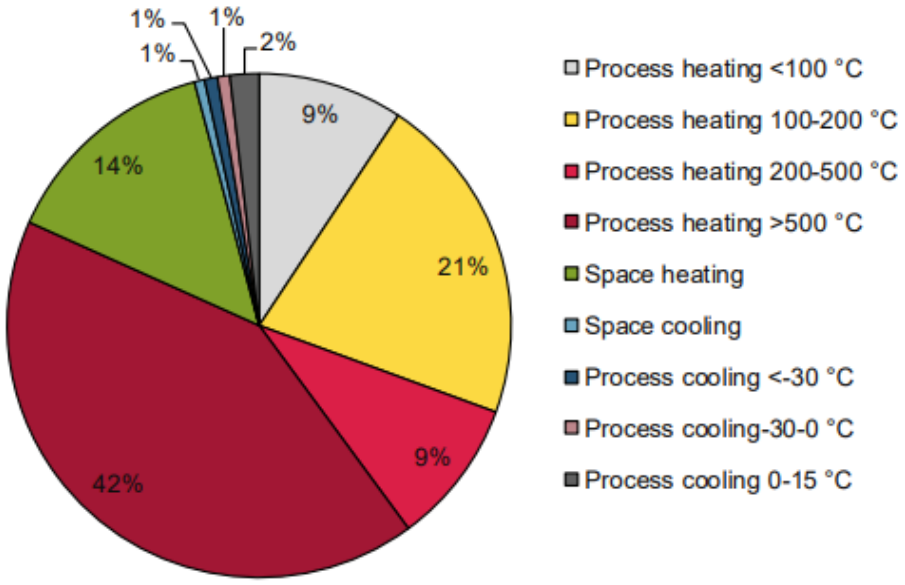

Figure 4: Overview of process heating and cooling demands [7].

Table 1 is an overview of different industrial sectors in need of process heating and the temperature level required for heating. In addition, the TRL level of industrial heat pumps are included and color-coded to illustrate the market availability for heat pumps within the different industrial sectors.

The temperature limit for commercially available systems is in general set to 100°C (TRL 9). Between 100 and 140°C, the heat pumps are regarded to be at prototype, demonstration or early commercialization stage (TRL 6-8), while above 140°C systems are still at conceptual, lab or prototype stage (TRL 3-5) [2]. It should be mentioned that this is a generalised definition as heat pump systems capable of delivering higher temperatures have been developed, as illustrated in Figure 5.

The table shows that there is a great demand for process heat for various industrial processes. Process heat is typically supplied above 80°C. Pulp and paper, chemicals and food & beverage industries have been recognized as industrial sectors with a significant heat demand at high temperatures [2]. Processes related to drying have a particularly high temperature requirement. Moreover, the plastic and wood and metal industries are sectors with process heating demand well above 100°C. There is also a great interest from the industry for production of low-pressure process steam from compression heat pumps [8].

In general, within all recognized industrial sectors there is a need for process heating above 100°C, which requires further development of HTHPs from concept and lab level, or prototype stage towards fully commercialized systems.

Table 1: Overview of industrial processes in need of temperature above 80°C, colour structure is based on TRL level of heat pumps. Reproduced from [2].

Sector	Process	Temperature [°C] 80	100	120	140	160	180	200	[°C]
Paper	Drying								
	Boiling								
	Bleaching								
Food & beverages	Drying								
	Evaporation								
	Pasteurization								
	Sterilization								
	Boiling								
	Distillation								
	Blanching								
	Scalding								
Chemical	Distillation								
	Compression								
	Thermoforming								
	Concentration								
	Boiling								
Automotive	Resin moulding								
Metal	Drying								
	Pickling								
	Degreasing								
	Electroplating								
	Phosphating								
Plastic	Injection moulding								
	Pellets drying								
Mechanical engineering	Surface treatment								
	Cleaning								
Textiles	Colouring								
	Drying								
	Washing								
	Bleaching								
Wood	Gluing								
	Pressing								
	Drying								
	Steaming								
	Cocking								
Several sectors	Hot water								
	Preheating								
	Washing/Cleaning								

	TRL 9: Commercially available HTHP 80 to 100°C
	TRL 6 - 8: Prototype status, technology development 100 to 140 °C
	TRL 3 - 5: Laboratory scale research, functional models, proof of concepts > 140°C

2.5 Heat Pump Market Overview

The potential delivery temperature of heat pumps is increasing as the research progresses and the market matures. Compared to the current market offer in 2014, the delivery temperature has increased from approximately 100°C to about 160°C, and the range of available industrial heat pumps has grown significantly over the recent years. Over 20 heat pump model from a total of 13 manufacturers have been developed capable of delivering heat above 90°C [2], as illustrated in Figure 5, which shows them sorted according to the maximum delivery temperature. Kobelco has set the benchmark with Kobelco SGH 165, which is an extension of the model SGH and utilize 120°C heat to produce steam directly by compressing it to 165°C. Heaten AS (formerly Viking Heat Engines AS) is further developing the Heat Booster model to a claimed delivery temperature up to 165°C [9].

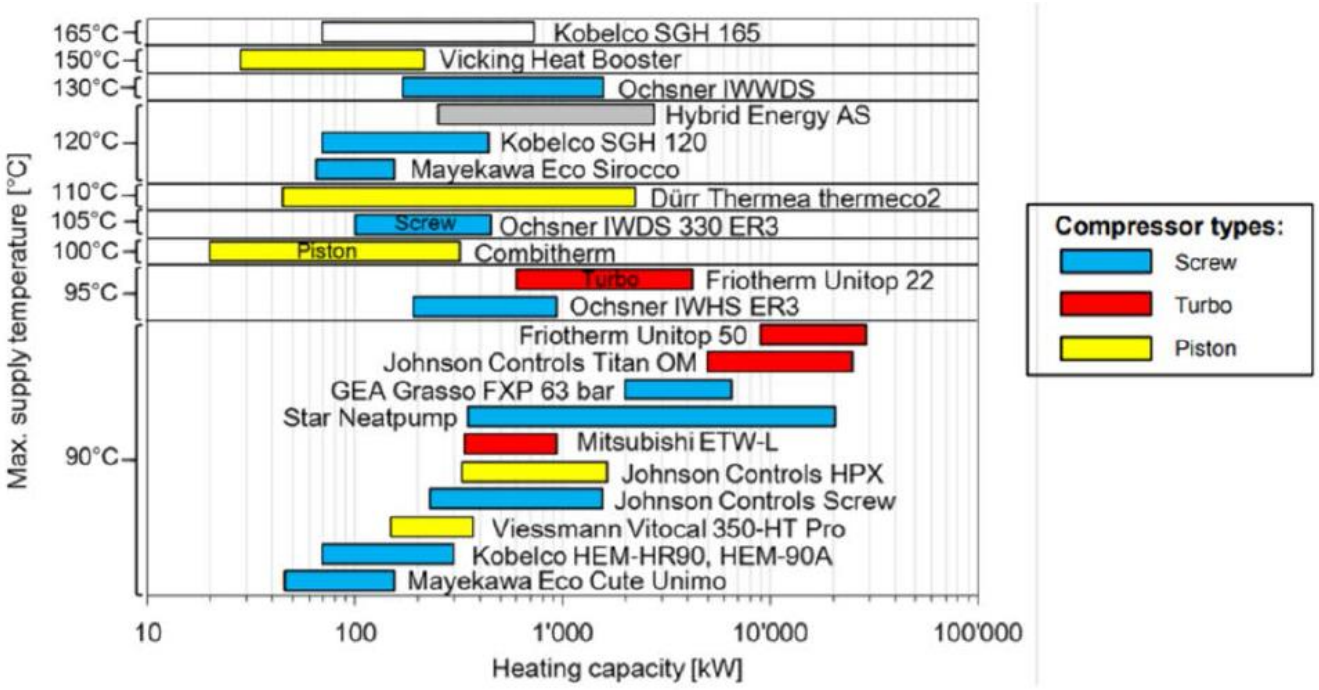

Figure 5: Industrial HTHP models developed by commercial vendors sorted according to sink temperature [2].

2.6 HTHP Research and Development Status

Mateu-Royo et al. have collected and summarized the status of the various R&D work so far. A graphical overview is shown in Figure 6 which includes commercially available systems, commercial R&D systems and research projects. Most of these systems utilise synthetic refrigerants, such as HFC-245fa (high GWP), HFO-1336mzz(Z), HFO 1234ze(E) (low GWP). Regarding natural fluids, water, CO_2, ammonia and butane have been used as refrigerants in some of these projects [3].

Moreover, the summary by Mateu-Royo found that most of these heat pumps systems use reciprocating, screw or scroll type compressors. A further review of refrigerants, component and systems layouts steam heat pumps and reversed Brayton heat pumps using CO_2 will be discussed later in the report.

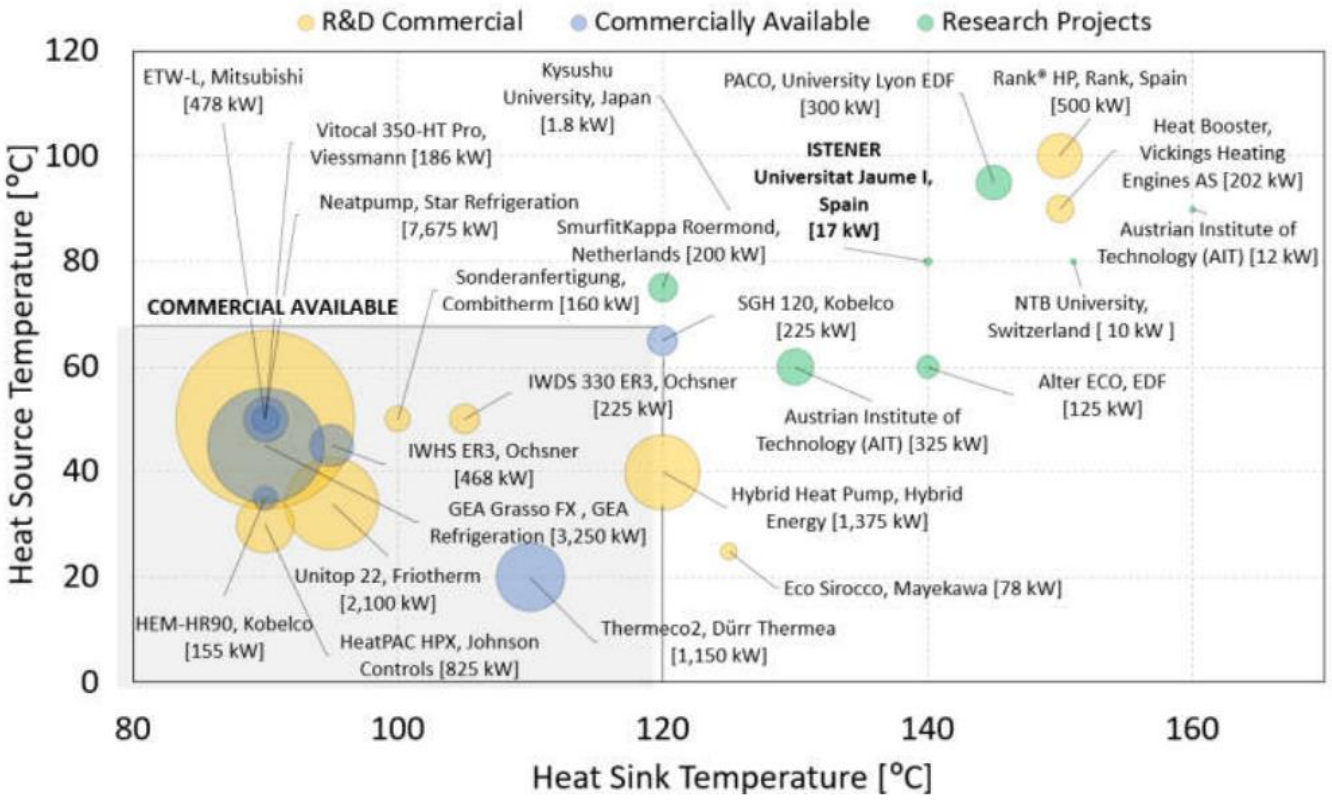

Figure 6: Graphical overview of the R&D development in HTTP [3].

2.7 Barriers

There are several barriers limiting the widespread implementation of HTHPs. They include low level of awareness of the technical and economic feasibility of using heat pumps for various industrial applications. Moreover, there needs to be developed more knowledge related to the integration of HTHPs in industrial processes. These barriers are also related to the fact that there are few large-scale pilot and demonstration systems that have been developed [2].

The technical barriers are due to operation at high temperatures, where there is a lack of suitable refrigerants with low GWP, and component limitations. This concerns the compressor in particular which, depending on the refrigerant, can reach very high outlet temperatures, which causes multiple challenges to both the cooling system and the lubrication system as the lubricating properties of oil starts to degrade above 140°C and material challenges.

Research efforts have been made to find new refrigerants with low GWP, among which water (R-718) and CO_2 (R-744) have been demonstrated to be capable of operating at higher temperature levels and suitable components [10], [11]. Moreover, research and investigations into certain components have been made, such as turbo-compressors which can potentially operate oil-free and thus not limited by the lubrication system [11]. Experiences from other application areas, such as oil and gas show that for example CO_2 compressors are technically feasible up to 480°C [12].

The economic barriers include large investment costs and longer payback periods compared to competing systems such as electrical, or gas or oil-fired boiler. In addition, in certain nations the fuel energy price compared to electricity is low, resulting in even longer payback periods [2]. At the same time, the ratio between the cost of electricity from renewables and fossil fuels is decreasing [11].

2.8 Key Performance Indicators

2.8.1 Coefficient of Performance – COP

The performance and efficiency of the heat pump is determined by its Coefficient of Performance (COP), which describes the relationship between heat delivered (Q_H) from the heat pump to work (W) input:

$$COP = \frac{Q_H}{W}$$

The added work typically comes from the electrical energy required to run the compressor. A heat pump is typically able to achieve COP values of 3-5 depending on the temperature difference between the heat source and the heat sink. The reason for this can be found in the difference in the working principle between traditional electric heating and heat pumps. In electric heating systems, heat is added directly from the exergy source (in this case electrical energy), and the consumer cannot utilize more energy than the input, giving a COP of 1.

In a heat pump, exergy (mechanical energy) is used to transfer heat from a low-temperature area to a high-temperature area. This operation is considerably less energy demanding than adding heat directly, with the result that the power input from the compressors is significantly lower than the heat delivery from the heat pump.

2.8.2 Carnot COP and Efficiency

Thermodynamically the ideal heat pump can be described as a reverse Carnot Engine as illustrated in Figure 7. where heat (Q_C) is pumped from a low temperature reservoir, or heat source (T_C), using work and rejected as heat (Q_H) to a high temperature reservoir or heat sink (T_H).

The work input to the process can be described by:

$$W = Q_H - Q_C$$

And the COP relation becomes:

$$COP = \frac{Q_H}{Q_H - Q_C}$$

Since the Carnot process involves isentropic compression and expansion, and isothermal heat absorption and rejection, heat absorption and rejection are a function of the temperature and the change in entropy (S):

$$Q = T\Delta S$$

Hence, the Carnot COP can be simplified to a function of the temperatures of the heat source and heat sink:

$$COP_{Carnot} = \frac{Q_H}{Q_H - Q_C} = \frac{T_H \Delta S}{T_H \Delta S - T_C \Delta S} = \frac{T_H}{T_H - T_C}$$

In a real heat pump, the COP therefore becomes strongly dependent on the temperature lift that is required, which is the temperature difference between the evaporator and the condenser. Furthermore, in a real heat pump, thermodynamic losses occur in all the main components: in heat exchangers due to temperature differences between the cold and hot fluids; during compression, due to compressor inefficiencies causing non-isentropic compression; during expansion, which in most heat pumps is a throttling valve operating according to isenthalpic Joule-Thomson's expansion; and due to pressure losses in the heat exchangers and tubing.

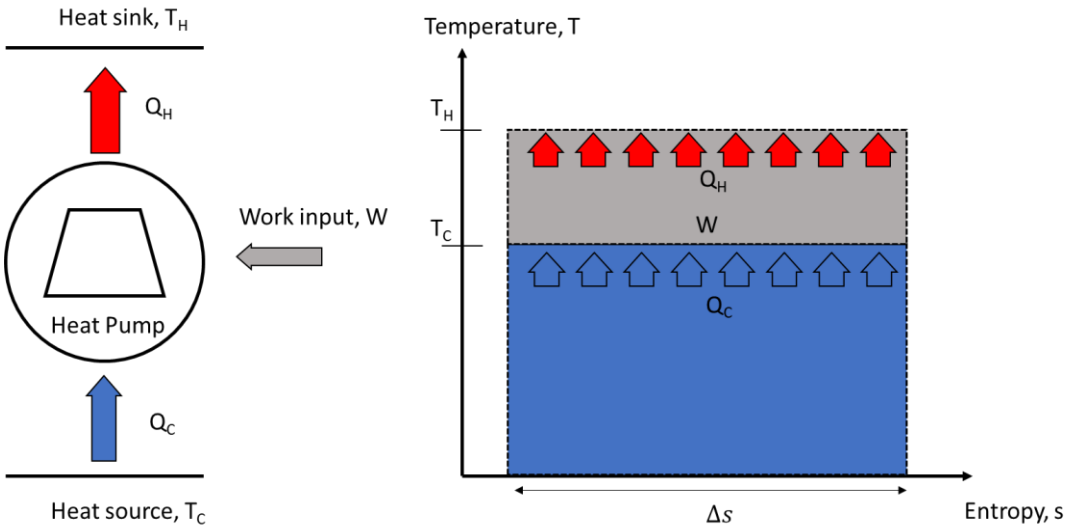

Figure 7: Heat pump as a reverse Carnot heat engine and corresponding temperature-entropy diagram.

Since the temperature lift of a heat pump is the dominant factor of deciding its COP, a better way of determining its efficiency compared to other heat pumps is the relation of the COP to the Carnot COP, which is the maximum theoretical COP. This is called the Carnot efficiency and becomes:

$$\eta_{Carnot} = \frac{COP_{real}}{COP_{Carnot}}$$

Typically, industrial heat pumps can achieve a Carnot efficiency between 40 and 60%. A graphical comparison between the Carnot COP and the COP for industrial heat pumps with 40-60% Carnot efficiency is illustrated in Figure 8. In this example the heat source temperature is set to 140°C. As an example, with a temperature lift of 40 Kelvin, a COP value of 4.5 and 6.8 can be expected.

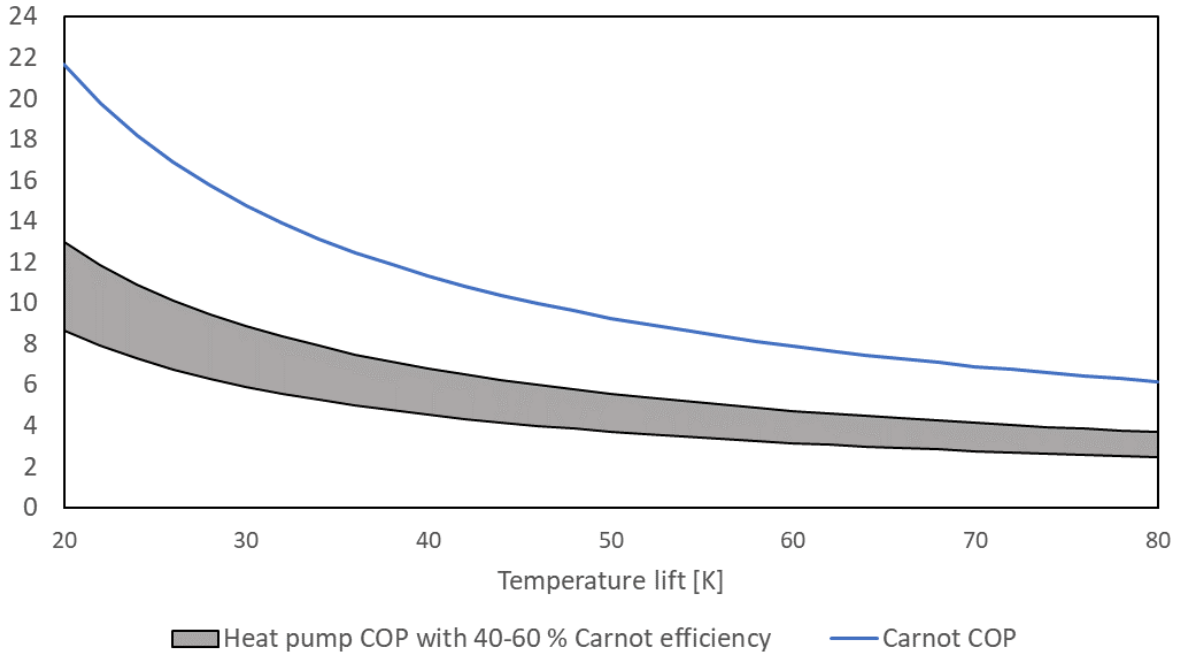

Figure 8: COP comparison between the ideal heat pump operating with Carnot COP and real heat pumps operating at 40-60% of the Carnot efficiency.

2.8.3 Lorenz COP and Efficiency

Although the Carnot efficiency is most frequently used to measure the efficiency of a heat pump, it assumes isothermal heat exchange with the source and sink. However, in many cases heat is exchanged at gliding temperatures. In those cases, with large temperature glides in the sink and source, the Lorenz COP and efficiency is more useful because it takes these temperature glides into account, providing a more accurate COP. The Lorenz COP is defined as:

$$COP_{Lorenz} = \frac{T_H}{T_H - T_L}$$

Where,

$$T_H = \frac{T_{H,out} - T_{H,in}}{\ln\left(\frac{T_{H,out}}{T_{H,in}}\right)}$$

$$T_L = \frac{T_{L,in} - T_{L,out}}{\ln\left(\frac{T_{L,in}}{T_{L,out}}\right)}$$

The Lorenz efficiency becomes:

$$\eta_{Lorenz} = \frac{COP_{real}}{COP_{Lorenz}}$$

As opposed to traditional heat pumps, where the refrigerant in the heat pump cycle undergoes latent heat transfer through evaporation and condensation, the Lorenz efficiency is especially suited for Reversed Brayton cycle heat pumps where the working fluid stays in the gas phase during the entire cycle, and where the sensible heat exchange occurs with large temperature glides in the gas cooler and gas heater.

3 Steam (R-718) Heat Pump Cycle

3.1 Working Principle

The SHIP200 heat pump concept for short term heat delivery up to 200°C is a steam heat pump, using water (R-718) as working fluid, which is based on a vapor compression refrigeration cycle (VCRC). In its simplest form, the cycle consists of four components: compressor, condenser, expansion valve and evaporator, as illustrated in Figure 9, and the corresponding temperature-entropy diagram in Figure 10. Heat is transferred from the heat source to the working fluid in the evaporator where it evaporates at low temperature and pressure. It then enters the compressor where mechanical energy from electricity is added to the working fluid by compressing it to a high temperature and pressure. The working fluid then enters the condenser where latent heat is transferred to the heat sink through condensation. The last step in the cycle is expansion through a throttling valve, where the refrigerant is released to low temperature and pressure again to repeat the cycle.

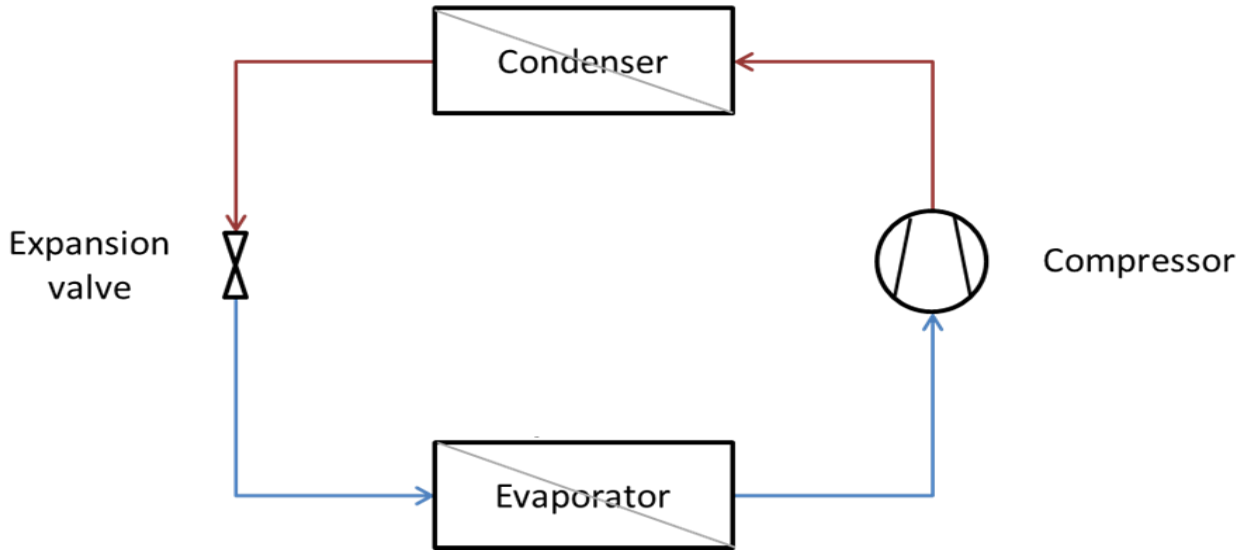

Figure 9: Simple vapor compression refrigeration cycle.

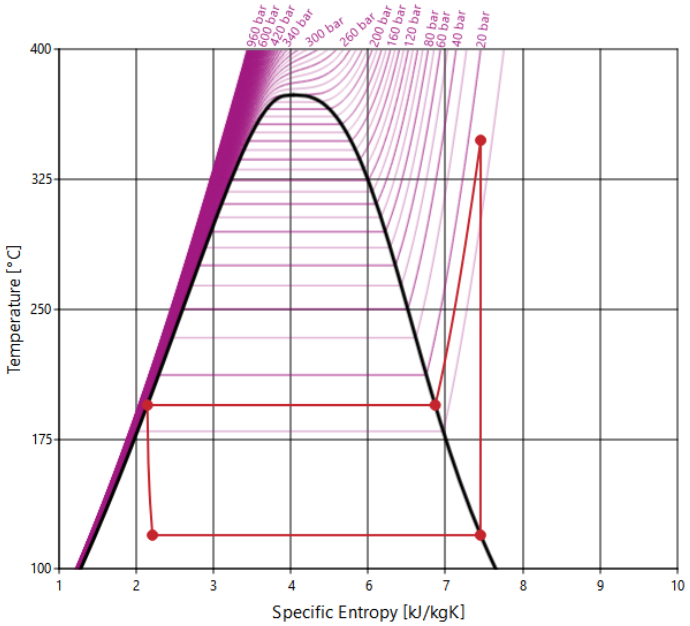

Figure 10: Temperature-entropy diagram for simple vapor compression refrigeration cycle, using water as working fluid operating between 120 and 195°C.

3.2 Refrigerants – R718

One of the most important parameters in a heat pump is the selection of working fluid or refrigerant. This choice is constrained by the temperature boundaries that the heat pump will operate within, as the evaporation and condensation temperatures need to match the boundary while operating at reasonable pressures. This means typically evaporation at or above atmospheric pressure and condensation at not too high pressures. Furthermore, the refrigerant needs to be chemically stable to avoid degradation.

In the existing industrial HTHPs that are commercially available, synthetic refrigerants are dominating. R-245fa (pentafluoropropane) and R-134a (tetrafluroethane) are two of the most common fluids but are not a future possibility due to their relatively high GWP. Previous reviews show that that current and previous research initiatives are dominated by a mix of different refrigerants, from the old conventional high GWP working fluids, such as R-245fa, new-generation synthetic refrigerants with low GWP, such as R-1336mzz(Z) and R-1234ze(Z), and natural refrigerants such as R-600 (butane), R-744 (CO_2), R-718 (Water), R-717 (Ammonia) and R-717/R-718 (Ammonia-water mix) [2], [3].

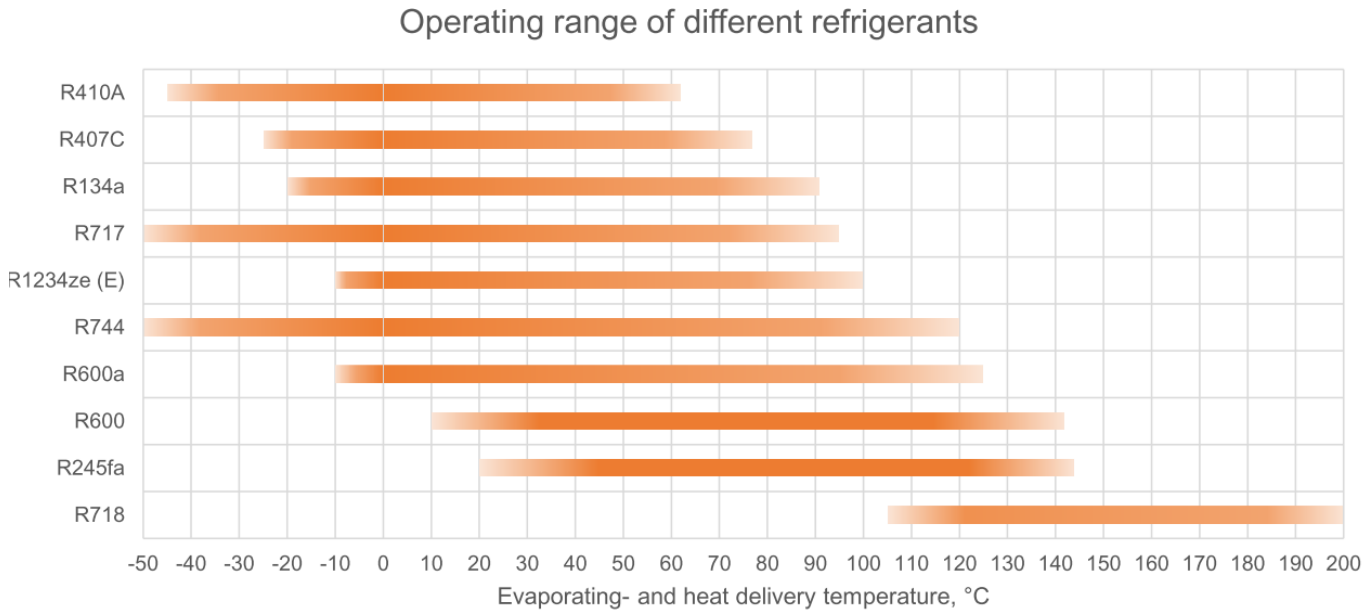

Figure 11: Operating range of different refrigerants [13].

Among the natural refrigerants, water stands out with a significantly higher critical temperature at 373.9°C, as illustrated in Figure 12, but also compared to synthetic fluids. This property makes it one of few practical fluids for heat delivery via condensation at temperatures around 200°C. In previous refrigeration applications, the use of water has been limited to absorption systems. For heat pump applications, the use of water was in the past not a subject. A main reason for this is its boiling temperature of 100°C, at atmospheric pressure, which means that it is less suited when heat sources are available below this temperature since evaporation then needs to take place at a sub-atmospheric pressure. However, in the later years with R&D increasing delivery temperatures from HTHPs, the use of water for applications above 100°C has become an attractive alternative.

Ashrae number	IUPAC name	ODP	Net GWP 100-yr	Molar mass (g mol^{-1})	Normal boiling point(s) (°C)	Critical temp. (°C)	Critical pressure (absolute) (kPa)
R-290	Propane	0	3.3	44.1	–42.1	96.7	4,248
R-600	Butane	0	4.0	58.1	0.0	152.0	3,796
R-600a	Isobutane	0	3.0	58.1	–11.7	134.7	3,640
R-601	Pentane	0	4.0	72.1	36.1	196.6	3,358
R-601a	Isopentane	0	4.0	72.1	27.7	187.8	3,378
R-717	Ammonia	0	0.0	17.0	–33.3	132.4	11,280
R-718	Water/Steam	0	0.2	18.0	100.0	373.9	22,060
R-744	Carbon dioxide	0	1.0	44.0	–78.0	31.0	7,380

Figure 12: Common natural working fluids and their properties [4].

Water displays many attractive properties. It is chemically stable, non-toxic and non-flammable, which makes it one of the safest known working fluids with no environmental impacts. Furthermore, it naturally has no ozone depletion or global warming potential. It also has the lowest cost and is available anywhere.

Compared to other refrigerants, it has a high latent heat of evaporation, which means that high heat deliveries can be achieved with modest refrigerant mass flow rate [14]. Still, the high specific volume [m^3/kg] of water leads to high compressor volumetric flow rates. As the corresponding vapour density [kg/m^3] increases with increasing evaporation temperature, the thermal capacity of the heat pump with a compressor at a given size will increase when the evaporation temperatures are increased.

The thermal conductivity of liquid water (0.68 W/mK at 100°C) is higher than the thermal conductivity for other typical working fluids, a property beneficial to achieve higher heat transfer coefficients during heat exchange with the source and sink.

Due to its thermodynamic properties, Madsboell et al. argued that water is the most promising working fluid for high-temperature heat pumps. Given that identic compressor efficiencies can be achieved, the COP by using water is higher than for competing working fluids [15].

Since many process applications use steam, e.g. as a drying agent, in distillation or boiling, the use of water as working fluid allows for an open loop solution where the compressed steam can be directly used in the process, either using MVR systems or other forms of open heat pumps. It also allows for the possibility to use direct contact condensers and evaporator, given that water is used as a heat-transfer-fluid. This can potentially reduce system capital cost and improve the cycle performance.

Refrigeration systems using steam have achieved high efficiencies when the heat source and sink are at relatively constant temperatures. When paired with sources and sinks with larger temperature glides i.e. single phase fluids, zeotropic mixture refrigerants or gas cycles have shown superior efficiencies. This would suggest that in order to achieve the best possible COP for a closed cycle steam heat pump in a SHIP200 system, temperature glides should be minimized [11].

To summarize water displays many advantageous properties, there are, however, shortcomings, which needs to be addressed during the design of the heat pump. Still, for a VCRC system delivering heat at temperatures around 200°C there are few other realistic alternatives, and the use of water (R-718) appears to be the most attractive option.

3.3 Research and Development Status of Steam Based HTHPs

Research and development on HTHPs are dominated by systems using other working fluids than steam (R-718). However, in the recent years steam has received more attention.

Chamoun et al. investigated the potential of using water vapor and performed experimental simulation of a HTHP. The investigations showed that the largest obstacles were related to the compressor technology and that existing industrial compressors designed for water vapor were constrained by cost, low efficiency or low compression ratios. With a newly developed twin-screw compressor adopted for water vapor, their heat pump could recover waste heat from 85-95°C and satisfy high temperature heat demand with a condensation temperature of 145°C [14].

Madsboell et al. developed a steam compressor designed to operate in the temperature range 90-110°C with a capacity of 100-500 kW. The compressor was able to achieve a temperature lift of 35-30°C per stage. It was highlighted that using planetary gear from automotive superchargers, would allow for the use of standard electrical motor at a relatively low cost compared to high-speed direct drive motors [15].

Zühlsdorf et al. introduced a multistage cycle using R-718 (Water) as working medium for heat pump-based process heat supply above 150°C. The heat pump cycle was a cascade cycle using butane in the two bottom cycles, and R-718 as the top cycle operating with three compression stages, each with a compression ratio of around 3. The operating temperature for the top cycle for one of the cases was between 125°C (evaporator) and 280°C (stage 3 condenser), achieving a COP of 3.0. Their analysis indicated that it is possible to economically supply process heat up to 280°C from electrically driven heat pumps, and technically feasible up to temperatures up to 300-400°C using compressor technologies from other industries, such as oil & gas [11].

3.3.1 Research Projects

In the Paco project, University of Lyon EDF, together with Johnson Controls, developed a twin screw compressor used in a closed loop heat pump delivering around 300 kW 145°C, from 95°C. The twin screw compressor was developed to overcome the challenge with low temperature lifts associated with centrifugal compressors and blowers. The compressor featured significant modifications to the sealings and included water injection. However, due to mechanical problems it was later replaced by a two-stage centrifugal compressor with magnetic bearings [16], [6].

In the HeatUp project SINTEF together with Rotrex and Epcon developed a single stage turbo compressor, which during tests achieved a pressure ratio of 2.4 and, corresponding to a temperature lift of 25K from 100°C.

Later, in the DryFiciency project AIT and SINTEF developed a two-stage turbo compressor MVR heat pump system in cooperation with Rotrex and Epcon. Experimental results showed that it was capable of compressing steam from atmospheric pressure up to 3 barA, delivering 300 kW at 133°C, reaching a COP of 5.9. Sealing challenges were observed as a small amount of steam penetrated into the gearbox, which created oil/water emulsions [17]. For future applications, an improved sealing should be investigated. The dryFiciency project ultimately aims for real production demonstration at TRL7 of both closed loop and open loop heat pumps.

In both the HeatUp and DryFiciency projects, the turbo compressor was based on a mass-produced automotive turbocharger, with the benefit of potentially reaching investment costs as low as 200€/kW.

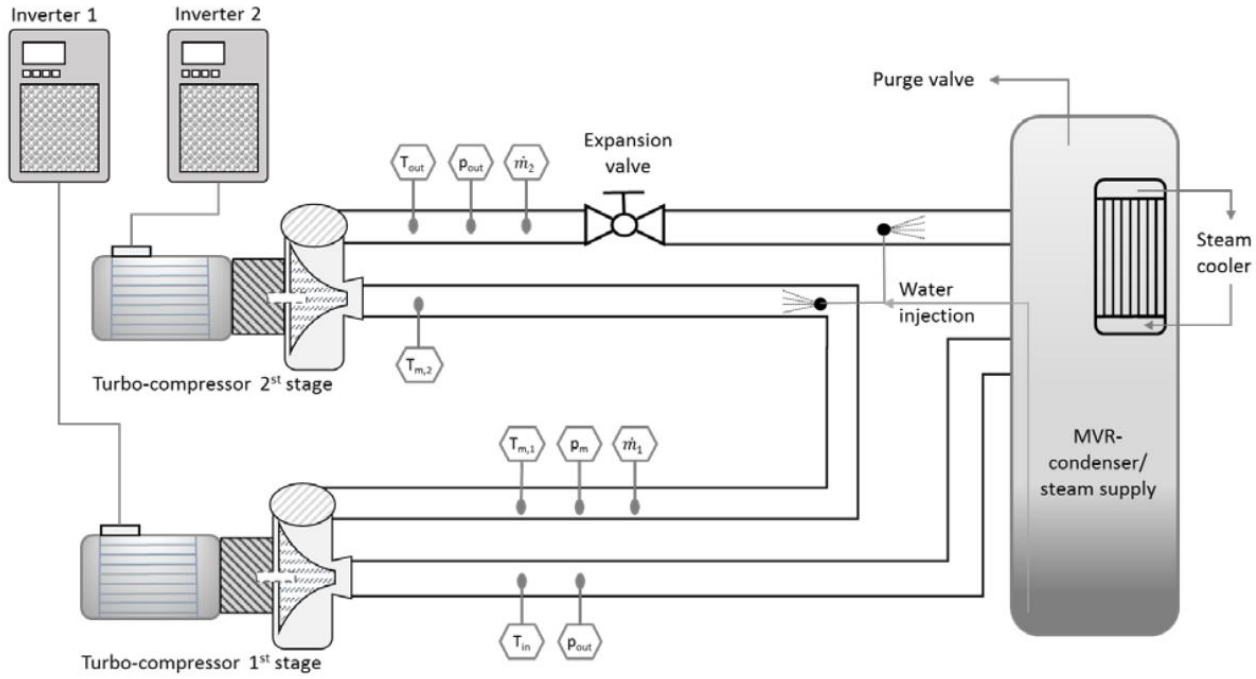

Figure 13: Process sketch of the 2-stage turbo compressor MVR heat pump test rig in the DryFiciency project [17].

Recently, in the ongoing Free2heat project, which is a collaborative project between SINTEF, NTNU and ToCircle, the aim is to develop a heat pump capable of delivering heat at 180°C. The compressor is based on a rotary vane machine, which compresses water-steam in the two-phase area. This, together with water injection, which also lubricates the compressor, avoids the production of superheated steam. This reduces the thermal stress by reducing the maximum temperatures, eliminates the use of oil-based lubrication and the need for external de-superheaters [18], [19].

3.4 Cycle Components Design Considerations

3.4.1 Compressor Technologies

The compressor is the heart of the heat pump and is essential for reaching heat delivery at high temperatures. The compressor needs to have sufficient capacity by providing the correct volumetric flow rate, while at the same time being efficient, reliable and have a reasonable cost.

Several potential compressor technologies exist for high-temperature heat pump applications for water vapor:

- Piston compressors
- Screw compressors
- Turbo compressors
- Centrifugal fans and blowers

In Figure 5 the compressor technologies used by the commercial actors show that piston and screw compressors dominate the market. Scroll compressors are also used in some experimental research projects, but these typically have too small capacity to be realistic for industrial applications [3]. However, in most of these heat pumps, other working fluids than water are used.

Piston compressors or reciprocating compressors are positive-displacement compressors, where a piston driven by a crankshaft moves up and down in a cylinder compressing the gas from a large volume to a smaller volume. Because water has very high swept volumes, which limits the volumetric flow rate, piston compressors have typically been used for other refrigerants with lower specific volumes [15]. However, an Austrian research project, SteamUP has shown that using a piston compressor is feasible for high temperature steam compression [13]. Still, a disadvantage is relatively high investment costs.

Screw compressors are rotary-type positive displacement compressors that use helical screws to compress the refrigerant. With this technology, high-capacity compressors for steam can be realized, and it exists with both lubricated and lubrication free compressors. However, the lubrication free compressors suffer from reduced efficiencies. The PACO project showed that using a twin screw compressor is technically feasible. However, as with the piston compressors, a downside to using screw compressors are high investment costs [11].

In the case of centrifugal fans and blowers, they provide cost-efficient compression for high capacities > 4 MW. However, the compression ratios per stage are rather low, which typically corresponds to a temperature lift of 5-7K. Multiple stages of blowers or fans need to be employed to achieve high temperature lifts [20].

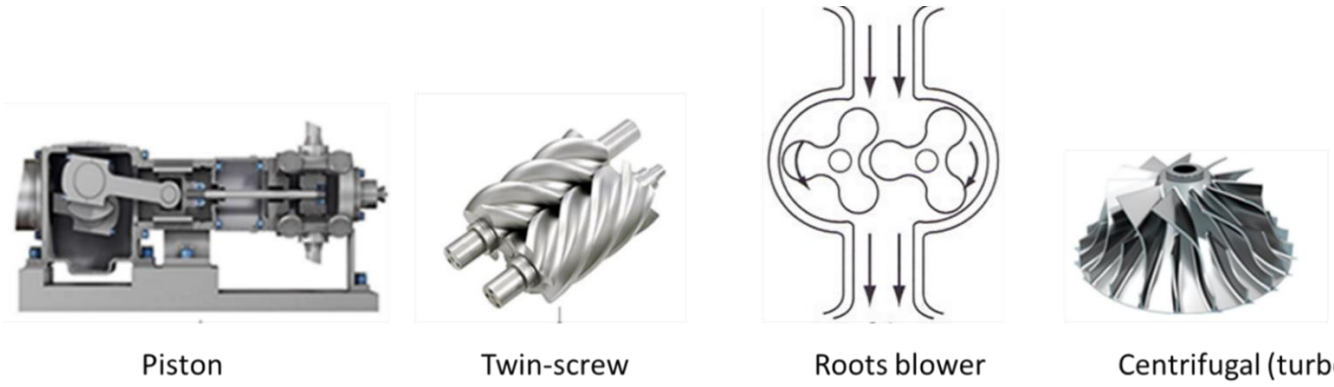

Figure 14: illustration of different compressor technologies [21], [22].

3.4.1.1 Turbo Compressors

Turbo compressors are electrically driven compressors based on a centrifugal or axial flow. The pressure rise through a turbo compressor is achieved by adding kinetic energy to the working fluid through the rotor or impeller, followed by a conversion to potential energy or static pressure as the fluid is slowed down by a stator or diffuser.

Compared to other compressor types, the advantage of turbo compressors is that a relatively compact design can be achieved due to high rotor speeds, which allows for high inlet velocities and volume flow rates [15]. The compact design also allows for reduced capital costs. As the compressor is one of the main cost components in heat pumps, and because few steam compressor alternatives exist for thermal capacities between 500 kW to 4 MW, the turbo compressor technology could provide a cost effect option in this segment [20].

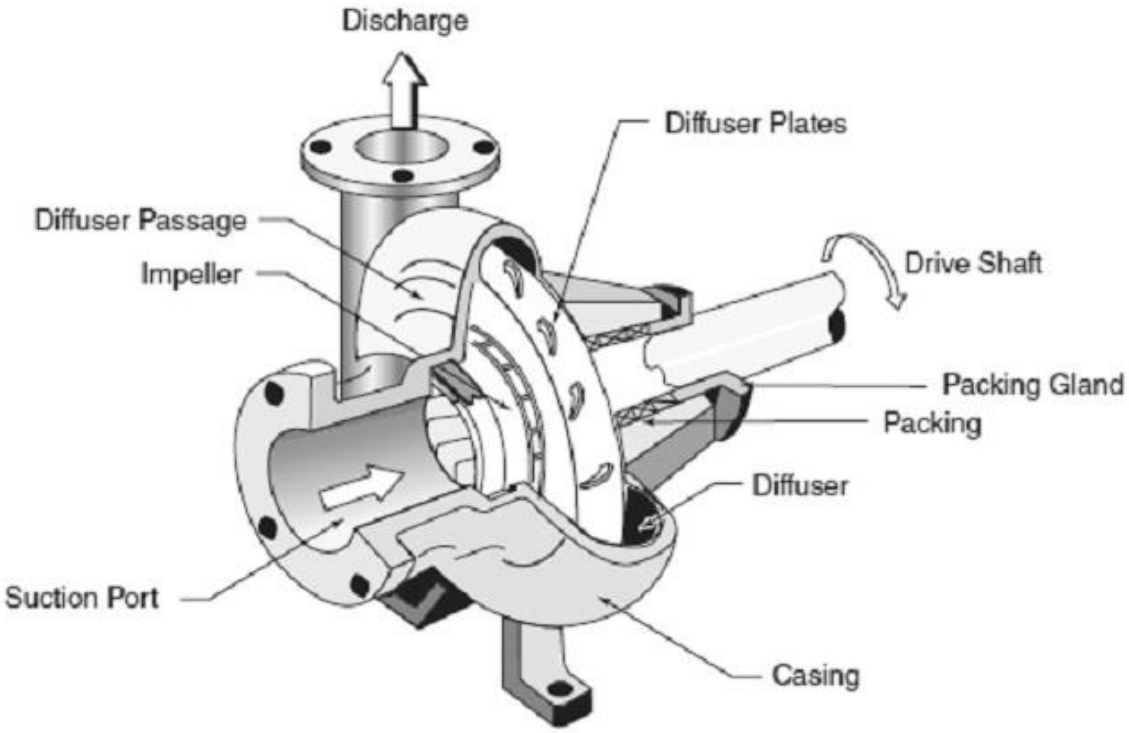

Figure 15: Section view of a centrifugal compressor [23].

Comparing the axial and centrifugal compressor, the advantage of the centrifugal compressor is increased pressure ratio per stage, while axial compressors allow for slightly higher efficiencies and more compact design [15]. From existing commercial technologies and research initiatives, centrifugal compressors appears to be the most utilized option [15], [2], [20], [24], [25]. Several projects have identified the turbo compressor and the most promising alternative, including the PACO project, HeatUP and DryFiciency.

Most turbo compressors are developed for air. In terms of component development towards steam, the difference between air and steam lies in the density, temperature and atomic weight. This requires small alterations to the impeller design and the planetary gear. The main challenge when using gears is sealing leakage between the process steam and the gear lubrication oil [15].

Even though a turbo compressor is a compact solution compared to other compressor technologies, the low vapor density of water means that a larger compressor is required compared to other refrigerants with higher densities. Another disadvantage of steam is that it has a high temperature lift for a given pressure lift. This is illustrated in the temperature-entropy diagram in Figure 10 where a single stage isentropic compression of water vapor from 120°C and 3 barA to 14 barA to achieve a 75K temperature lift, results in a compressor outlet temperature of 350°C, which is much higher than the corresponding condensation temperature at 195°C. Such an approach with high temperatures is very challenging for the compressor and would lead to significant material stress and correspondingly high costs for using a material with high durability.

Another challenge with high temperature lift in a single-stage compressor is that it is limited by factors such as the low atomic weight of water and the compressor pressure ratio. The compressor tip speed depends on both of these parameters and is in itself limited by the choice of material and mechanical design in the compressor. An illustration of the relationship between compressor tip speed and temperature lift is given in Figure 16. As a consequence the temperature lift in each compression stage is limited to around 20-25 K [15].

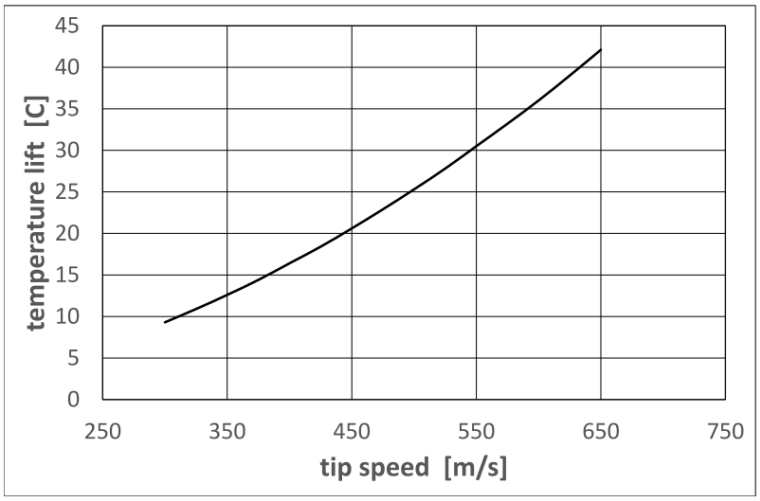

Figure 16: Temperature lift as a function of impeller tip speed for a centrifugal compressor[15].

In order to avoid both high stage temperature lifts and very high compressor outlet temperatures, multiple compression stages, with corresponding de-superheating will instead need to be implemented. As illustrated in Figure 17, when the single-stage compression heat pump cycle in Figure 10 is replaced by a 3-stage compression cycle, followed by de-superheating of the refrigerant down to saturated steam conditions, the maximum cycle temperature at the end of compression stage 3 is 237°C.

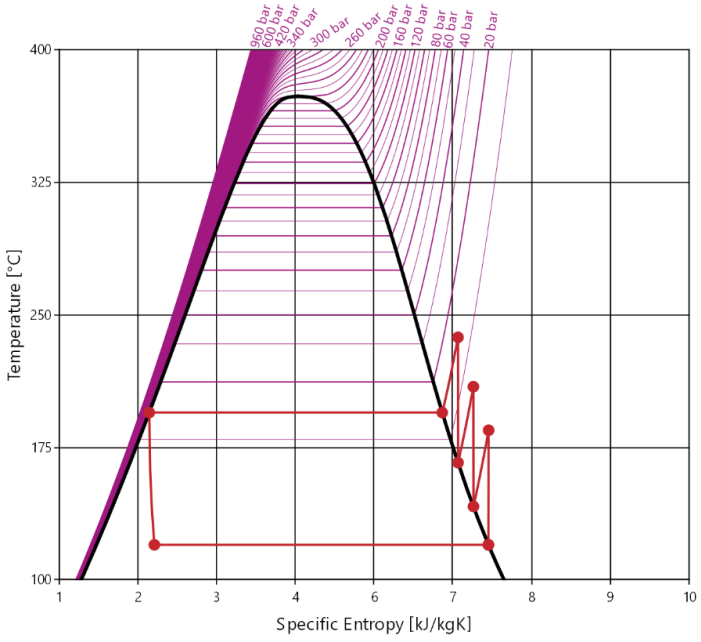

Figure 17: Temperature-entropy diagram of a heat pump cycle with three stage compression and corresponding de-superheating.

Still, even at temperatures around 200°C degradation of planetary gear lubrication oil is a concern. Although sealing technologies exist, the safest option from an operational reliability point of view would be to use a direct-drive system without gears. However, such a solution is also more expensive.

Since a turbo compressor is very sensitive to liquid droplets causing material damage, the system should be designed with a minimum superheating of 5-10K at the inlet of each compression stage [24].

3.4.2 De-superheating

De-superheating after compression is performed in order to reduce the overall compressor work and the maximum cycle temperature. It is comparable to traditional intercooling for air compressors, but instead of using a heat exchanger, the steam is typically cooled down by the evaporative effect from water, for example by spraying water directly into the pipes.

The mixing of vapor and water reduces the overall temperature and increases the total mass flow rate, such that for each compression stage works with higher mass flow rates than the previous stage. This has the effect of increasing the compressor duty compared to using a traditional intercooling, but also increases the heat delivery in the condenser. The capital cost of de-superheating by injecting water is significantly reduced compared to using heat exchangers for intercooling.

Zühlsdorf et al. investigated different concepts for de-superheating R-718 high temperature heat pumps with multiple compression stages. As illustrated in Figure 18, there are two main approaches to de-superheating: liquid injection into the gas stream (a, d), or an open intercooler concept where a bubbling of the gas stream into the liquid holdup (b,c) [24].

The liquid injection concepts can either be performed using a liquid injection atomizing nozzle (a), or with an open intercooler with packings (d). Both technologies allow for a precise temperature control of the superheated steam after liquid injection, which is important in order to avoid liquid droplets at the inlet of the next compressor. While (a) is a is a fully established technology and frequently used in industrial steam plants, (d) is at a concept level, but with proven components. However, while (a) requires a certain length of the pipe downstream the injection point to allow all injected water to evaporate prior to the next compression stage, (d) can be realized with a small-sized intercooling due to the packings, which increase the heat exchanger area [24].

The open intercooler concepts can be performed by using a conventional open intercooler with vapor injection (b) or using an absorption de-superheater (c). Both concepts allow for economizing the heat pump cycle, where the flash gas after a first stage throttling is recovered in the intercooling stage. However, there is a limited possibility to control the outlet temperatures [24].

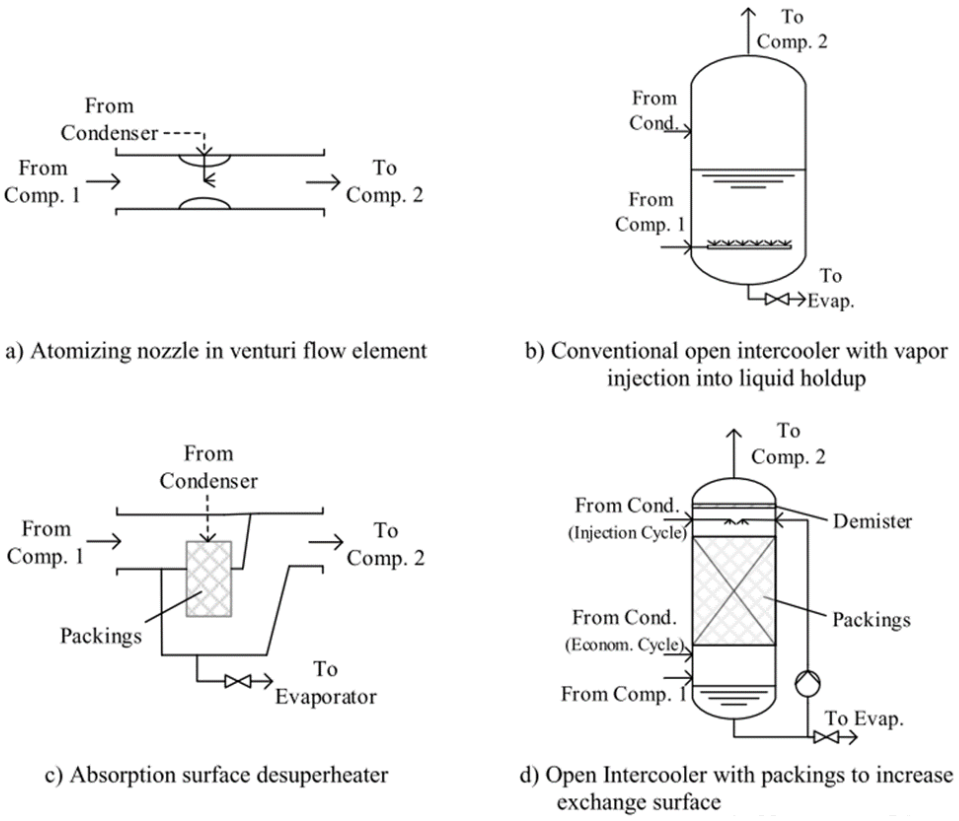

a) Atomizing nozzle in venturi flow element

b) Conventional open intercooler with vapor injection into liquid holdup

c) Absorption surface desuperheater

d) Open Intercooler with packings to increase exchange surface

Figure 18: Possible technologies for de-superheating [24].

In the two-stage test facility built by SINTEF for the DryFiciency project de-superheating was realized using solution (a). However, instead of injecting water through throttling from the condenser, the water was pumped from the steam generator (evaporator) tank. This was a cost-effective solution, and experience during testing showed that this resulted in good control of the temperature after de-superheating. However, the setup was space demanding due to above-mentioned reasons [17], which to some extent contradicts the purpose of using a heat pump based on compact turbo compressors. Thus, if a compact solution similar to (d) can be realized to a low cost it would potentially give the best solution for large-scale industrial applications.

3.4.3 Heat Exchangers

In a closed cycle heat pump, there are two main heat exchangers, the condenser and the evaporator. Compared to the compressor, the heat exchanger technology is fully commercialized to operate at temperatures in excess of 200°C. However, in order to select a suitable heat exchanger, the characteristics of the heat exchanger, the working fluid and the operating conditions need to be taken into account. In terms of the working fluid and operating conditions, the heat exchanger encounter a few challenges as the steam have high temperatures and high specific volumes. The change in specific volume when water condenses at 200°C is approximately 1:100, while for R-245fa the ratio is 1:15 when condensation occurs at 100°C. These changes will lead to deceleration and acceleration of the flow in the condenser and evaporator, which potentially could give large pressure drops.

In terms of heat transfer capabilities steam has high heat transfer coefficients compared to other working fluids. For film heat transfer the heat transfer coefficients can be estimated to 5000-15000 W/m^{2}K for condensation and 2000-10000 W/m^{2}K for evaporation [26].

Shell and tube heat exchangers and plate and frame heat exchangers are the most common heat exchanger types, both of which can be considered as evaporator, condenser and internal heat exchanger in an HTHP.

The plate and frame heat exchangers are advantageous in terms of offering compact size as they have a much larger heat transfer area relative to their size than shell-and-tube heat exchanger. They have high performance with low exergy losses as they can achieve very low logarithmic mean temperature differences [LMTD] between the hot and cold fluid.

They are also typically less costly and are easier to maintain. Several HTHP systems are known to use plate heat exchangers, such the ammonia-water hybrid heat pump with 650 kW thermal capacity, delivered by Hybrid Energy [27], and the SGH 165 and SGH 120 delivered by Kobe steel and rated up to 650 kW [28].

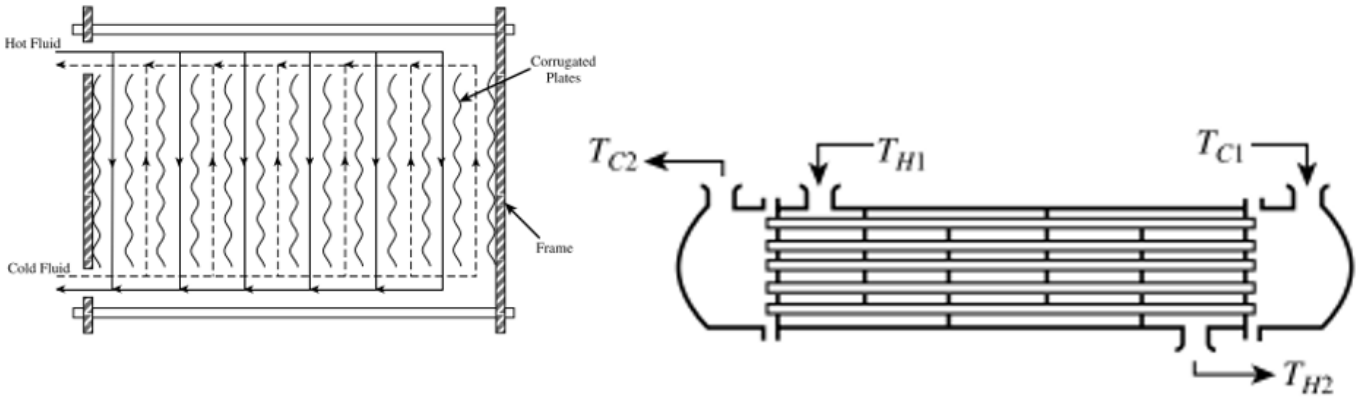

Figure 19: Principle sketch of a plate-and-frame heat exchanger (left) and a single-tube pass shell-and-tube heat exchanger (right) [26].

Typically, gasketed plate heat exchangers are offered, which are common, relatively cheap and offer simple maintenance through mechanical cleaning. However, the gaskets are typically limited to 180-200°C, which is far below the expected steam entry temperature, which will be in the range of 250-300°C.

Potential options were therefore investigated. A search for suitable commercial plate heat exchangers from Alfa Laval and SWEP showed that brazed or fusion bonded plate heat exchangers are capable of reaching higher temperatures than gasketed plate heat exchangers. The most promising alternatives are listed in Table 2. For the

condenser, the two potential options are the Alfa Laval Compablock, which is a plate and block type heat exchanger with potentially large capacities, up to 6000m^3/h and the Alfa Laval Alfanova HP400, which utilizes fusion bonding for to handle high temperature and pressure requirements. For the evaporator, where the temperature requirements are around 160°C potential options in addition to the two others can be Alfa Laval AC1000DQ or Alfa Laval CB400, of which both are rated for temperatures well around 200°C.

A disadvantage with these plate heat exchangers is that, with the exception of Compablock, they are not sized for very large scales. It is estimated that a heat pump with a capacity of 12 MW will require multiple plate heat exchangers for both the condenser and the evaporator. If pressurized water is used as HTF, a minimum of 2 is required each for the condenser and the evaporator. If Wacker Helisol is used as HTF, the amount of heat exchangers would be minimum 4.

Table 2: List of potential plate heat exchangers.

Heat Exchanger options	Max flow [m^3/h]	Max T [°C]	Max P [barG]	Minimum number of heat exchangers required
Alfa Laval Compablock, plate and block heat exchanger	6000	400	42	1
Alfa Laval Alfanova HP400 (fusion bonded plate heat exchanger)	200	550	28	4
Alfa Laval AC1000DQ	200	204	30	4
Alfa Laval CB400	200	225	35	4

Figure 20: Left Alfa Laval AC100DQ Brazed plate HX, right: Alfa Laval Alfanova HP400 fusion bonded HX [29], [30].

3.4.3.1 Internal Heat Exchanger

The use of an internal heat exchanger (IHX) is a modification to the basic vapor compression heat pump cycle and is used to increase the performance of the heat pump. This is done by transferring heat via a heat exchanger from the hot working fluid after the condenser stage to the working fluid before entering the compressor. The hot fluid is subcooled, while the cold fluid is superheated. By using an IHX the effective temperature lift that the compressor needs to achieve can be reduced as the temperature of the working fluid in the evaporator can be increased since it no longer needs to account for superheating.

Previous studies have shown that including IHX on HTHPs can have significant effects on the performance, increasing the COP over 10% [31]. However, the effect of IHX depends on the working fluid and operating conditions and should be investigated specifically for each cycle. The downside of the IHX is added complexity and costs.

3.4.4 Expansion Valve

The expansion valve is used to reduce the pressure of the working fluid prior to entering the evaporator.

Different types of expansion valves exist:

- A thermostatic expansion valve TXV is used to control the superheat of the working fluid at the outlet of the compressor. A sensing bulb at the outlet of the evaporator is thermally connected to the valve, and the gas inside the sensing bulb forces the TXV at a certain amount of superheat.
- Electronic expansion valves (EXV) are more sophisticated and accurate compared to TXVs. They can also use pressure and temperature sensors at the outlet of the evaporator as a feedback to regulate the superheat by adjusting the valve opening. Opening itself is driven by electric motors.

Both types can thus be used to regulate the superheat of the working fluid as it exits the evaporator. Another control strategy would be to control the pressure in the condenser or in the evaporator, thus controlling either the high or low pressure of the heat pump cycle.

In practical applications the evaporator and condenser pressure may vary due even though the temperature boundaries i.e. source inlet temperature and sink outlet temperature stay constant. The reason for this is because the temperature difference between the working fluid and HTF can change as the thermal load increases or decreases. It is therefore easier to set up a control strategy based on compressor inlet superheat as this should be set to a constant value.

In terms of temperature ratings, a few valves are limited to temperatures below 200°C. However, there exist commercial suppliers such as Spirax, which delivery pneumatically or electronically controlled valves rated to 300°C.

3.4.5 TRL and Potential Barriers

A summary of the review of heat pump components in the sections above is given in Table 3. It lists the main components of the heat pump, and the expected TRL level of the components based on the available literature from the research on HTHPs and investigations on commercial suppliers. The TRL is set in relation to the definitions by the European commission given in Figure 21. As expected, the compressor is the component with the lowest TRL level, mainly due to challenges related to high temperatures. For the other components, it is expected that fully commercialized systems are available. However, the selection of some technological solutions, such as for the heat exchanger and de-superheater may be at the expense of compactness as the preferred solutions may not be available at sufficient size for a large-scale HTHP system.

Table 3: Summary of expected components TRL level and potential barriers.

Component type	Estimated TRL level	Comments and identified barriers
Compressor	5-7	Turbo compressors: Main challenges are sealing, lubrication oil degradation, and limited ΔT for each compression stage. Lubrication free, direct-drive compression are preferable in terms of reliability, but have a higher cost. Few manufacturers for medium scale and large-scale systems designed for 200°C HTHP. Other Compressor types: Typically limited capacity, due to high specific volumes for steam, With the exception of screw compressors, there is lack of research. Blowers and centrifugal fans can handle high capacities but have a very limited ΔT per compression stage.
Heat exchanger (Evaporator, condenser, IHX)	9	Plate heat exchangers: Potential lack of existing commercial options with sufficient capacity for large-scale systems at required operating temperature and pressure. Shell and tube heat exchangers are possible but requires larger space. Alfa Laval's Compablock heat exchanger is a potential alternative.
De-superheating	7-9	Water atomizing injection systems are fully commercialized but may lack sufficient capacity for large-scale systems. Long stretch of pipes required to evaporate all water droplets, which is space consuming. Open intercooler with packings is very compact, and can handle large capacities, but is not fully commercialized.
Throttle valve	9	Fully commercialized technology for EXVs capable of handling high temperatures exist.
Overall heat pump system	3-4	Limited by the compressor technology. No existing commercial or large-scale pilot steam-based heat pump system using turbo compressors.

Figure 21: Definition of TRL by the European Commission.

4 Reversed Brayton Cycle

4.1 Introduction

The reversed Brayton cycle is used to describe the operation of heat pumps where the working medium is in a gas phase throughout the cycle. Heat is then received and rejected at gliding temperatures, which is an advantage if the external systems transfer heat at gliding temperatures. The working medium temperature glide can be adjusted to match those at the boundary systems to minimize the exergy loss.

The ideal reversed Brayton cycle consists of four processes. Heat is received by the working medium at constant pressure. The working medium is then compressed with constant entropy to the higher temperature. Heat is rejected at the higher temperature at constant pressure before the working medium is expanded with constant entropy to the starting state.

A gas or supercritical fluid is usually used as a working medium in implementations of the reversed Brayton cycle. Heat is transferred to and from the working medium through heat exchangers. Real heat exchangers have associated pressure drops due to fluid dynamic effects. Often there is a trade-off between heat transfer properties and pressure drop performance, as heat transfer and pressure drop usually increase with turbulence formation. There must be a sufficient temperature difference between the working medium and the external heat transfer fluid to drive the heat transfer. There is also a trade-off between heat transfer area and temperature difference performance as a higher area (and therefore also size, cost, pressure drop, etc.) is needed for a smaller temperature difference (higher efficiency). A compressor is used to compress the working medium to increase the temperature. Real compressors have some irreversible losses leading to higher required work input, and therefore higher temperatures, than an isentropic compression between the same pressures. An expander is used to decompress the working medium from the high to low-pressure sides while recovering some of the exergy through work. The expander also has irreversibility associated with it. A real reversed Brayton cycle will therefore operate with lower efficiency than a corresponding ideal reversed Brayton cycle. Schematics of a reversed Brayton heat pump is presented in Figure 22. Schematics of ideal and real cycle temperature-entropy diagrams are presented in Figure 23.

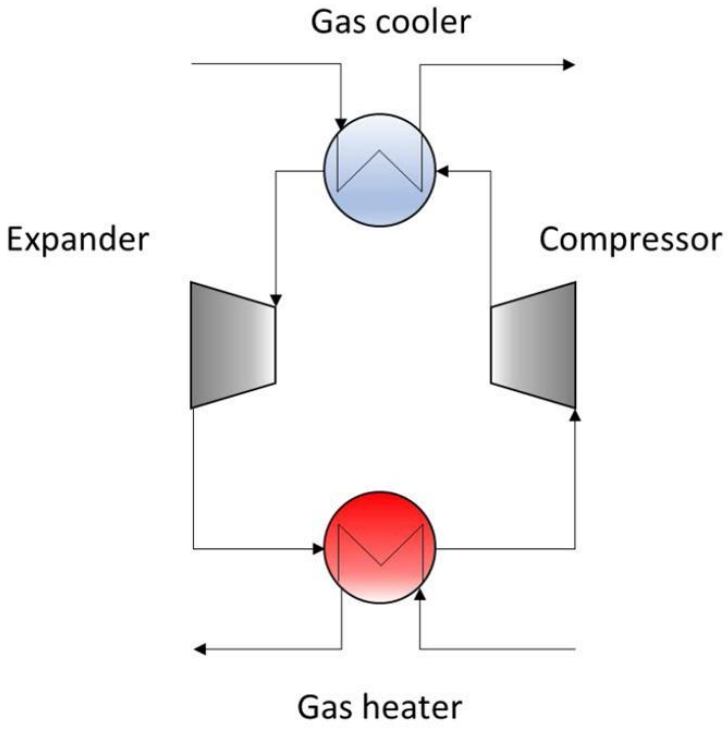

Figure 22: Schematic of basic reversed Brayton heat pump.

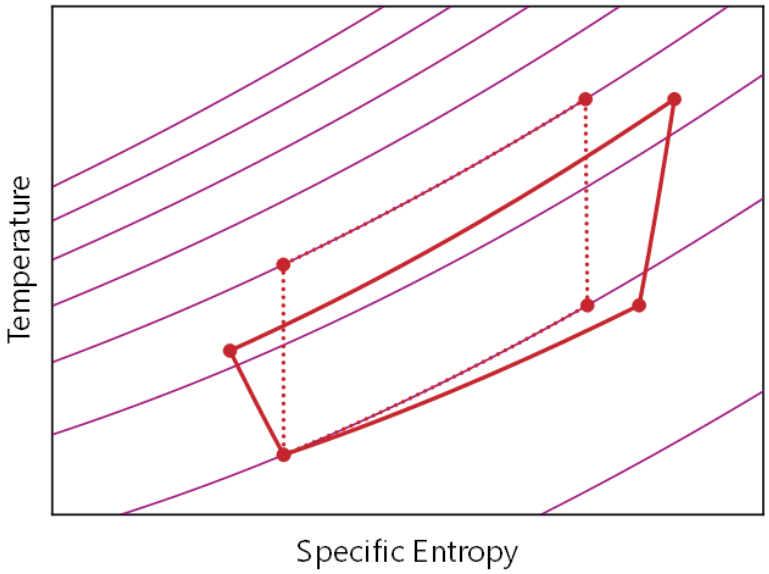

Figure 23: Schematic temperature-entropy diagram of ideal (dotted) and real (solid) reversed Brayton cycle.

4.2 Working Media

Different working media have been proposed for use in high temperature reversed Brayton cycles. A reversed Brayton heat pump with air as the working medium is being developed by DLR with the goal of reaching at least 250°C [32]. MAN Energy solutions has tested a system using CO_2 in a transcritical cycle [33]. Helium has been used in a reversed Brayton cycle cryo-refrigerator with cooling down to a temperature of 20 K [34].

In general, a high volumetric heat capacity is desirable due to associated smaller sizes which in turn carry less cost and potentially less fluid dynamic losses for the same heat delivery.

High specific volume has been found to generate lower turbomachinery losses. Irreversible losses in the compressor have important effects on the system performance [35]. Real gas effects due to intermolecular interactions such as the increased mass density, while keeping sufficient gas-like properties, such as low viscosity, associated with supercritical states could therefore increase the performance of a reversed Brayton heat pump.

Supercritical carbon dioxide (sCO_2) has been proposed as a candidate for use as the working medium in reversed Brayton heat pumps. The supercritical state of carbon dioxide is achieved relatively easily with the critical temperature of 31°C and pressure of 73.8 barA. sCO_2 is also chemically stable, not flammable or toxic, has no ozone depletion potential and relatively low global warming potential.

Due to the harmful effects on the ozone layer and climate of many synthetic refrigerants, natural refrigerants have gained increased attention. Ammonia and hydrocarbons have been investigated as well, although ammonia is toxic and hydrocarbons are flammable. In addition to high cycle coefficient of performance (COP), environmental friendliness, non-toxicity and non-flammability are important selection criteria [2]. A review from 2017 reports renewed interest in CO_2 as the working medium in high-temperature heat pumps and mentions research work on CO_2 heat pumps delivering heat up to 100 °C and that development of heat pumps for higher temperatures would require development of component technology [4].

The highly non-linear thermodynamic properties around the critical point have been proposed to improve the efficiency of a heat pump system. To take advantage of the non-linear behaviour the system must be operated close to the critical point, which is not possible for high-temperature applications. However, the high mass density with low viscosity in the supercritical region can still provide advantages with compact and efficient turbomachinery and heat exchangers for high-temperature heat pumps.

SCO_2 has been studied for use as the working medium in power cycles, e.g. for thermal power plants, to a higher extent than for its use in heat pumps. Figure 24 is copied from [36] and shows a comparison of working media in

a Brayton power cycle. sCO_2 cycles have similar efficiencies as helium cycles for lower temperatures and is less sensitive to penalties from core bypass flows and pressure drops [37]. Several components in a power cycle work in a similar way to those in a heat pump and the comparison between working media in Brayton power cycles could indicate relative suitability between them for their use in a reversed Brayton cycle.

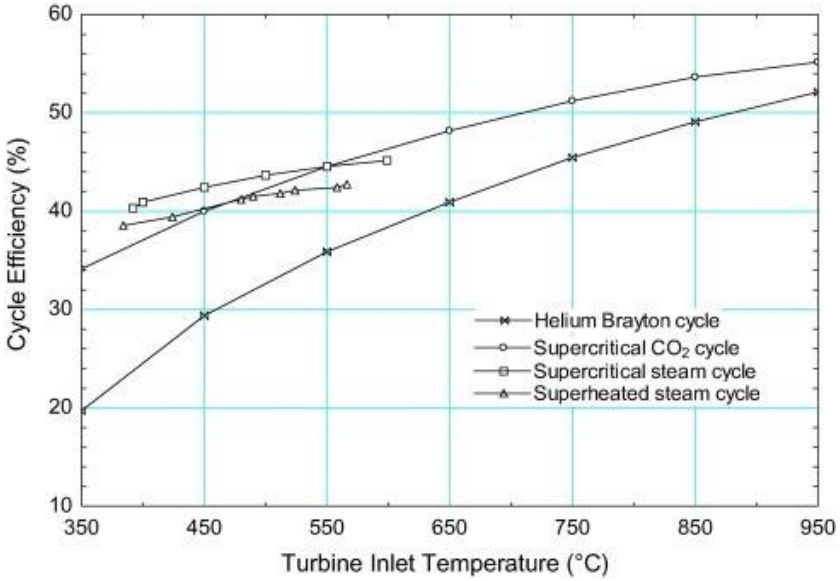

Figure 24: Cycle efficiency in Brayton power cycles with different working media [36].

4.3 Research Projects on the Use of Reversed Brayton Heat Pump Cycle

An sCO_2 heat pump system comprised of commercially available components has been suggested by General Electrics for lifting heat from 60°C to 480°C at 100 MW discharge heat rate. The highest electrical power of CO_2 compressors on the market was reported to be in the range 30-40 MW_e. The COP of the suggested system was estimated to be around 1.3 [12].

A pilot project in Cottbus, Germany is planned by DLR where air is used as the working medium to lift heat from the temperature range 20-100°C to at least 250°C at around 100 kW [32].

The review by White et al. focuses on the current R&D of sCO_2 power cycles, but some of the system components are relevant for a potential reversed Brayton heat pump cycle, such as heat exchangers and turbomachinery [38].

4.4 Cycle Component Design Considerations

4.4.1 Turbomachinery

The high operating pressures and densities in a sCO_2 system allows compact turbomachinery and therefore relatively small system sizes and low cost [38]. Important challenges associated with high-speed turbomachinery for sCO_2 systems are related to fluid dynamic losses. Numerical and experimental research is being done to find optimal designs for various operating conditions.

4.4.1.1 Compressors

For sCO_2 applications, centrifugal compressors have been recommended over axial compressors due to a simpler structure and a relatively high efficiency [37]. For capacities over 100 MW_e axial compressors are recommended [38].

From the cases presented in the review by White et al. compressors for sCO_2 are currently on the stage of theoretical and experimental development at smaller scale, and the TRL can from this be estimated to 4 [38].

Peregrine Turbine Technologies is developing an sCO_2 compressor designed to reach 429 barA with a rotation speed of 118000 rpm [39].

4.4.2 Expanders

Research on expansion devices for sCO_2 is also reported in the review by White et al. In many cases the compressor and expander share a common shaft. The development of expanders is closely related in a power cycle and much of the research is done on the combined turbomachinery. The TRL of sCO_2 expanders can be estimated to be similar to the TRL of sCO_2 compressors [38].

4.4.3 Heat exchangers

Research into the use of sCO_2 as the working medium has involved investigation on suitable heat exchanger designs [38]. Some aspects of heat exchanger design for sCO_2 differ from those for use with steam. E.g., higher mass flow rates are needed for the same heat output which puts stronger constraints on piping length to minimize the pressure drop.

The heat exchanger type that best fits the application depends on the operational conditions. An sCO_2 reversed Brayton cycle typically involves high pressures which puts constraints on the possible heat exchanger types.

Printed circuit heat exchangers (PCHEs) have been suggested as suitable with sCO_2 [40]. PCHEs are made up of a stack of relatively thin metal sheets where the channels are formed through photochemical machining of each plate before being stacked and bonded through diffusion welding. The channels can have different layouts and straight channels, zigzag, and s-shapes are among layouts that have been investigated. The cross section of each channel is often semi-circular. For counterflow arrangements, hot and cold fluid flow in opposite directions in alternating layers of channels.

Typical hydraulic diameter and distance between channel walls are on the order of 1 mm. PCHEs can therefore be made relatively compact. PCHEs are also relatively robust and can be used under high pressures and temperatures, which make them suited for sCO_2. There exist PCHEs able to operate at pressures up to at least 500 barA and 800°C [41]. With zig-zag channels, a compactness of 1050 m^2/m^3 has been achieved experimentally with a power density up to 4.4 MW/m^3 [40]. From these numbers, a required heat transfer area could be expected to be at minimum 240 m^2/MW.

One drawback with PCHEs is that the channels are inaccessible for maintenance. Another drawback is the relatively high cost, up to 90% percent of the cost of an sCO_2 reversed Brayton cycle could be associated with heat exchangers if PCHEs are used [38].

Further development is needed for heat exchangers operating with sCO_2 at pressures over 200 barA [40]. However, PCHEs have been reported to be able to operate at much higher pressures by other authors. Since Chai and Tassou reports on the use of sCO_2, a conservative TRL estimate could be reasonable. For this project the TRL of heat exchangers were set to 4.

4.4.4 Estimation of TRL

Table 4: Estimated components and systems TRL and main challenges.

Component	Estimated TRL	Main challenges
Compressor	4	High pressure and temperature demands. No commercially available options for required pressures. Potential candidate under development by Peregrine Turbine Technologies. Efficiency challenges with fluid-dynamic losses for high-speed compressors.
Expander	4	Similar challenges and development status as with compressors. Often research in combined system.
Heat exchanger	4	Commercial PCHEs exist but further development is needed for operation at required pressures.
Overall system	2-3	All major components, except gas heater, need further development to meet pressure requirements.

5 Evaluation of heat pump concepts and system integration

5.1 Boundary conditions

Table 5 lists the boundary conditions and other relevant input/output parameters that will be used in the concept evaluations and Modelica simulations. The parameters have been obtained through a review of previous FRIENDSHIP deliverables D1.1, D1.2 and D1.3, as well as through meetings with project partners Absolicon and CEA.

Table 5: Heat pump boundary conditions and input / output parameters

Component/ Property	Input/ Output	Heat pump concepts		Comments	Ref
		Steam heat pump	Reversed Brayton heat pump		
Evaporator / Gas heater					
HTF Maximum inlet temperature	Input	160°C	160°C	Can be assumed constant under all conditions	[42]
HTF expected outlet temperature	Input	140°C	140°C	Can be assumed constant under all conditions	[43]
HTF type	Input	Therminol 66	Therminol66	For conceptual evaluations and Modelica simulations therminol66 is utilized, which offer similar properties as Wacker Helisol, which is the proposed HTF on both the source and sink side of the heat pump	
HTF and working fluid heat transfer coefficients (alpha)	Output	-	-	Calculated in Modelica simulations. In concept evaluations a minimum ΔT of 10K is assumed.	
HTF Operating fluid pressure	Input	10 barA	10 barA		[42]
Working fluid target evaporation temperature / gas heater outlet temperature	Input	130°C	150°C	Based on minimum ΔT of 10K between hot and cold fluid in heat exchanger	
heat exchanger Pressure drop	Output	-	-	To be calculated as one of the output properties defined in D1.2	[42]
Required heat exchange area	Output	-	-	To be calculated as one of the output properties defined in D1.2	[42]
Turbo compressor					
Superheat prior to inlet	Input	10K	n/a	Based on typical values from the literature and experimental results from of SINTEFs turbo compressor test rig	[20], [17]
isentropic efficiency	Input	0.75	0.75	Based on achievable efficiencies for steam-based turbo compressors, and compressors for reversed Brayton heat pumps based on CO_2. In the concept evaluations the sensitivity from varying the isentropic efficiency will be investigated. In Modelica simulations an isentropic efficiency of 0.75 is specified at design point, however lower values will occur when the heat pump is operating outside design conditions	[20], [11], [44]
Compression power	Output	-	-	To be calculated as one of the output properties defined in D1.2	[42]
Compressor outlet temperature	Output	-	-	To be calculated as one of the output properties defined in D1.2	[42]
Compressor outlet pressure	Output	-	-	To be calculated as one of the output properties defined in D1.2	[42]
De-superheater					
Required de-superheating flow rate	Output	-	-	To be calculated as one of the output properties defined in D1.2	[42]
Condenser / Gas cooler					
Heat pump condensing temperature / maximum cycle temperature	Input	200°C	250°C	Based on target temperatures defined in Grant Agreement	
HTF fluid outlet target temperature	Input	190°C	240°C	Based on target condensing temperature / maximum cycle temperature – minus minimum ΔT of 10K between hot and cold fluid in heat exchanger	

HTF fluid inlet temperature	Input	160°C	160°C	Nominal temperature is 160°C. However, temperature variations between 140 and 170°C can be expected during charging. Effect of varying temperatures is investigated in concept evaluations and Modelica simulations.	
heat exchanger Pressure drop	Output	-	-	To be calculated as one of the output properties defined in D1.2	[42]
Required heat exchange area	Output	-	-	To be calculated as one of the output properties defined in D1.2	[42]
HTF type	Input	Therminol 66	Therminol66	For conceptual evaluations and Modelica simulations therminol66 is utilized, which offer similar properties as Wacker Helisol, which is the proposed HTF on both the source and sink side of the heat pump	
HTF Operating fluid pressure	Input	5 barA	5 barA	Based on discussions with Absolicon and CEA	
Nominal Steam supply pressure	Input	4.9 barA	n/a	Based on operating conditions for the Gendorf plant. Relevant for Open cycle heat pump. Sensitivity analysis for different pressure levels will be performed in the concept evaluations	[42]
Expander					
isentropic efficiency	Input	N/A	0.75	Assume same isentropic efficiency as compressor	
Thermal capacity					
Full-scale system	Input	12 MW	12 MW	Based on Full-scale heat pump system as defined in D1.2	[42]

5.2 Steam Heat pump Concepts for Short Term 200°C Heat Delivery for SHIP200

5.2.1 Open vs Closed Cycle Steam Heat Pump Systems for SHIP200

In D1.3 - Test plan and validation methods for all components or subsystems and global SHIP 200&SHIP 300, two different heat pump concepts were proposed; a closed cycle heat pump, illustrated in Figure 25, and an open-cycle heat pump, illustrated in Figure 26. These heat pump concepts were listed in the appendix as figured in the SHIP200 PID options 1 and 6, respectively [43].

The closed cycle heat pump is the base concept, as it is the most flexible in terms of integration with the other parts of the heat generation process and be used for any type of heat generation. Most emphasis has therefore been put on that concept in this report. However, the open cycle concept has its advantageous in certain scenarios, such as when heating is used to produce steam. A heat pump using steam as a working fluid can then be opened up to deliver steam directly to the process, without having to go through two steps of heat exchange through a condenser and in a combined heat storage, both causing a certain amount of temperature loss at each stage. Hence, it can then provide a more energy-efficient production of steam for process heating. Both the open-cycle and closed cycle concepts will be described and evaluated more in depth in this chapter.

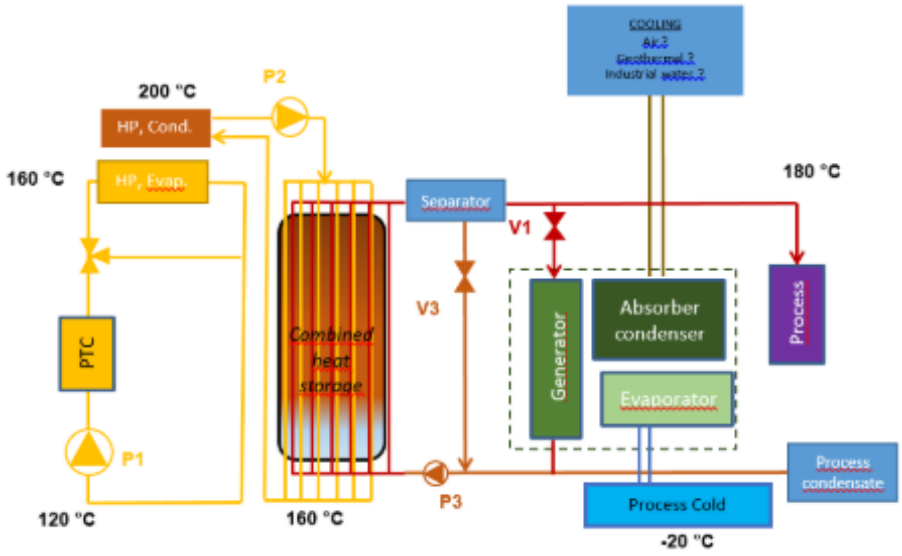

Figure 25: Closed cycle heat pump concept in SHIP200.

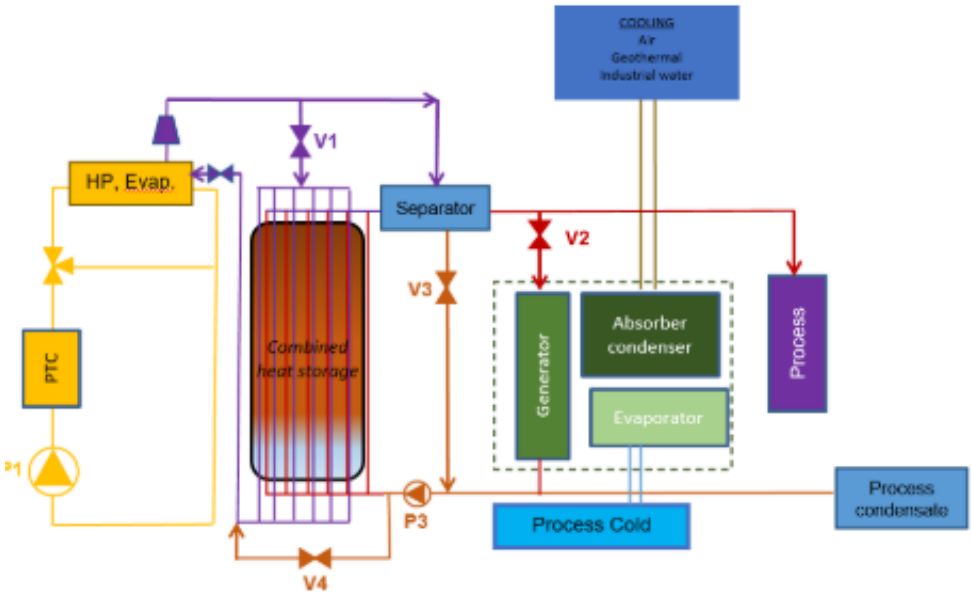

Figure 26: Open cycle heat pump in SHIP200.

5.3 Closed Cycle Steam Heat Pump

The closed cycle steam heat pump is the main heat pump concept in the SHIP200 system design. In this heating system solar heat is upgraded using a closed cycle heat pump, consisting of an evaporator, three-stage compression with intermediate de-superheating, a condenser and a throttling valve. The base concept is illustrated the top left corner of Figure 28. Within the main concept, a variation of concepts, four in total, will be evaluated to find a suitable concept that fits to the SHIP200 system.

Table 6 lists the boundary conditions and the input parameters that will be used in all concept evaluations. The parameter values are based on [42], [43] and meetings with the project partners. The heat is transferred to the heat pump via the HTF in the solar loop. The HTF enters the evaporator at 160°C and leaves at 140°C. The pressure is 10 barA. The heat is transferred to the combined heat and storage via the HTF on the sink side in the condenser. The HTF enters the condenser between 140 and 170°C, with 160°C being the nominal temperature. It leaves at approximately 190°C. Depending on the specified minimum temperature difference in the heat exchanger this temperature may be increased. However, for the purpose of simplicity, the minimum temperature difference between the hot and cold fluid in all heat exchangers is set to 10K.

With an outlet temperature of 140°C for the HTF in the evaporator, the evaporation temperature of the working fluid becomes 130°C, which corresponds to 2.7 barA. The aimed condensation temperature is 200°C, which corresponds to 15.5 barA. This gives a total cycle pressure ratio of 5.55. Based on what typically can be achieved for turbo compressors and previous test results [20], the most feasible solution is to use three compression stages which, given equal pressure ratios, results in a pressure ratio of 1.79 for each stage.

Table 6: Parameters used in the closed-cycle heat pump evaluations.

Parameter	Temperature
Steam condensation conditions	15.5 barA, 200°C
Steam evaporation conditions	2.7 barA, 130°C
HTF fluid evaporator inlet	10 barA, 160°C
HTF fluid evaporator outlet	10 barA, 140°C
HTF fluid condenser inlet	5 barA, 140-170°C
Minimum compressor superheat	10°C
Minimum ΔT in heat exchanger	10°C
Heat delivery	12 MW

From the results on the evaluations of the heat transfer fluid by CEA in WP5 and Absolicon in WP2, the most promising fluid appears to be Wacker Helisol. However, Wacker Helisol is not readily available in the TLK fluid library which will be used for the Modelica simulations of the heat pump concepts.

It was therefore investigated to use a replacement fluid for Wacker Helisol, which possessed similar properties such as density, heat capacity, dynamic viscosity and thermal conductivity. This resulted in the selection of Therminol66 as the replacement fluid. Its properties at 10 barA, 140-160°C are listed in Figure 27.

For the sake of the initial concept evaluations of the closed-cycle heat pump, which have been conducted using a specified minimum ΔT in the heat exchanger, relevant HTF properties are density and heat capacity as this will provide estimations of the HTF flow rates.

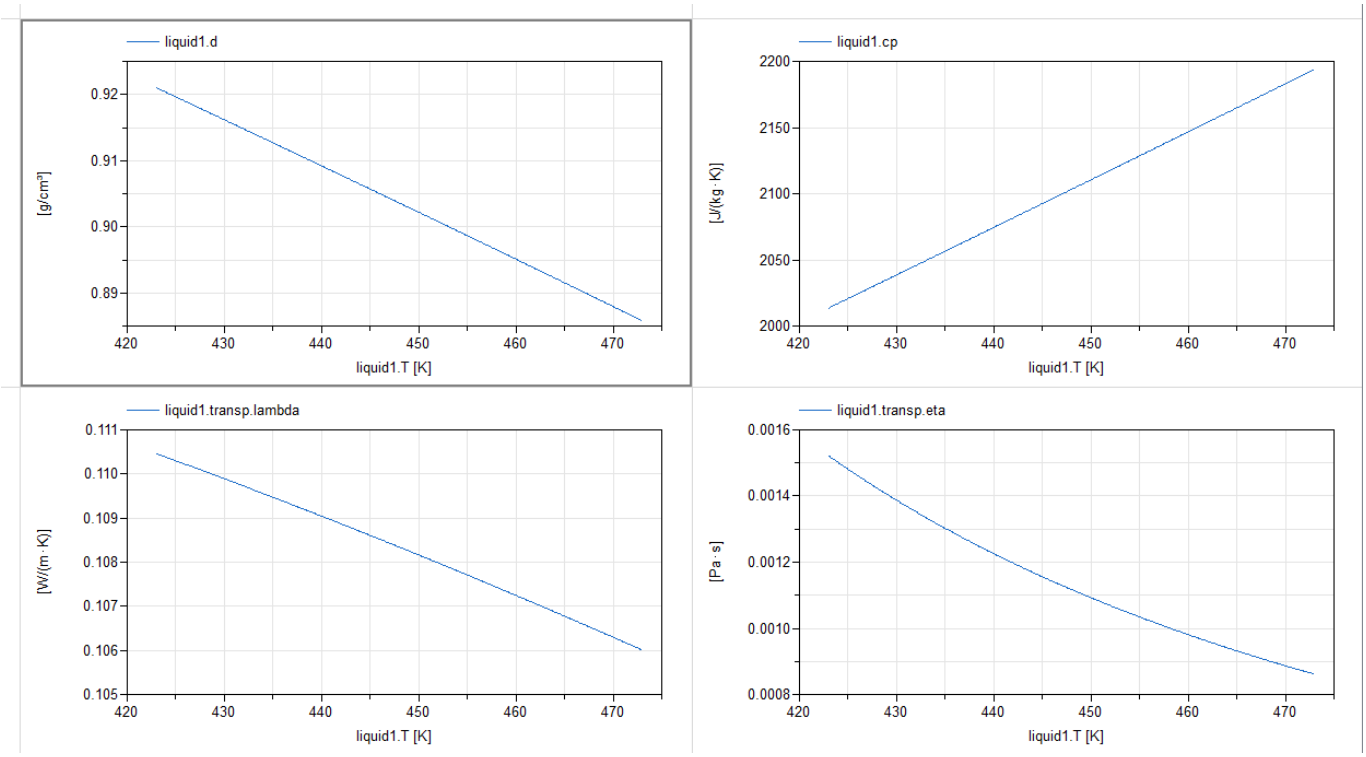

Figure 27: properties of Therminol66 at 10 barA and 140-200°C, top left: density, top right: heat capacity, bottom left: thermal conductivity, bottom right dynamic viscosity.

5.3.1 Concept Descriptions

An evaluation of four different closed cycle heat pumps concepts has been made. The concepts are based on the parameters listed Table 6, and are evaluated according to both performance and sizing.

These four main concepts for the closed-cycle steam heat pump have been evaluated:

1. Concept 1: Base case
2. Concept 2: Subcooling (SC)
3. Concept 3: De-superheater (DSH) after 3rd compressor stage
4. Concept 4: Internal heat exchanger (IHX)

The concepts are similar in terms of cycle evaporation and condensation pressures and temperatures, as the boundary conditions are similar for each concept. However, the concepts differ in terms of offering different solutions for heat exchange, superheating and de-superheating of the working fluid.

Concept 1 is illustrated in the top left corner of Figure 28. In this concept the steam is compressed in three turbo compressors with intermediate de-superheating after each stage. De-superheating is performed by pumping a fraction of the liquid after the expansion valve and spraying it back into the cycle after the first and second compression stage. After the last compressor stage de-superheating of the working fluid is performed in the condenser in addition to condensation at 200°C and 15.5 barA through heat exchange with the HTF, bringing the working fluid to saturated water conditions.

In the expansion valve, the working fluid undergoes isenthalpic expansion reducing its pressure back to 2.7 barA. Finally, in the evaporator the working fluid is evaporated by heat transferred from the PTCs to the working fluid via the HTF. The necessary heat required to superheat the working fluid by 10K prior to the inlet of the first compressor stage is also transferred in the evaporator.

Concept 2 is illustrated in the top right corner of Figure 28. This concept is almost similar to concept 1. However, here the working fluid is subcooled in the condenser past its saturation point to a minimum of 10K above the inlet temperature of the HTF. When the inlet temperature of the HTF in the condenser is significantly below the condensation temperature, subcooling can be employed to increase the amount of heat transferred to the sink and improve the COP. Since the HTF fluid inlet temperature varies from 140°C to 170°C, it means that with a 10K minimum temperature difference, subcooling the working fluid by 20-50K is possible.

Concept 3 is illustrated in the bottom left corner of Figure 28. This concept employs the subcooling from concept 2 and an additional de-superheater is employed after the third compression stage. The addition of a superheater will limit the steam inlet temperature in the condenser to 200°C. Although an additional de-superheater is used, this concept could be beneficial from a cost point of view since it reduces the required temperature rating of the condenser, and could potentially reduce overall costs as gasketed plate heat exchangers may be used. It may also reduce the overall heat transfer area in the condenser since it does not need to de-superheat steam, which gives a relatively low heat transfer coefficient compared to steam condensation.

Concept 4 is illustrated in the bottom right corner of Figure 28. This concept differs the most from the other concepts as an internal heat exchanger is used to provide the required superheating prior to the inlet of the first compressor stage, which can economize the cycle and improve the COP, especially if it allows the working fluid to evaporate at a higher pressure and temperature. This concept also includes subcooling from concept 2.

The working principle is as follows: after the condenser, the working fluid is subcooled and flows to the internal heat exchanger (IHX) where it transfers heat to the working fluid in the low-pressure side of the cycle prior to the inlet of the first stage compressor. A downside of the IHX, in addition to added cost and complexity is that it could reduce the amount of subcooling and thereby reduce the heat rate in the condenser.

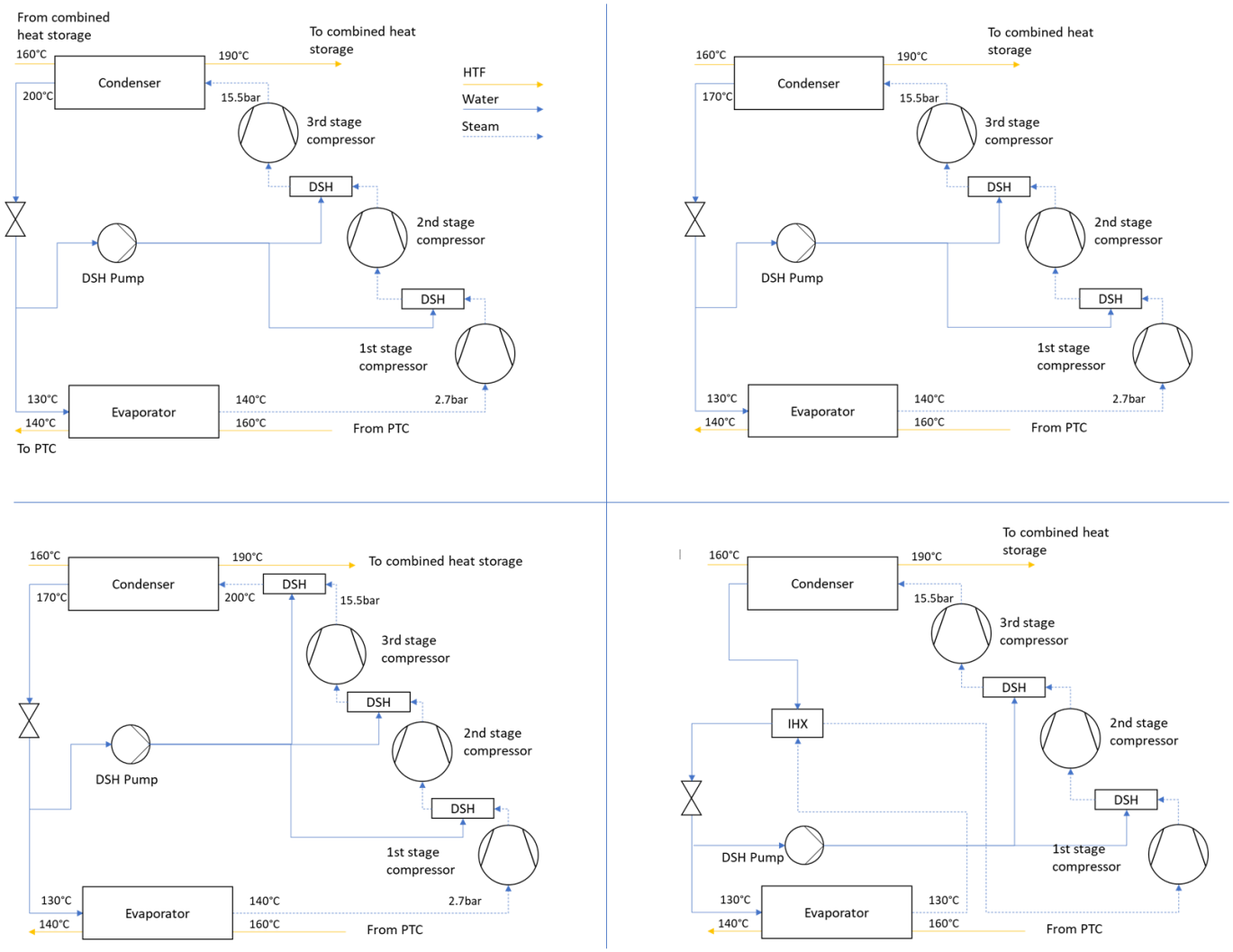

Figure 28: Top left corner: Concept 1, Top right corner: Concept 2, Bottom left corner: Concept 3, Bottom right corner: Concept 4.

5.3.2 Results and Discussion

The COP values for the four concepts are given in Figure 29, which shows how the COP values change for varying heat sink HTF inlet temperatures.

The best COP values are achieved with concept 3 (COP: 4.98, η_{Carnot}: 34.4%), followed by concepts 2 and 4, which obtain equal COP values. Concept 1, the base case, performs the worst. However, the differences between the concepts in terms of COP is rather small. With a nominal HTF condenser inlet temperature of 160°C, the drop in COP is only 6% from concept 3 to concept 1. The variations in the Carnot efficiency ranges from 34%-40%. Compared typical Carnot efficiencies achieved by industrial heat pumps, these values are on the lower end. The main reason for this is the large temperature glide, especially on the source side, which effectively increases the required temperature lift by 30K.

The main contribution to the increased performance from the base case is due to the addition of subcooling (SC), which is employed in concepts 2,3 and 4. This effectively increases the specific heat output for the heat pump, and allows for the heat pump to deliver the same amount of heat, but with a reduced working fluid flow rate, which then leads to reduced compressor work.

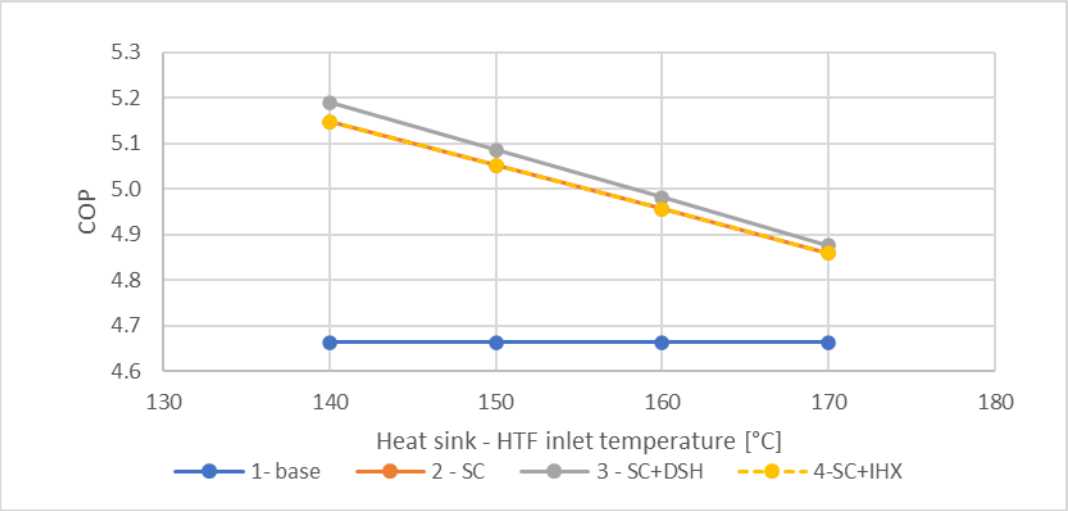

Figure 29: COP vs HTF inlet temperatures for the different concepts.

For concept 3, the employment of a de-superheating stage after the last compressor stage allows for slightly reduced mass flow through the compressors, leading to reduced compressor work. Injection of water leads to the working fluid entering the condenser at saturation conditions, 200°C. For the other concepts, the steam enters the condenser in a superheated state at 267°C, potentially allowing for significantly higher HTF outlet temperatures.

However, it is not possible to utilize the increased inlet temperature to further heat the HTF to temperatures far beyond 190°C, as this is limited by the pinch point that occurs when the steam reaches saturated conditions. This problem is illustrated in Figure 30, which shows the temperature-heat flow diagrams for the heat pump concepts. In the top diagram, which is from concept 1 there is a clear pinch point in the condenser, while in the bottom diagram, which is from concept 3, there is no such pinch point, and the smallest temperature difference occurs at the outlet. As seen in Figure 31 the reduction in the HTF outlet temperature from the condenser in concept 3 compared to the other concepts is only between 1.5-4°C.

Concepts 2 and 4 achieve equal COP values for all temperature glides. Concept 4 includes an internal heat exchanger (IHX), which is used to provide the required superheating before the first compression stage. The superheat was kept at 10°C. Even if it could be raised with IHX, initial evaluations showed that it was beneficial to minimize the amount of superheat into the first compressor stage as this reduces compressor work.

Using IHX will in many cases contribute to increasing the COP because the evaporator pressure can be raised, which leads to lower overall compressor pressure ratio. However, in this case the PTCs heat the HTF from 140°C to 160°C, which means that the highest evaporator temperature possible is 130°C, given a minimum temperature difference of 10K between the HTF and the working fluid. If the temperature glide of the HTF was small, e.g. only 5°C (150-145°C), the evaporation temperature could be increased from 130°C to 135°C.

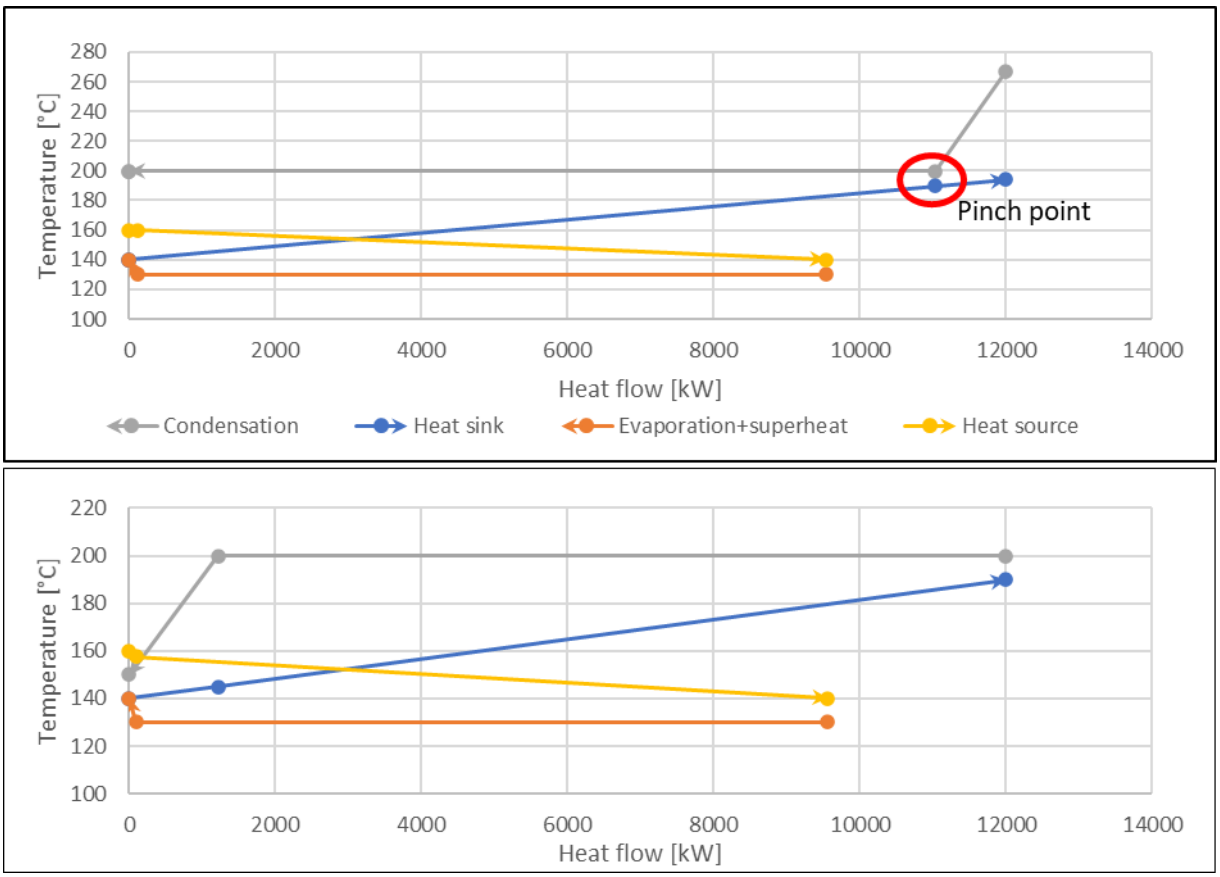

Figure 30: Temperature - heat flow diagram: Top - Concept 1 -base , bottom: Concept 3 SC+DSH.

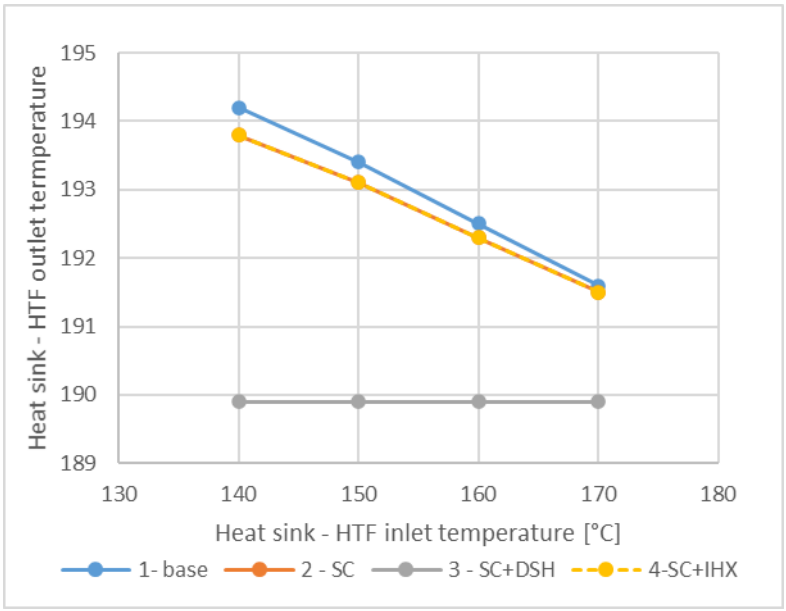

Figure 31: HTF outlet and inlet temperature in the condenser for the different concepts.

5.3.2.1 Compressor

Figure 32 shows the total compressor power consumption for the various cases on the left side, while the suction volume flow for each compressor stage is shown on the right side for all four concepts at all HTF condenser inlet temperatures. The power consumption naturally follows the opposite trend compared to the COP values in Figure

29 since the heat rate is constant at 12 MW. The compressor suction volume flow is important as it is one of the main parameters for sizing of the compressor. The volumetric flow rates at an HTF inlet condenser temperature of 160°C are 11675, 7160 and 400 m^3/h for stage 1, 2 and 3, respectively, which all are at the lower end of the value ranges in the graph.

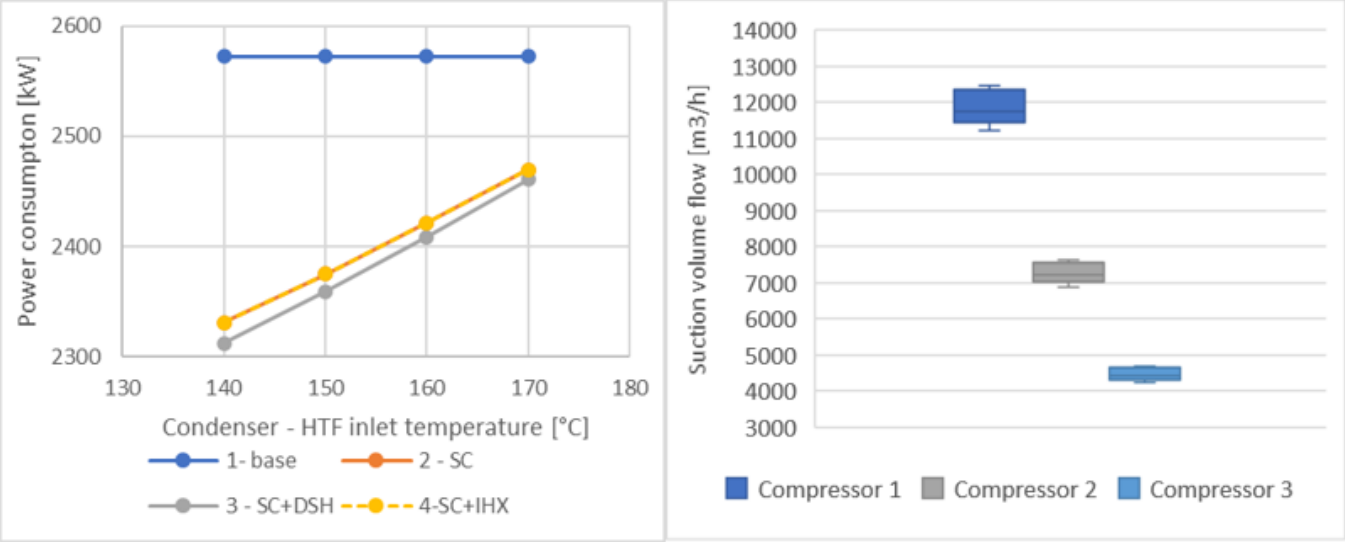

Figure 32: Left graph: Compressor power consumption, Right graph: compressor suction volume flow.

5.3.2.2 Heat Exchanger Area Calculations

In order to get an indication of the size of the heat exchanger, the heat transfer area has been calculated for the different concepts.

The area is calculated based on the following equation:

$$\dot{Q} = UA * LMTD$$

$\dot{Q}$: Heat load

U: Overall heat transfer coefficient

LMTD: Logarithmic mean temperature difference

The heat load is known, as this is specified to 12 MW for a large-scale industrial system. The U-value is calculated based on the equation below, which is suitable for plate heat exchangers, using typical fluid film heat transfer coefficients, given in Table 7.

$$\frac{1}{U} = \frac{1}{h_{hot}} + \frac{1}{h_{cold}} + \frac{\delta}{\mathrm{k}}$$

The plate thickness, δ, is based on the gasketed plate thickness from Alfa Laval, while the plate conductivity is based on typical value for stainless steel, which is lower than aluminium, but typical for plate heat exchangers designed for high temperatures and pressures.

The resulting U-values are given as a minimum, maximum and average values in Table 9. In the heat exchanger area calculations, the average values have been used. In order to calculate the area more accurately the evaporation, condensation, subcooling, and superheating/de-superheating processes have been separated as these will result in different U-values.

Table 7: typical film heat transfer coefficients [26].

Fluid	Film heat transfer coefficient [W/m²K]
Liquid – no phase change (Water)	2000-6000
Gas – no phase change	10-500
Evaporation (Water)	2000-10000
Condensation (Steam)	5000-15000

Table 8: Plate heat exchanger properties.

Property	Value
Plate thickness, δ	0.4 mm [45]
Plate conductivity, k (stainless steel)	15 W/mK [46]

Table 9: Calculated U-values based on film heat transfer coefficients and plate heat exchanger properties.

Heat exchanger	Hot fluid type/process	Cold fluid type/process	Calculated U value [W/m²K]		
			Min	Max	Average
Evaporator	Liquid	Evaporation	1000	3400	2200
Condenser	Condensation	Liquid	1400	3800	2600
Subcooler	Liquid	Liquid	1000	2800	1900
De-superheater	Gas	Liquid	10	450	260
IHX/Superheater	Liquid	Gas	10	450	260

The results from the area calculations are shown in Figure 33 for the heat sink side and in Figure 34 for the heat source side.

The largest area variations are found on the heat sink side. Here, depending on the concept choice the processes of subcooling, condensation and de-superheating occur in the condenser. The process of condensation requires the largest amount of heat transfer area. However, due to the low U-value for the process of de-superheating, this process requires a relatively high transfer area compared to the amount of heat transfer. For this reason, the calculated area for concept 3 is significantly lower than for the other concepts since de-superheating is handled by water injection outside the condenser. With an HTF inlet temperature of 160°C, the calculated heat transfer area is 226m^2.

The results also show that the heat exchanger area is dependent on the HTF inlet temperature, and increases for increasing HTF inlet temperatures due to reduction in LMTD. The process of subcooling requires a very small heat transfer area.

For concept 4 additional heat exchanger area is required to perform the internal heat exchange to superheat the steam prior to first stage compression.

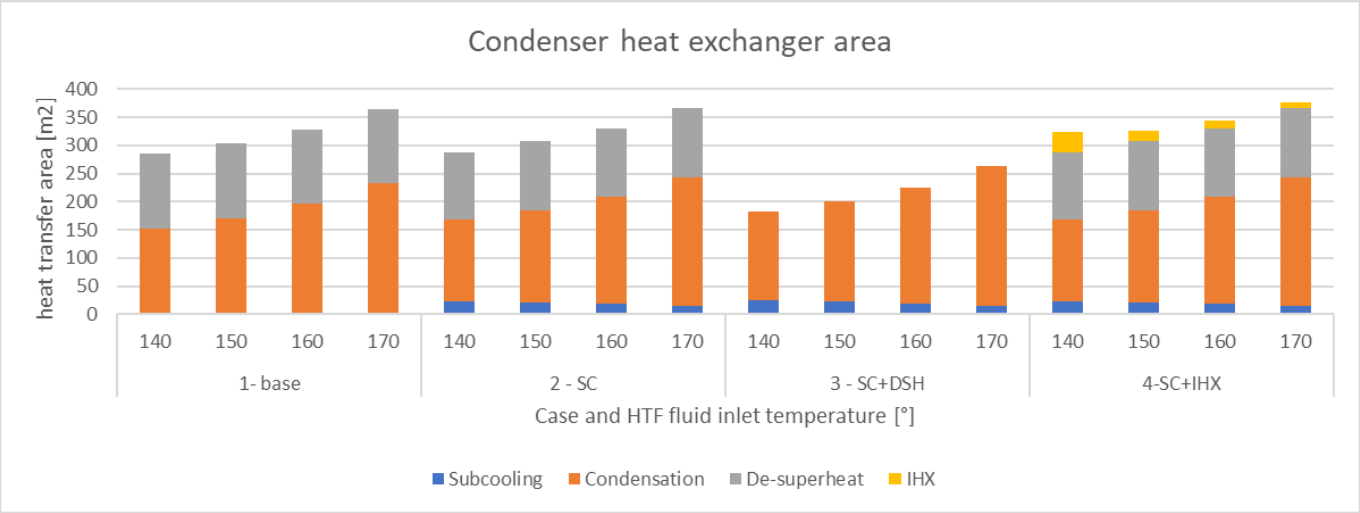

Figure 33: Condenser heat exchanger area.

There were very small variations between the concepts for the calculated heat transfer area on the heat source side. Here, the processes of evaporation and superheating occurs in the evaporator. The total calculated heat transfer area was around 225m^2. For concept 4 the superheating is handled by the internal heat exchanger.

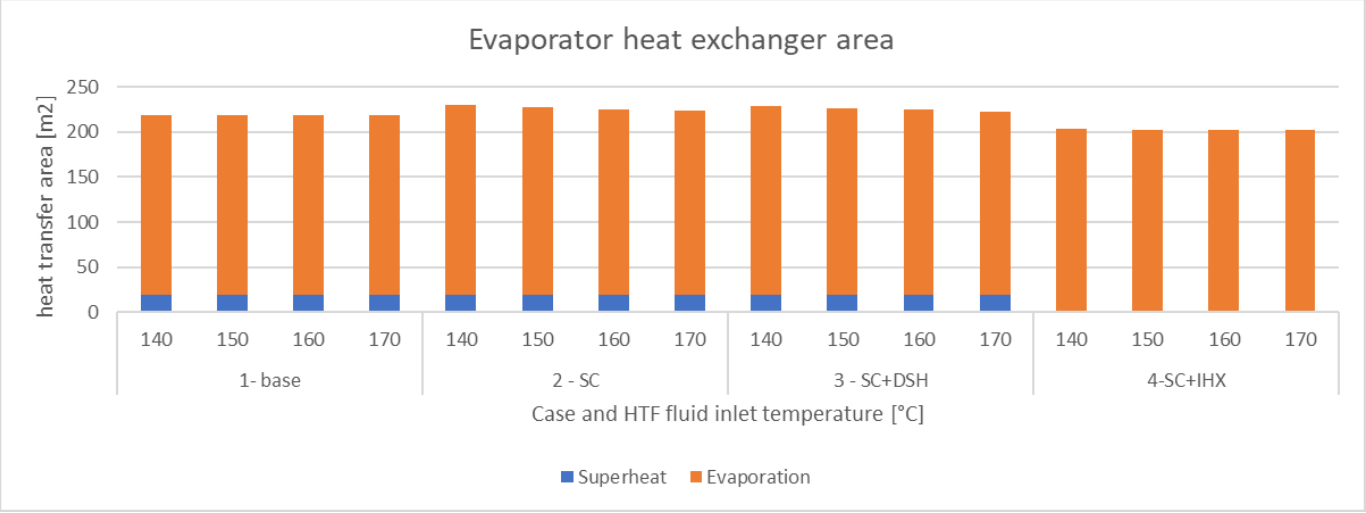

Figure 34: Evaporator heat exchanger area.

5.3.2.3 Summary of Main Results

The temperatures and pressures at all cycle points for all concepts are shown in Figure 35 and Figure 36, respectively.

The best performing concept was concept 3, which uses subcooling and de-superheating with water injection after the last compression stage. Tables 10, 11 and 12 summarize the main results for this concept based on different thermal capacity for the heat pump:

- Table 10: Summary of results for large-scale system - 12 MW capacity
- Table 11: Summary of results for small-scale system – 500 kW capacity
- Table 12: Summary of results for SHIP200 lab-scale system (Grenoble) – 110 kW capacity.

The 110 kW capacity for the SHIP200-scale system is based on estimation from deliverable D3.1, which showed that it would be useful to utilize up to 90 kW from the PTCs solar field based on seasonal variations [43]. With an added 20 kW of electrical input from the compressors, the heat pump would be capable of delivering 110 kW.

More in-depth evaluations of concept 3 are performed using Modelica and are described in chapter 6.1.

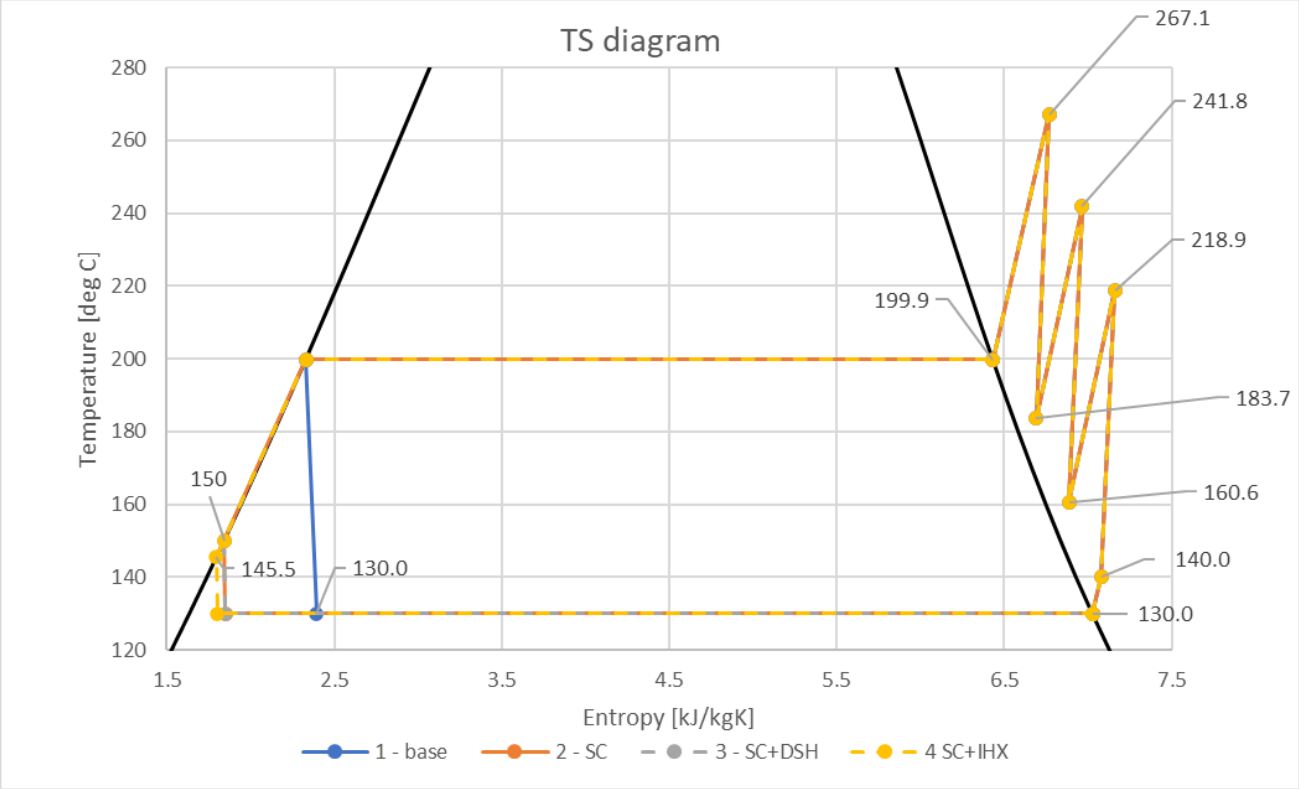

Figure 35: Temperature-entropy diagram for all 4 concepts for the case with heat sink inlet temperature of 140°C.

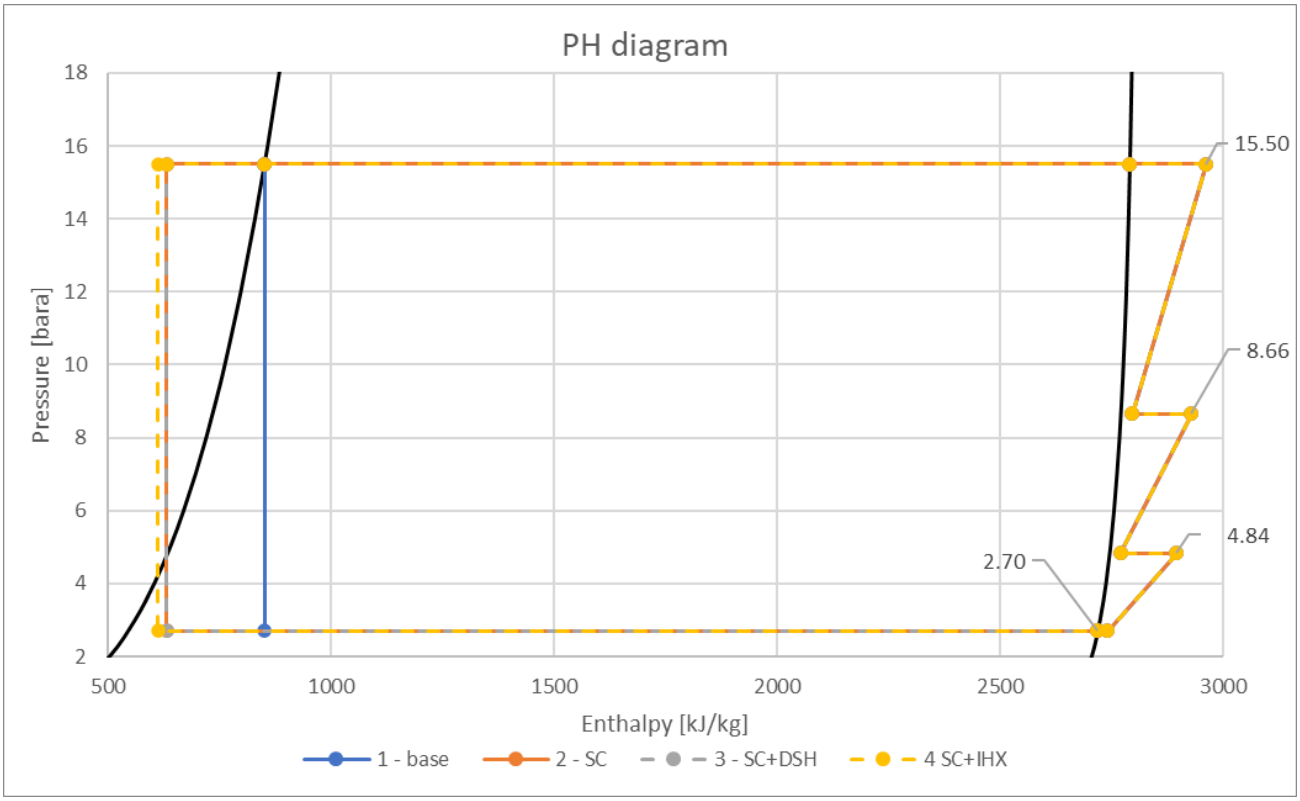

Figure 36: Pressure-enthalpy diagram for all 4 concepts for the case with heat sink inlet temperature of 140°C.

Table 10: Summary of the main parameters of the best performing concept for a large-scale heat pump system with a thermal capacity of 12 MW.

	Condenser: HTF inlet temperature [°C]			
Parameter	**140**	**150**	**160**	**170**
Condenser:				
HTF mass flow [kg/s]	110	137	183	275
Working fluid mass flow [kg/s]	5.6	5.7	5.8	5.9
Total heat transfer area [m^2]	182	200	226	263
Evaporator:				
HTF mass flow [kg/s]	233	233	233	233
Working fluid mass flow [kg/s]	4.5	4.6	4.7	4.8
Total heat transfer area [m^2]	229	227	225	223
Heat transfer from PTC [kW]	9558	9553	9548	9543
1st stage Compressor:				
Power [kW]	700	715	729	745
Volumetric flow rate, inlet [m3/h]	11207	11436	11675	11927
2nd stage Compressor:				
Power [kW]	768	784	800	817
Volumetric flow rate, inlet [m3/h]	6873	7013	7160	7315
3rd stage Compressor:				
Power [kW]	844	861	879	898
Volumetric flow rate, inlet [m3/h]	4223	4309	4400	4495
Total compressor power [kW]	2312	2359	2409	2461
De-superheating:				
1st stage water injection flow rate [kg/s]	0.27	0.27	0.28	0.29
2nd stage water injection flow rate [kg/s]	0.31	0.32	0.32	0.33
3rd stage water injection flow rate [kg/s]	0.45	0.46	0.47	0.48
Total injection flow rate [kg/s]	1.03	1.05	1.07	1.09

Table 11: Summary of the main parameters of the best performing concept for a small- scale heat pump system with a thermal capacity of 500 kW.

	Condenser: HTF inlet temperature [°C]			
Parameter	**140**	**150**	**160**	**170**
Condenser:				
HTF mass flow [kg/s]	5	6	8	11
Working fluid mass flow [kg/s]	0.23	0.24	0.24	0.25
Total heat transfer area [m^2]	8	8	9	11
Evaporator:				
HTF mass flow [kg/s]	10	10	10	10
Working fluid mass flow [kg/s]	0.189	0.193	0.197	0.201
Total heat transfer area [m^2]	10	9	9	9
Heat transfer from PTC [kW]	398	398	398	398
1st stage Compressor:				
Power [kW]	29	30	30	31
Volumetric flow rate, inlet [m3/h]	467	476	486	497
2nd stage Compressor:				
Power [kW]	32	33	33	34
Volumetric flow rate, inlet [m3/h]	286	292	298	305
3rd stage Compressor:				
Power [kW]	35	36	37	37
Volumetric flow rate, inlet [m3/h]	176	180	183	187
Total compressor power [kW]	96	98	100	103
De-superheating:				
1st stage water injection flow rate [kg/s]	0.0112	0.0114	0.0117	0.0119
2nd stage water injection flow rate [kg/s]	0.0129	0.0132	0.0135	0.0137
3rd stage water injection flow rate [kg/s]	0.0187	0.0191	0.0195	0.0199
Total injection flow rate [kg/s]	0.0428	0.0437	0.0446	0.0455

Table 12: Summary of the main parameters of the best performing concept for a SHIP200 lab-scale heat pump system with a thermal capacity of 110 kW.

	Condenser: HTF inlet temperature [°C]			
Parameter	**140**	**150**	**160**	**170**
Condenser:				
HTF mass flow [kg/s]	1.00	1.26	1.68	2.52
Working fluid mass flow [kg/s]	0.05	0.05	0.05	0.05
Total heat transfer area [m^2]	1.67	1.84	2.07	2.41
Evaporator:				
HTF mass flow [kg/s]	2.14	2.14	2.13	2.13
Working fluid mass flow [kg/s]	0.042	0.042	0.043	0.044
Total heat transfer area [m^2]	2	2	2	2
Heat transfer from PTC [kW]	88	88	88	87
1st stage Compressor:				
Power [kW]	6.42	6.55	6.69	6.83
Volumetric flow rate, inlet [m3/h]	103	105	107	109
2nd stage Compressor:				
Power [kW]	7.040	7.184	7.335	7.493
Volumetric flow rate, inlet [m3/h]	63	64	66	67
3rd stage Compressor:				
Power [kW]	7.74	7.89	8.06	8.23
Volumetric flow rate, inlet [m3/h]	39	40	40	41
Total compressor power [kW]	21.19	21.63	22.08	22.56
De-superheating:				
1st stage water injection flow rate [kg/s]	0.0025	0.0025	0.0026	0.0026
2nd stage water injection flow rate [kg/s]	0.0028	0.0029	0.0030	0.0030
3rd stage water injection flow rate [kg/s]	0.0041	0.0042	0.0043	0.0044
Total injection flow rate [kg/s]	0.0094	0.0096	0.0098	0.0100

5.3.3 Cost and Size Analysis

As costs are one of the main barriers for widespread industrial high temperature heat pump implementation, it is important to evaluate the potential for the implementation of heat pumps on an industrial scale from an economic point of view.

In economic evaluations of heat pumps two terms are often discussed. The first is the levelized cost of heat, which is expressed in €/MWh and used to assess the energy generation costs for different technologies e.g. gas fired boiler, electric boiler and heat pumps.

The second, which is estimated in this section, is the specific investment costs. This is expressed in €/KW and describes the capital costs per kW heating capacity of the heat pump. This term is often used to benchmark different types of heat pump systems against each other.

A cost analysis was performed for the base concept; the closed-cycle steam heat pump as this is the main heat pump concept for SHIP200. Aspen Process Economic Analyzer was used to provide more cost details for the main components of the heat pump. The cost analysis was made for the compressors, condenser and evaporator, which is expected to be the major cost drivers. The input parameters are based on calculated values for heat pump concept 3, for a system with a thermal capacity of 12 MW, which are summarized in Table 10.

The cost analysis for the compressors is based on centrifugal compressors using water as working fluid. The main input parameters were the motor driver power, actual compressor inlet volumetric flow rate, and design pressure and temperature at compressor inlet and outlet. It was not possible to specific higher inlet temperatures than 90°C, so this value was used for all compressors. The cost estimate includes the compressor, motor and miscellaneous costs such as electrical, instrumental and piping, but not an eventual gearbox. For each compressor the material costs, which is the total investment including installation came to around € 882,000-943,000.

For the evaporator and condenser, the cost analysis is based on a plate and frame type heat exchanger. The estimated heat transfer area for concept 3 was used as an input parameter, along with the expected material type (stainless steel, grade 316L), the operational pressures and temperatures for the condenser and evaporator were also used as input. Similar to the compressors the cost estimate includes both the costs of the heat exchanger and miscellaneous costs such as electrical, instrumental and piping. The estimated costs were in the range of €220,000-240,000.

The investment costs are summarized in Table 13 and the total estimated investment cost was estimated to €3.2 million, which results in a specific investment cost of 265€/kW. As this only includes the major components, the estimated costs for the entire heat pump are expected to be higher if various materials such as piping, auxiliary systems, valves, support structures and gearboxes were included.

Table 13: Investment cost estimations for the main components of the steam heat pump.

Equipment	Main cost input parameters	Material costs	Installation costs	Total costs
Compressor 1st stage	Fluid type: water Design inlet gauge pressure/temperature Design outlet gauge pressure/temperature inlet actual volumetric flow rate Driver power	€ 889,000	€ 54,000	€ 943,000
Compressor 2nd stage		€ 846,000	€ 48,000	€ 894,000
Compressor 3rd stage		€ 836,000	€ 46,000	€ 882,000
Condenser	Heat transfer area Material type design gauge pressure design temperature	€ 194,000	€ 44,000	€ 238,000
Evaporator		€ 181,000	€ 42,000	€ 223,000
Sum costs				**€ 3,180,000**
Specific investment costs (12 MW_{th} capacity heat pump)				**265 €/kW**

Compared to other studies an estimate of 265€/kW appears reasonable; Bantle et al. estimated the costs for a two-stage vapor turbo-compression MVR heat pump at 200 €/kW [17]. Zühlsdorf et al. estimated investment costs as low as 179 €/kW, indicating that R-718 heat pumps can be economically feasible [24]. Based on literature studies, previous installed systems and the and current market analysis, the specific investment cost for high-temperature heat pumps is estimated to decrease with increasing thermal capacity as shown in Figure 37.

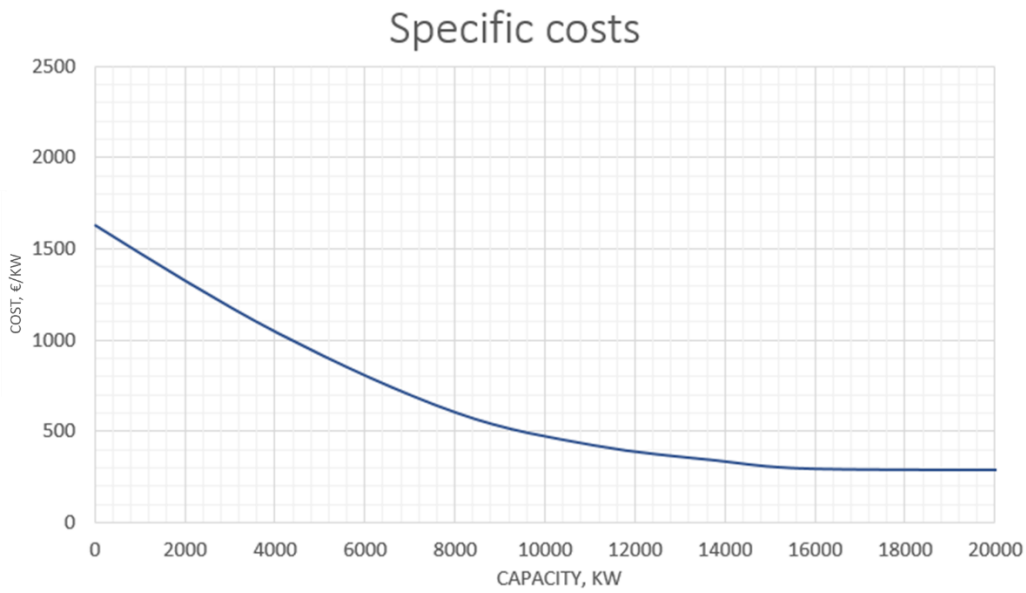

Figure 37: Specific costs vs capacity for high-temperature heat pumps.

The weights estimate for the major components are given in Table 14, which is also based on Aspen Process Economic Analyzer. The estimated weight for compressors is around 6000 kg each, while the weights of the condenser and the evaporator are estimated to 3300 kg. This gives a total weight estimate of 25 tons for the major components. Eventual gearboxes, piping, support structures refrigerant and HTF-filling will increase the weight of the overall system. Based on other known large scale >10 MW turbo-compressor heat pumps 25 tons is within the expected weight range.

Table 14: Weight estimations for the main components of the steam heat pump.

Equipment	**Weight**
Compressor 1st stage	5900 kg
Compressor 2nd stage	6000 kg
Compressor 3rd stage	6100 kg
Condenser	3300 kg
Evaporator	3300 kg
Total	24,600 kg

5.4 Open Cycle Steam Heat Pump

In the open cycle steam heat pump concept, the proposal is to deliver the steam directly to the process itself, which eliminates the need for a condenser. After the process, the steam has condensed and is returned to heat pump cycle as condensate. The condensate then needs to be heated and evaporated.

The open cycle heat pump may give associations to MVR heat pumps. However, for MVR heat pumps the process itself acts as the evaporator, while a condenser is used to utilize to condensate the steam produced by the MVR compressor, while the cold steam is heated by the condenser.

The concept of an open cycle heat pump can reduce costs due to the elimination of a condenser, while performance can be increased since steam can be delivered directly from the heat pump, avoiding the exergy losses that occur during heat exchange, both in the condenser, but also in the combined heat and storage tank. Figure 38 gives an overview of the saturated vapor pressure for varying temperatures. In this case it is assumed that condensate is returning from the process, which means that the pressure would need to be > 1 barA if it is returned at 100°C, and > 2.7 barA if returned at 130°C.

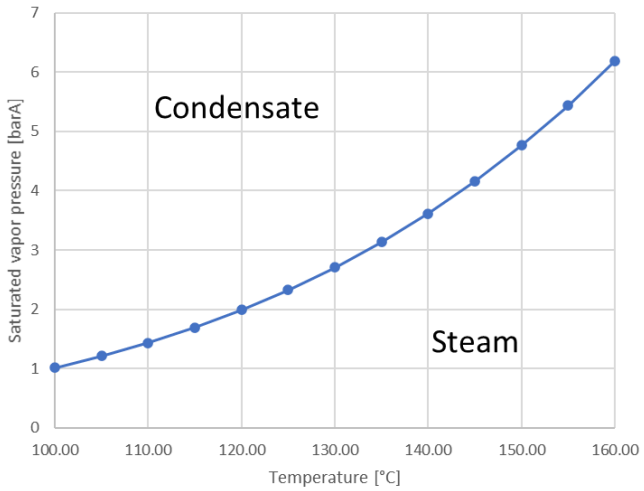

Figure 38: Saturated vapor pressure vs temperature.

To minimize the power required for the compressors, the inlet steam pressure and temperature should be as high as possible. The maximum compressor inlet temperature is limited by the inlet and outlet temperature of the HTF in the evaporator, which is 160°C and 140°C, respectively. If the minimum ΔT between the hot and cold fluid in the evaporator is 10K, this gives an evaporation temperature of 130°C, which corresponds to a pressure of 2.7 barA.

If the return condensate pressure is below 2.7 barA, a pump can be used to increase the pressure. Correspondingly if the pressure is above 2.7 if a valve can be used to reduce the pressure. It is assumed that the process condensate returns with a temperature well below 160°C in order to utilize the solar heat as a heat source to the heat pump.

5.4.1 Concept Description

An evaluation of an open heat pump concept has been made. Table 15 lists the input parameters to the model simulation, while the corresponding process diagram of the evaluated concept is illustrated in Figure 39.

Compared to the closed-cycle heat pump, the process is simplified with fewer components in the heat pump. The condensate is heated and evaporated in the evaporator by the HTF fluid coming from the solar PTCs. Depending on the temperature of the condensate entering the evaporator, it is both heated, evaporated and superheated, as illustrated in Figure 40, which shows the temperature-entropy diagram of the heat pump process.

It is assumed that the process condensate enters the evaporator at 2.7 barA, as this allows for evaporation at 130°C. Any pumping duty required to increase the pressure to 2.7 barA is negligible compared to the compressor duty, so any sensitivity evaluation in inlet pressure has therefore not been considered. However, an evaluation of the impact of the condensate temperature has been made with a variation between 100°C – 130°C with increments of 10°C.

The process steam is delivered from the heat pump at 200°C. The required steam pressure varies for different industrial plants. For example, the lowest steam pressure level for the steam network in Gendorf is 4.9 barA [42], the JTI plant steam network pressure is 8 barA [43], while the steam network in the plant in Tarragona is 14 barA. Using these plants as reference, it was therefore decided to evaluate with pressure levels ranging between 4.9 and 14 barA, with 2 bar increments.

With an outlet pressure of 14 barA, the total cycle pressure ratio (Pr) is 5.2. In this evaluation two compressor stages were used, resulting in a stage Pr of 2.28, which is on the upper end of what steam turbo compressors are capable of. However, for simplification it was decided to use the same amount of compression stages for all pressures.

De-superheating (DSH) is utilized between the first and second compression stage. The water used for DSH is taken from the condensate upstream the evaporator. DSH is assumed to be pumped to the required pressures. However, any pumping duty required for DSH is negligible. After the first compression stage DSH is used to de-superheat the steam to 10°C above the saturated temperature, while after the second compression stage DSH is used to de-superheat steam to 200°C if necessary. This was performed for almost all evaluation cases. The only exception was the Gendorf plant case where the temperature after the second compression stage was so low that DSH was not required, while DSH after the first stage was significantly reduced in order for the second stage to even reach 200°C.

Table 15: Parameters used in the open-cycle steam heat pump.

Property	Temperature
Process condensate	2.7 barA, 100-130°C
Process steam	4.9-14 barA, 200°C
HTF fluid evaporator inlet	160°C
HTF fluid evaporator outlet	140°C
Minimum compressor superheat	10°C
Minimum ΔT in heat exchanger	10°C
Steam heat delivery	12 MW

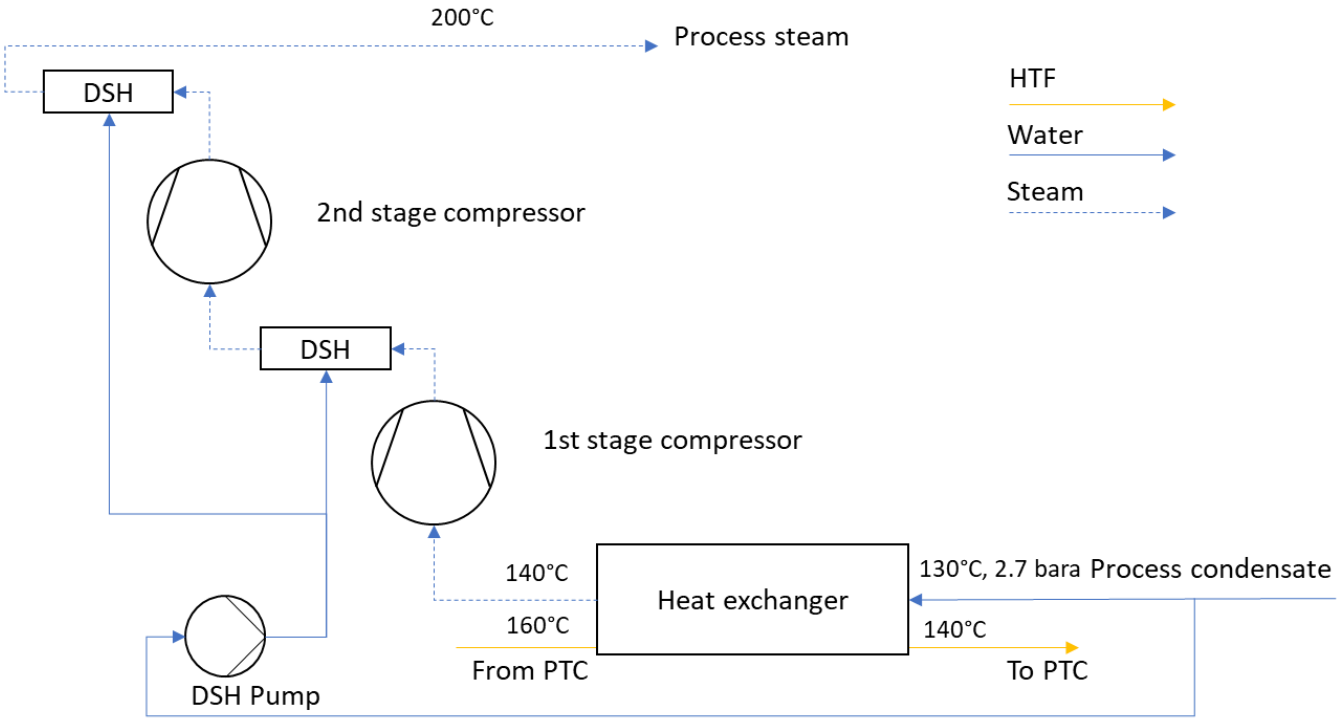

Figure 39: Process diagram of an open cycle heat pump for direct steam generation.

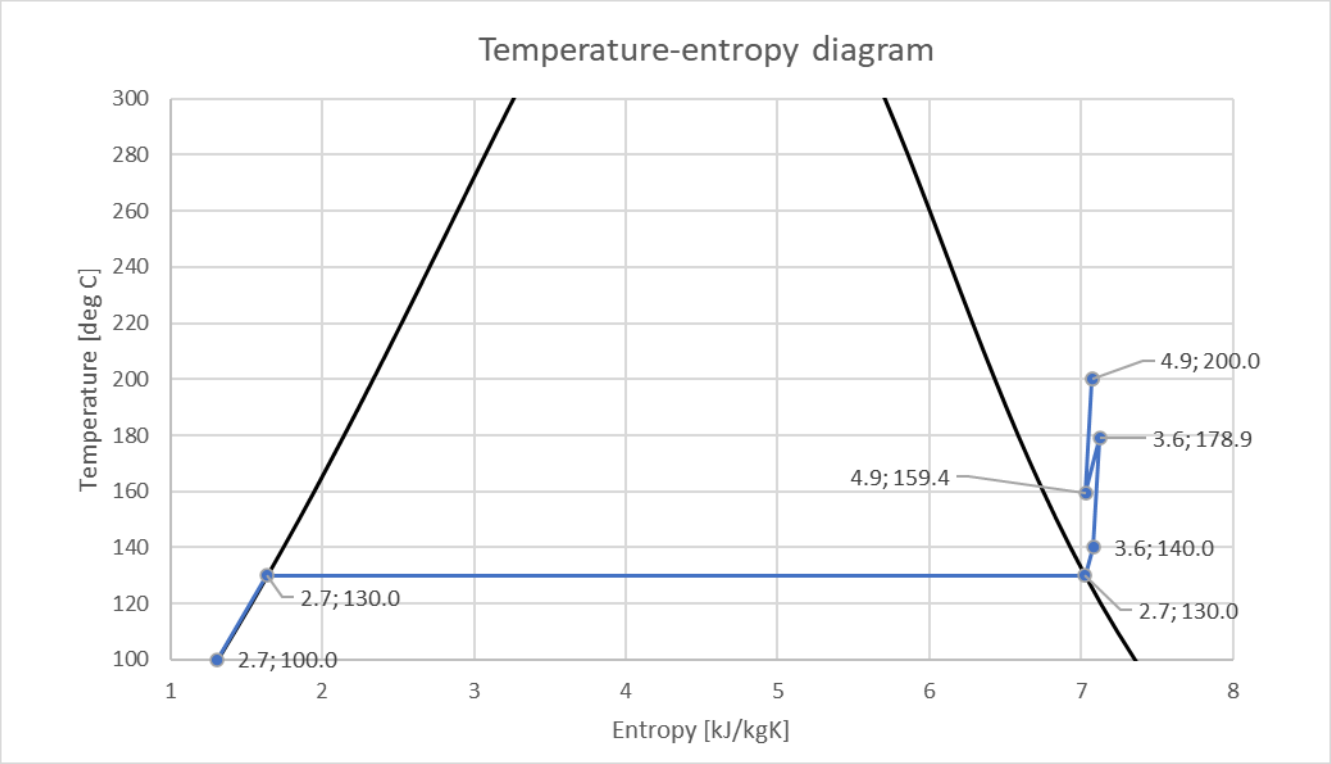

Figure 40: Temperature-entropy diagram for an open-cycle heat pump delivering 200°C steam at 4.9 barA.

5.4.2 Results and Discussions

The COP is calculated based on the total heat delivery to the steam network i.e. the enthalpy change from the steam supply and the condensate return, and the total compressor power consumption.

Figure 41 shows how the COP of the heat pump varies with different steam pressures and condensate return temperatures. When the steam supply pressure is as low as 4.9 barA (Gendorf case) COP values up to 15.8 are achieved. On the other end, a steam supply pressure of 14 barA, results in a COP value up to 5.9. The COP reduces with increased steam supply pressures since the compressor duty is a direct consequence of the pressure ratio, increasing around 2.5 times from total duty of 800 kW to over 2000 kW from the lowest to the highest supply pressure, as illustrated in Figure 42.

Very small variations in COP as a function of the condensate return temperature are observed. A high condensate return temperature gave slightly lower COP values than a low return temperature, which may appear contradictory. However, a low return temperature also means more specific heat delivery since the temperature glide in the steam network has been increased. For a constant heat delivery this results in a reduced steam mass flow through the compressors, which reduces the power consumption.

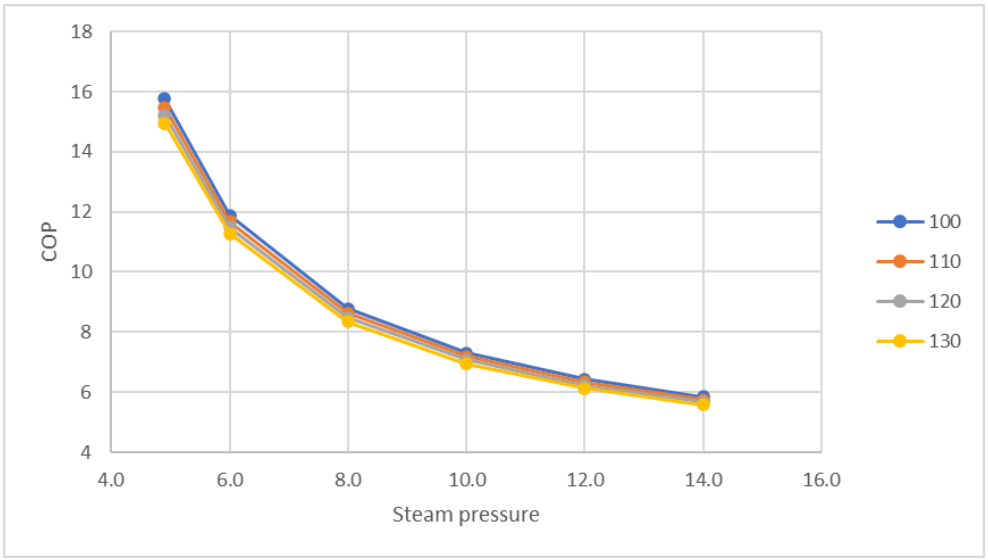

Figure 41: COP vs steam delivery pressure for steam return temperatures.

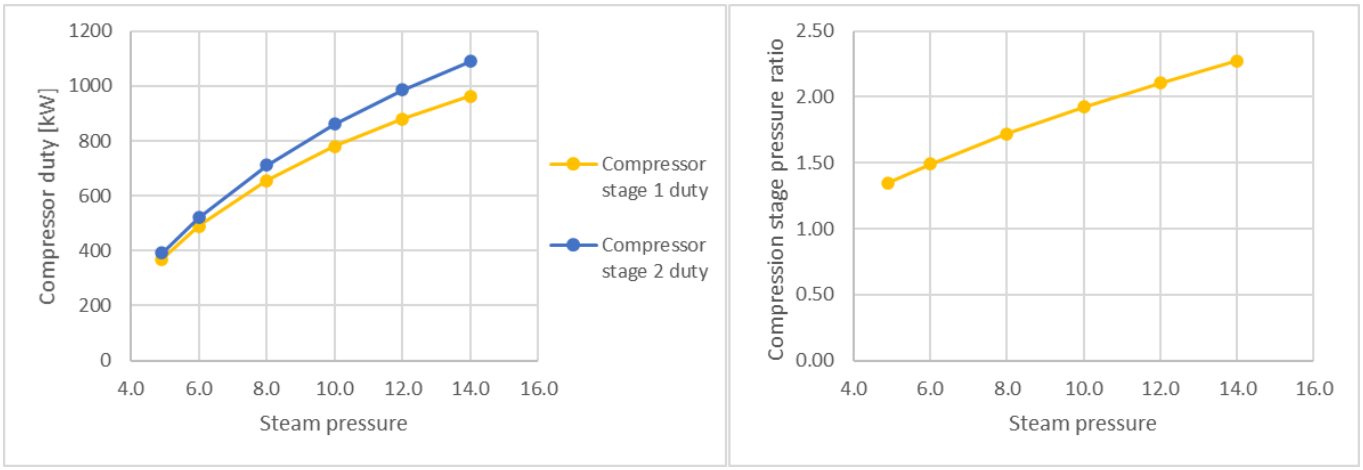

Figure 42: Left: Compressor duty as a function of steam supply pressure. Right: Compression stage pressure ratio as a function of steam supply pressure. Simulated with condensate return pressure of 100°C.

Compared to the closed cycle steam heat pump, the COP values achieved by the open-cycle heat pump are very high, especially when the steam supply pressure is low. This can be explained by the fact that the delivery temperature at low supply pressures is much higher than the condensation temperature. As an example, when the supply pressure is 4.9 barA, the saturated vapor temperature is 151°C, which is the temperature the heat will primarily be delivered at if the steam is condensed in the steam network. A comparison between the Gendorf plant, JTI plant and Tarragona plant is made in Figure 43, showing the distance from the steam supply conditions and the saturated vapor line (black line). The dotted line shows the isobars at the supply pressure. The steam supplied for the Tarragona plant is very close to saturated vapor, with a condensation temperature of 195°C.

Another important consideration is the compressor outlet temperature, which is significantly higher when steam is supplied at high pressures (Tarragona case), compared to low pressures. This is because steam is supplied close to the saturated vapor line, which results high compressor outlet temperatures and significant de-superheating, when only two compression stages are used. The overall compressor work and maximum outlet temperatures can be reduced by increasing the number of compression stages, though at the expense of increased component costs.

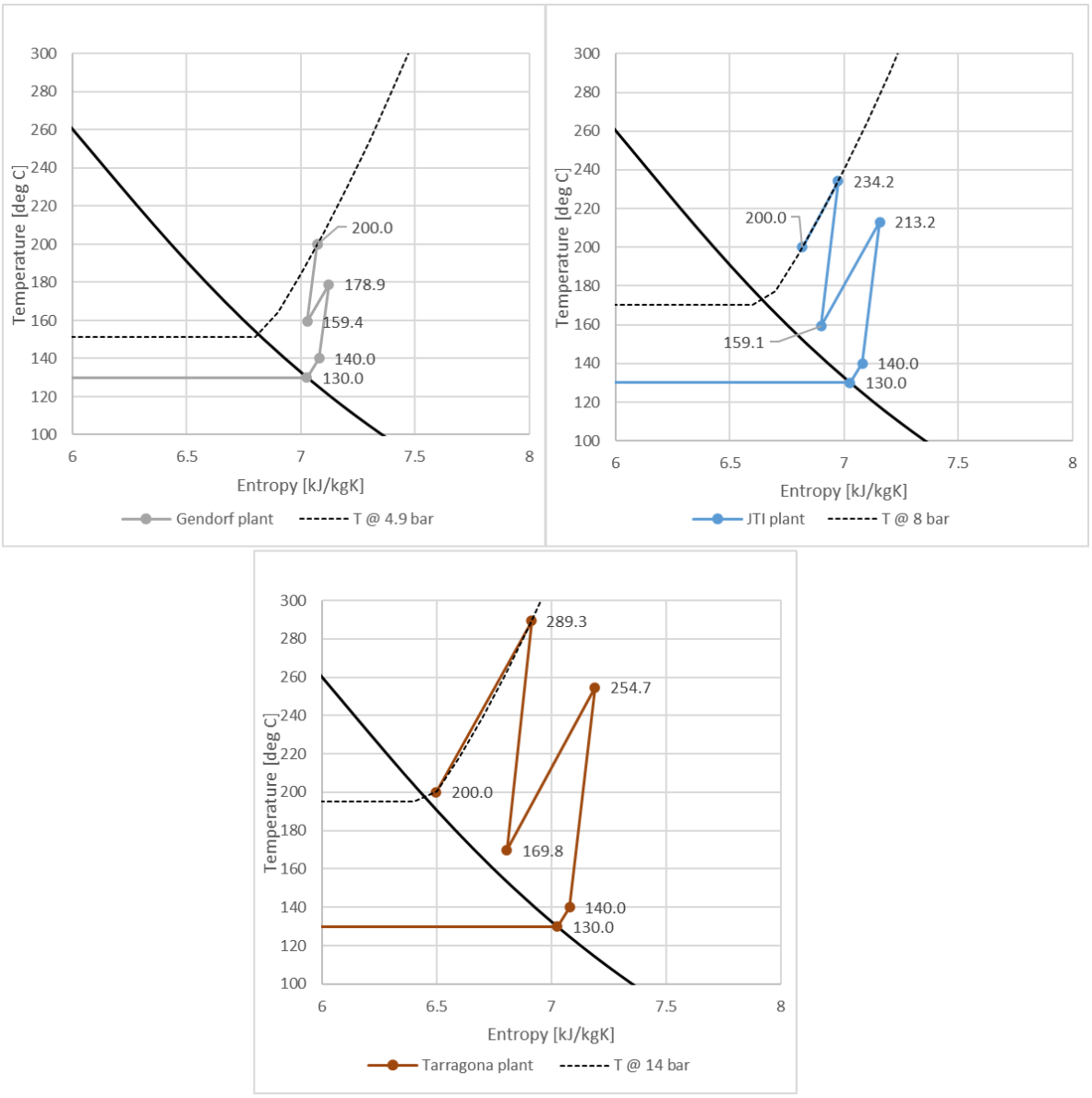

Figure 43: Cut out of the temperature-entropy diagrams comparing Gendorf, JTI and Tarragona plants.

5.5 Reversed Brayton Heat Pump Concept for Long Term 250°C Heat Delivery for SHIP200

5.5.1 Case Description

The reversed Brayton heat pump will use supercritical CO_2 (sCO_2) as the working medium to lift heat delivered from parabolic trough solar collectors at 160°C up to around 250°C. The system will be designed with a temperature difference of 10°C between the working fluid and boundary systems will be used to drive the heat exchange at the high temperature side and the system will be designed with an exit temperature of 240°C which further can be delivered to thermal storage or as process heat.

At design point the external heat transfer fluid (HTF) at the sink side will have an inlet temperature of 160°C. A variation from this value down to 140°C and up 170°C will be tested on the system to investigate the effect of realistic off-design operation. At design point the heat will be delivered at a rate of 12 MW and off-design heat rate operations will be studied at 10 MW, 8 MW and 6 MW. The temperature of the working medium will be elevated from 150°C to 250°C with a single-stage turbo compressor. The working fluid will then deliver heat to the HTF until it reaches 240°C. The mass flow will be adjusted so that this process delivers 12 MW. The working medium will then be expanded to the initial pressure through an expansion machine before being heated to the compressor inlet conditions. The boundary and cycle conditions are summarized in Table 16 and Table 17, respectively.

A preliminary simplified heat pump model will be made using Excel and the NIST Refprop database to get estimations of the impact of different pressure conditions and turbomachinery isentropic efficiency on the system COP. The inclusion of an internal heat exchanger (IHX) in the simplified model was also investigated.

Table 16: Boundary conditions used reversed Brayton sCO_2 cycle.

Property	Value(s)
HTF fluid gas heater inlet temperature [°C]	160
HTF fluid gas heater outlet temperature [°C]	140
HTF fluid gas cooler inlet temperature [°C]	140- 170 (160 nominal)
HTF fluid gas cooler outlet temperature [°C]	240
Cycle heat delivery [MW]	6-12 (12 nominal)

Table 17: Cycle design conditions used reversed Brayton sCO_2 cycle.

Property	Value(s)
Gas heater outlet temperature [°C]	150
Gas heater outlet pressure [barA]	150
Gas cooler inlet temperature [°C]	250
Gas cooler inlet pressure [barA]	355.748
Gas cooler outlet temperature [°C]	170

5.5.2 Preliminary Simplified Model

The simplified model included isobaric heat exchange at the source and sink and used an isentropic efficiency to model the compressor and expander. The simplified model did not depend on the scale of the system and all calculations were done on a per mass unit basis. An isentropic efficiency of 75% was used for both compressor and expander. Specification of the lower pressure in the cycle implicitly specifies the higher pressure through the isentropic efficiency. A parameter study where the compressor inlet pressure was varied from 70 barA to 200 barA for each sink HTF inlet temperature case was done to find an optimal set of lower and higher pressures. With the design value of the sink HTF inlet temperature, the same pressure variation study was performed with different turbomachinery isentropic efficiencies from 70% to 85%.

5.5.3 Heat Exchangers

For the design of the reversed Brayton heat pump, the components used for heat exchange are based on the PCHE type due to its suitability for high-pressure sCO_2 systems. If the thermal performance is similar, the heat exchanger model could be replaced with a different type without much difference in results from the system since the calculations are quite generic.

The geometric properties of the channels are based on a PCHE studied by Ren et al. where the semicircle diameter was set to 2.8 mm giving a hydraulic diameter of 4A/P = 1.71 mm (A is the cross-sectional area and P is perimeter length). Figure 44 shows a unit cell of the heat exchanger cross section where the colder fluid passes through the blue area and the hotter fluid through the red area [47]. From values used in the model design, the heat transfer area density for each fluid side can be estimated to approx. 600 m^2 / m^3, which is around half of reported achievable area densities for PCHEs of 1050 m^2 / m^3 [40], and will therefore be a conservative value.

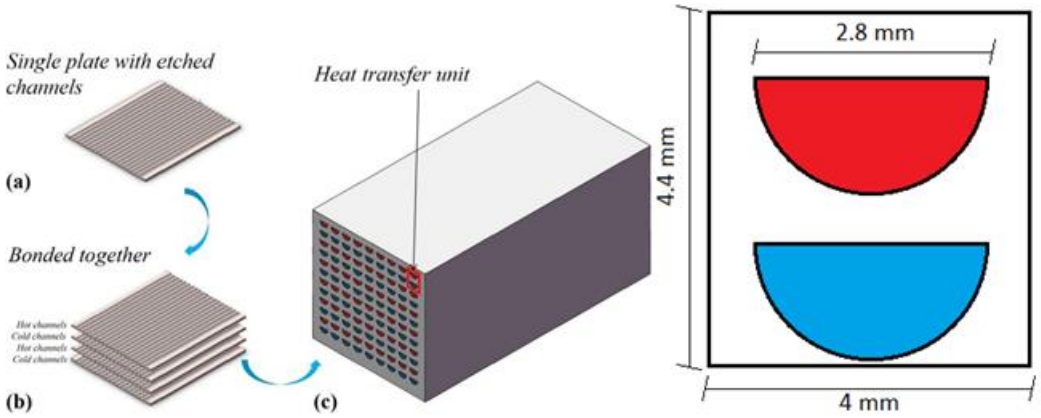

Figure 44: Schematic of PCHE. Images (a), (b) and (c) describe the assembly of channelled plates to form the heat exchanger. The schematic on the right shows the cross section of a heat transfer unit where the red and blue area represent the warm and cold side fluids. The geometric properties were adopted from the article by Ren et al. [47].

As the heat transfer properties of the system depend on the Reynolds number of fluid flows, a Reynolds number of 10000 in the sCO_2 channels was used to estimate the geometric properties of the heat exchangers. This value was somewhat arbitrarily chosen based on Reynolds number values used in research on PCHE models in the literature and to ensure turbulent flow for enhanced heat transfer.

At design point the HTF inlet temperature on the sink side was 160°C and the outlet 240°C. A temperature difference in the gas cooler of 10K between the fluids was chosen, giving a temperature glide from 250°C to 170°C on the sCO_2 side. A design point heat delivery of 12 MW was used to calculate the mass flows of the fluids, giving approx. 97.7 kg/s of sCO_2 and 68 kg/s of therminol66. Using the average mass density of sCO_2 and the Reynolds number of 10000, the number of channels was calculated from the cross-sectional area of each channel. This gave 141784 channels for the sCO_2 side. Based on estimations of the heat transfer properties of the system, a length of 6.1 m was estimated for the tubes to deliver 12 MW. For simplicity, the same number of channels were used for both fluid sides. This gave a Reynolds number of approximately 263 for the therminol66 side. The length of the heat exchanger tubes was adjusted during Modelica simulations until correct heat transfer and outlet temperatures were achieved. Similar calculations were done for design of the gas heater.

The heat transfer coefficient for the sCO_2 side was estimated based on the Reynolds number and Prandtl number, obtained from NIST REFPROP, through Darcy friction factor and Nusselt number correlations for straight channel circular pipe flow based on hydraulic diameter using the Gnielinski correlation [47]. This gave a heat transfer coefficient of approx. 970 W/(m^2 K) which was in the lower range of values found in the literature, indicating that it is a conservative but reasonable estimate. A value of 232.9 W/(m^2 K) was used as an estimate for the heat transfer coefficient for therminol66 based on a representative calculation with the TIL heat exchanger model.

Thermal properties of the solid wall was specified with a thermal conductivity of 21 W/(m K) [47], wall thickness estimated to 1 mm. The total heat transfer area was estimated from the total channel surface area for one fluid side.

The pressure drop pr. unit length on the sCO_2 side was estimated from the calculated Darcy friction factor to be approx. 1 kPa/m. Pressure drop at off-design mass flow through the heat exchanger is calculated by multiplication with the square of the mass flow ratio to the mass flow at design point.

The heat exchanger properties of the gas heater and gas cooler are summarized in Table 18 and Table 19, respectively.

Table 18: Gas heater properties.

Property	Value
Number of channels, each side	210711
Length [m]	1.26
Total heat transfer area [m^2]	1911
Heat transfer coefficient sCO_2 [W/m^2 K]	798.1
Heat transfer coefficient HTF [W/m^2 K]	232.9
Thermal conductivity wall [W/m K]	21 (Inconel 617)
Wall thickness [mm]	1

Table 19: Gas cooler properties.

Property	Value
Number of channels, each side	141784
Length [m]	8.518
Total heat transfer area [m^2]	8879
Heat transfer coefficient sCO_2 [W/m^2 K]	970
Heat transfer coefficient HTF [W/m^2 K]	232.9
Thermal conductivity wall [W/m K]	21 (Inconel 617)
Wall thickness [mm]	1

5.5.4 Results and Discussion

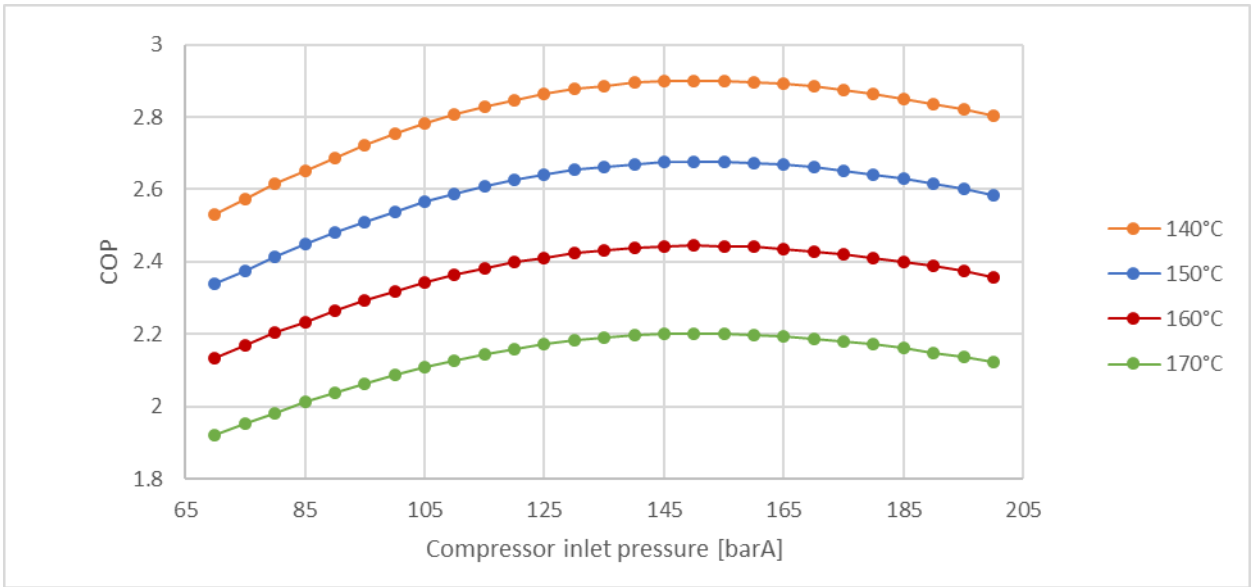

Figure 45: COP as function of compressor inlet pressure for different HTF inlet temperatures.

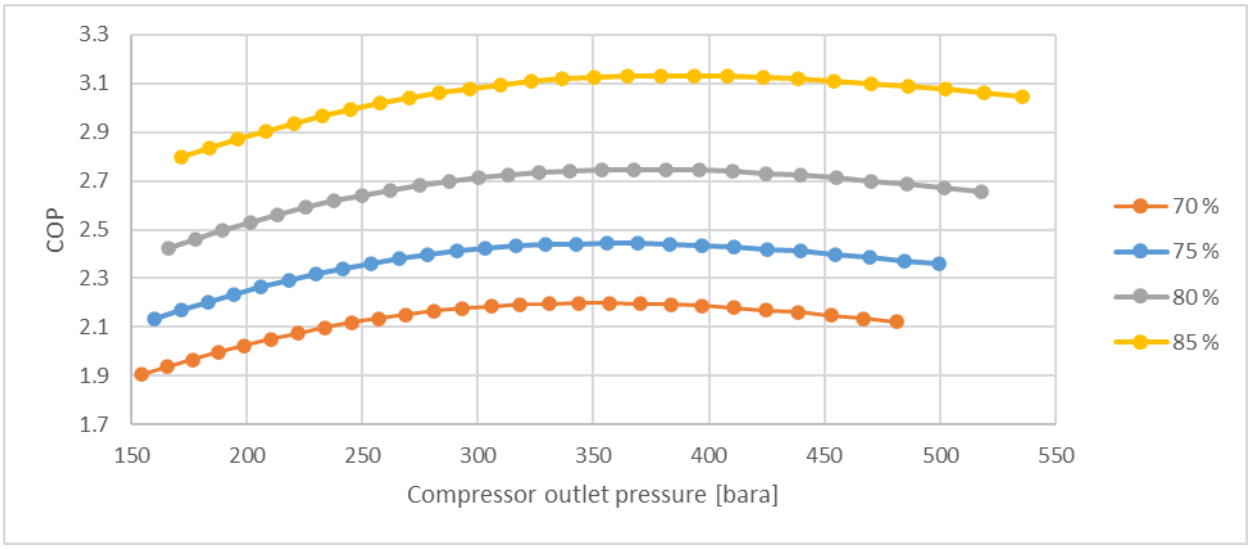

Figure 46: COP as function of compressor outlet pressure for different isentropic efficiencies. HTF inlet temperature is 160°C.

The results from the parameter study on different pressure conditions are presented in Figure 45. The compressor inlet pressure giving the highest COP was found to be 150 barA which gave a compressor outlet pressure of 356 barA. The COP increases nearly proportionally to the temperature glide interval which is reasonable due to the heat output being nearly proportional to the temperature glide for the same mass flow rate. For the same mass flow rate the compressor works are identical, but the expander work can vary somewhat with the gas cooler outlet temperature, however, with a smaller impact on the COP than the compressor. The equal compressor conditions used for all the studied cases could be the reason for why the curve shapes, and therefore optimal pressure conditions, are the same. During off-design operation, the compressor outlet temperature and pressure could vary. The calculations for the off-design HTF inlet temperatures could therefore be less representative of a real system.

The results from the parameter study on the impact of the turbomachinery isentropic efficiency on the COP are presented Figure 46. The COP increases with increasing isentropic efficiency. In the studied interval, the increase seems to be non-linear, with increased sensitivity at higher isentropic efficiencies. There is roughly a 50% increase in COP when the isentropic efficiency is increased from 70% to 85%, but the optimal pressure values are higher which might cause additional challenges with the system implementation.

5.5.5 Size

5.5.5.1 Heat Exchangers

The cross-sectional area of the heat exchanger was calculated by multiplying the number of heat transfer units with the cross section occupied by each unit. Assuming the width and height of the total cross section to be the same, they could be estimated as the square root of the area. The length of the heat exchangers came from the design point calculations in Modelica. The mass of each heat exchanger was calculated by the fraction of volume occupied by the heat exchanger walls with the total volume and a mass density of Inconel 617 which was set to 8360 kg/m^3.

Table 20: Gas heater size

Property	Value
Length [m]	1.26
Height [m]	1.93
Width [m]	1.93
Occupied volume [m^3]	4.47
Mass [kg]	80627

Table 21: Gas cooler size

Property	Value
Length [m]	8.518
Height [m]	1.58
Width [m]	1.58
Occupied volume [m^3]	21.26
Mass [kg]	108505

5.5.5.2 Turbomachinery

The mass flow of sCO_2 in the system will be approx. 98 kg/s. A rough estimate of a centrifugal compressor diameter based on isentropic compression of an ideal gas and rotation speed of 90000 rpm was made. The compressor power was estimated in the calculations at the design point in the simplified model. Similar estimates were made for the expander for which the diameter was estimated to be on the same order as the compressor. Size parameters of turbo compressor and expander are presented in Table 22 and Table 23, respectively.

Table 22: Turbo compressor size estimates.

Property	Value
Inlet volume flow [m^3/h]	1508
Rotation speed [rpm]	90000
Diameter [m]	1-2 (rough estimate)
Power [kW]	7410

Table 23: Expander size estimates.

Property	Value
Inlet volume flow [m^3/h]	658
Rotation speed [rpm]	90000
Diameter [m]	1-2 (rough estimate)
Power [kW]	2926

5.5.6 Conclusion on Concept Design

Based on the optimal COP of the simplified heat pump model, a compressor inlet/outlet pressure of 150/356 barA will be used for the compressor component design. No commercially available turbomachinery was found to match the operational conditions, but currently ongoing research could produce components able to handle the high pressures in the near future.

Printed circuit heat exchangers will be used for heat transfer to the sink and source HTF as these have been suggested as good candidates for sCO_2 applications, although more research is needed before they can be applied to the high pressures in the gas cooler.

With the cycle conditions under consideration, there was not found any case where an IHX was feasible since sufficient heat was delivered at the heat sink for the working fluid to reach sufficiently low temperatures after expansion.

With the simplified heat pump model, it was shown that the COP increases with decreasing sink HTF inlet temperature, mainly since this increased the temperature glide.

Increments in isentropic efficiency of the turbomachinery could increase system performance significantly in terms of COP.

6 Simulation of Heat pump Concepts for SHIP200

6.1 Steam Heat Pump Modelica Simulations

A numerical model of a steam heat pump, similar to heat pump concept 3, described in chapter 5.3.1 has been built. A short recap of this heat pump concept: This utilized subcooling and de-superheating after all compressor stages. It achieved the best performance, with a COP of approximately 5 at design conditions.

The purpose of the numerical model is to enable a more detailed evaluation of heat pumps concepts. The following will be evaluated as part of the numerical simulations: Heat pump performance, operational stability and integration through simulations of both design and part load / off-design conditions. The latter represents the expected operational mode both during periods of low solar radiation, but also during system charge conditions, where the HTF condenser inlet temperature is expected to vary.

The numerical evaluation includes evaluation of all sub-components, but focuses especially the turbo compressor performance including isentropic efficiency, compressor mapping and potential surge conditions, which could limit operational range. The heat exchangers are also evaluated both in terms of the required heat transfer area and estimated pressure drop of the heat transfer fluid in the evaporator and condenser.

In addition, the numerical model of the heat pump will function as a basis for the implementation into a Modelica-based simulator of the entire SHIP200 system.

6.1.1 Model Description

The numerical model was modelled and simulated in Modelica. The TIL component library, a product by TLK-Thermo GmbH, was used to model the heat pump system. The model library is especially suited for refrigeration and heat pump systems. The graphical visualization in the results section is made using the visualization tool DaVE, which is also provided by TLK-Thermo GmbH. The graphical layout of the model is given in Figure 47. The main components of the heat pump system are named and connected to each other by a green line, representing the working fluid (water). The blue lines represent the boundary conditions of the heat pump which are the inlet and outlet conditions of the heat transfer fluid (Therminol66), at the condenser and evaporator. In addition, the numerical model consists of virtual sensors, controllers, setpoints and other inputs used to control the heat pump.

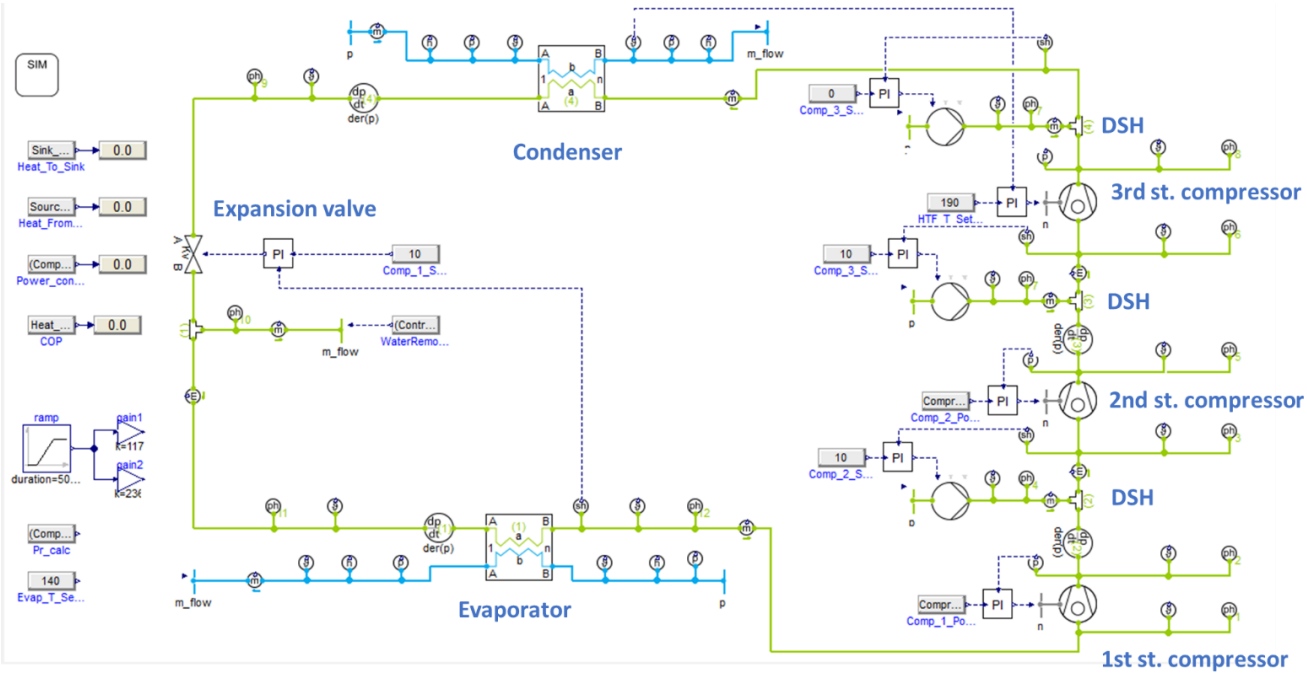

Figure 47: Modelica model of the steam heat pump, including main component names.

A summary of the key parameters and specifications of the model is given in Table 24.

Table 24: Model specifications.

Component	Model specification		
Turbo compressors	Gasparovic turbo compressor model Design pressure ratio: 1.79 Design speed: 90 000 rpm		
	Stage 1 design points: Max. stage efficiency: 0.85 Inlet temperature: 140°C Inlet pressure: 2.7 barA Mass flow rate: 4.72 kg/s	Stage 2 design points: Max. stage efficiency: 0.9 Inlet temperature: 161°C Inlet pressure: 4.84 barA Mass flow rate: 5.01 kg/s	Stage 3 design points: Max. stage efficiency: 0.97 Inlet temperature: 184°C Inlet pressure: 8.66 barA Mass flow rate: 5.32 kg/s
Condenser	Plate and frame heat exchanger. Plate length (825mm) and width (225 mm) based on Alfa Laval Alfanova HP400. Total heat transfer area: 470 m^2 Wall material: stainless steel Wall thickness 0.4 mm Heat transfer coefficient, h_water: 10 000 W/m^2K Heat transfer coefficient, h_HTF: calculated based on available correlation for single phase fluids in plate heat exchangers [48] Pressure drop HTF: calculated based on available correlation for single phase fluids in plate heat exchangers [48]		
Evaporator	Plate and frame heat exchanger. Plate length (817mm) and width (355 mm) based on Alfa Laval AC1000DQ. Total heat transfer area: 468 m^2 Wall material: stainless steel Wall thickness 0.4 mm Heat transfer coefficient, h_water: 6 000 W/m^2K Heat transfer coefficient, h_HTF: calculated based on available correlation for single phase fluids in plate heat exchangers [48] Pressure drop HTF: calculated based on available correlation for single phase fluids in plate heat exchangers [48]		
De-superheater system	Injection: Junction components Pump: simple pump component, power consumption neglected.		
Expansion valve	Orifice valve, Flow coefficient input		

6.1.1.1 Turbo Compressors

The turbo compressors are based on models according to the Gasparovic turbo-compressor. The benefit of this model is that it captures the characteristics of a turbo-compressor without the need to specify geometric input, which at this stage is unknown. Instead, the design point parameters, such as inlet pressure and temperature, pressure ratio, stage efficiency and rotational speed are given as input. The model adjusts the efficiency and performance as the operation falls outside design conditions. The isentropic efficiency at design conditions cannot be specified directly. Instead, a stage efficiency parameter is given. The stage efficiency of the three stages have been adjusted in order to achieve an isentropic efficiency of 0.75 at design conditions.

A compressor map of the Gasparavic model was made to get an understanding of how the general behaviour and performance varied with varying loads. It was done by varying the speed and the pressure at the inlet and outlet. The result is illustrated in Figure 48. The pressure ratio is given along the y-axis, while the x-axis represents the relative mass flow, which is the mass flow that would occur if the inlet conditions corresponded to standard conditions, i.e. 15°C and atmospheric pressure. The resulting isentropic efficiency is shown as data labels along the constant speed lines. The blue dotted lines are added to indicate lines of constant isentropic efficiency, also known as efficiency islands. As the operating conditions move away from design, the isentropic efficiency drops.

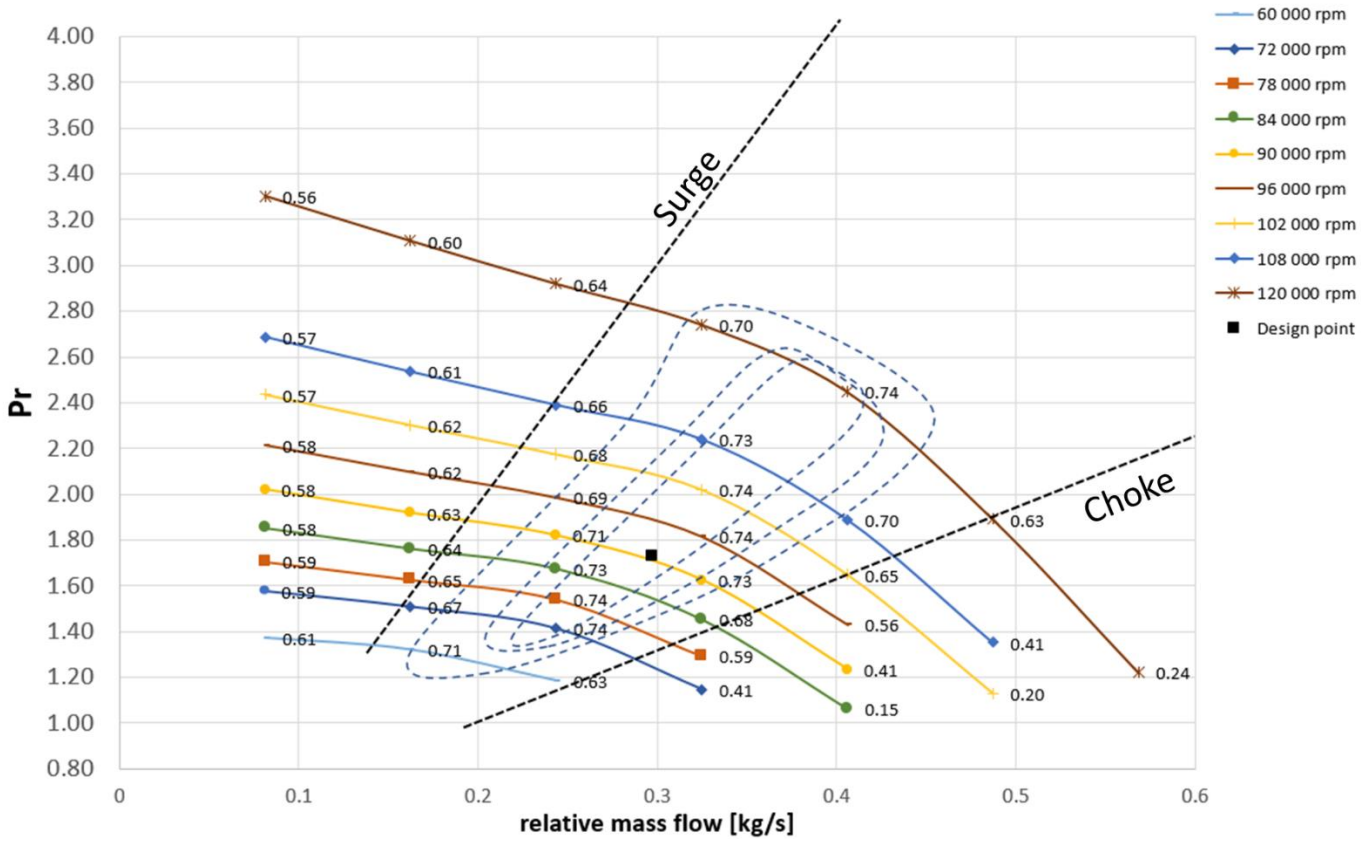

Figure 48: Compressor map of the turbo compressor model.

A weakness of the Gasparovic model is that it does not take compressors surge into consideration. As the flow through the compressor is reduced, it will eventually lead to a point where flow pattern becomes unstable, and even negative fluid velocities can occur. This is called surging and can have damaging effects on the compressor and should be avoided. The black dotted upper line in the map is an estimated line where surging potentially could occur in a real turbo-compressor. The compressor is not able to operate to the left of this line. Comparing the simulation results to the map may give an indication of surge conditions. The black dotted lower line on the map indicates potential choking conditions, where the compressor operates on its maximum flow for a given speed. The choking phenomenon is reflected in the model as the isentropic efficiency drops steeply along the constant speed line as the mass flow is increased.

The control strategy for the heat pump was based on three goals: achieving a HTF temperature of 190°C at the outlet of the compressor, maintaining a constant steam superheat at compressor inlet and maintaining equal compressor pressure ratios. The motive of the latter goal was to minimize total compressor power consumption and avoid potentially high- or low-pressure ratios for one or more stages, leading to reduced efficiency and surge or choke conditions.

In the first and second stage compressors, a PI-controller was used to control the outlet pressure by adjusting the rotational speed. The setpoint for outlet pressure was based on maintaining equal pressure ratios based on the following correlations:

$$p_{outlet,comp1} = P_{cycle,low} * P_r$$

$$p_{outlet,comp2} = P_{cycle,low} * {P_r}^2$$

$$P_r = \left(\frac{P_{cycle,high}}{P_{cycle,low}}\right)^{\frac{1}{3}}$$

The pressure ratio, Pr is calculated dynamically and given as input to the PI-setpoint values for the 1st and 2nd compressor stage. The high- and low-pressure of the cycle is not fixed, but changes depending on the load conditions. The reason for this is discussed in the results section. Feedback to the PI-controllers comes from pressure sensors at the outlet of each compressor. From this method the pressure ratio of the 3rd compressor stage becomes equal to the two other stages automatically, and it can instead be used to control the HTF condenser outlet temperature. This is done by altering the compressor speed until the setpoint of 190°C is reached.

6.1.1.2 Heat Exchangers

Both the evaporator and condenser were modelled as corrugated plate and frame heat exchangers. The geometries for the evaporator and the condenser were based on Alfa Laval AC1000DQ and HP400, respectively.

The HTF heat transfer coefficient and pressure drop calculations were based on available correlations for plate and frame heat exchangers, based on VDI Heat Atlas [48]. The calculated values are presented as part of the results.

It was also intended to use suitable available pressure drops and heat transfer coefficient relations for the working fluid. However, due to numerical instabilities this had to be specified. The heat transfer coefficient for the working fluid was set to 10 000 and 6000 W/m^{2}K in the condenser and evaporator, respectively. These values were based on averaged values from

Table 7. The pressure drop was set to zero.

The evaporator and condensers were sized according to design conditions: heat load of 12 MW and HTF condenser inlet temperature of 160°C. This resulted in a total heat transfer area of 468 and 470m^2, respectively. This is considerably higher than the results from the concept evaluations and will be further discussed as part of the results. The sizing of the condenser was also made taking subcooling into consideration. However, without an active controller it was difficult to control the degree of subcooling. Model improvements to part of the control strategy should be considered in the future.

For both the condenser and the evaporator, the mass flow of the HTF was controlled by a ramp function to simulate 50-100% load conditions for the heat pump, of which 100% load corresponded to design conditions and 12 MW heat rate to the combined heat storage.

In this setup the heat pump was integrated to the SHIP200 system by responding to changes in the heat demand by the combined heat and storage tank: As the mass flow of the HTF flowing through the condenser increases or reduces, the compressor speed of the 3rd compressor stage is altered in order to maintain a constant 190°C HTF outlet temperature, and the rest of the heat pump system adjusts accordingly.

Similarly, this means that the HTF mass flow through the evaporator needs to adjust to provide the required heat. By using this integration principle, it is assumed that there is communication between the combined heat and storage and PTC systems in terms of heat availability. This to avoid situations where there is insufficient solar heat to provide the required HTF mass flow through the evaporator, which eventually would lead to an HTF condenser outlet temperature below 190°C.

In this model the mass flow of the HTF in the condenser and evaporator was controlled by the same ramp function, and their percentage change during changing load conditions were equal. As the results will show, this was possible because only minor changes to the COP was observed during part load. However, a potential improvement to the model is to separate these two in order to take higher COP fluctuations into account.

The variations in HTF condenser inlet temperatures represent various stages of charge and discharge conditions and were set manually for each simulation case. These varied from 140 to 170°C with 10°C increments.

6.1.1.3 De-superheating

The de-superheating system was modelled as two separate systems as opposed to a closed loop for simplicity purposes. A pressure boundary was used to control the injection pressure, which was provided by a pressure sensor at the outlet of the previous compression stage. A PI-controller controls a simple pump model to provide the correct injection flow rate. The setpoint for the PI-controller was 10°C, which was the specified superheat conditions at the compressor inlet. The feedback was provided by a superheat sensor downstream the injection point. The point of

injection was modelled using a simple junction point in the heat pump cycle. The temperature of the injection water was automatically adjusted to saturated water conditions.

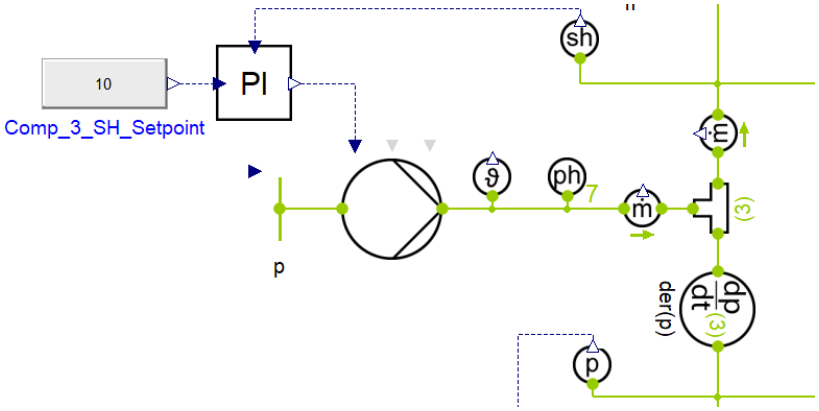

Figure 49: Model view of one of de-superheating stages

In order to avoid accumulation of working fluid in the simulation due of the injected water in the de-superheating stages, an equal amount of water to the injected water needs to be removed in the cycle. This occurs downstream the expansion valve where a junction point was used to remove the water. The flow rate was controlled by a set point equal to the sum of the injection flow rates.

6.1.1.4 Expansion Valve

The expansion valve was modelled using an orifice valve with a flow coefficient Kv as input. The Kv value was given by a PI-controller, which used a setpoint of 10°C and the superheat temperature at the evaporator outlet as feedback. Hence, the expansion valve was used to control the amount of superheat at the inlet of the 1st compressor stage.

6.1.2 Simulation Cases

A series simulation cases were constructed similarly to the concept evaluations of the closed-cycle steam heat pump. The simulation cases varied in terms of the HTF condenser inlet temperature, as listed in Table 25, which also lists the operational parameters used. For each simulation case heat delivery ranged between 6 and 12 MW in order to simulate 50-100% load variations.

Compared to the concept evaluations in chapter 5 there are fewer fixed cycle parameters. This is due to more detailed modelling on a component level, which results in dynamic values such as compressor isentropic efficiency and heat exchanger U-values.

Table 25: Parameter values used in the simulation cases.

Parameter	values
HTF fluid evaporator inlet	10 barA, 160°C
HTF fluid evaporator outlet	Ca 140°C
HTF fluid condenser inlet	5 barA, 140-170°C (design: 160°C)
HTF fluid condenser outlet	190°C
Steam superheat compressor inlet	10°C
Steam superheat at condenser inlet	0.05°C
Heat delivery	6-12 MW (design: 12 MW)

6.1.3 Simulation Results and Discussions

6.1.3.1 Performance

The resulting COP for each case (140-170°C) for varying heat deliveries i.e. load conditions is given in Figure 50. The results show COP values in the range of 4.75 - 4.96 which are similar to the results in the concept evaluations, although slightly lower.

An interesting observation is that higher HTF inlet temperatures result in improved COP values. This contrasts with the concept evaluations where the opposite results were observed. The main reason for these results is due to the HTF heat transfer coefficient in the condenser, which is improved when the HTF inlet temperature is increased. This is further discussed in section 6.1.3.2.

The COP varies with changing heat loads and is typically reduced as the heat load is reduced. However, the reduction is less than expected. Furthermore, the maximum COP is not at design point conditions but around 10400 - 10600 kW. Again, this can be explained by the heat transfer coefficients, but also the changes to the compressor isentropic efficiencies.

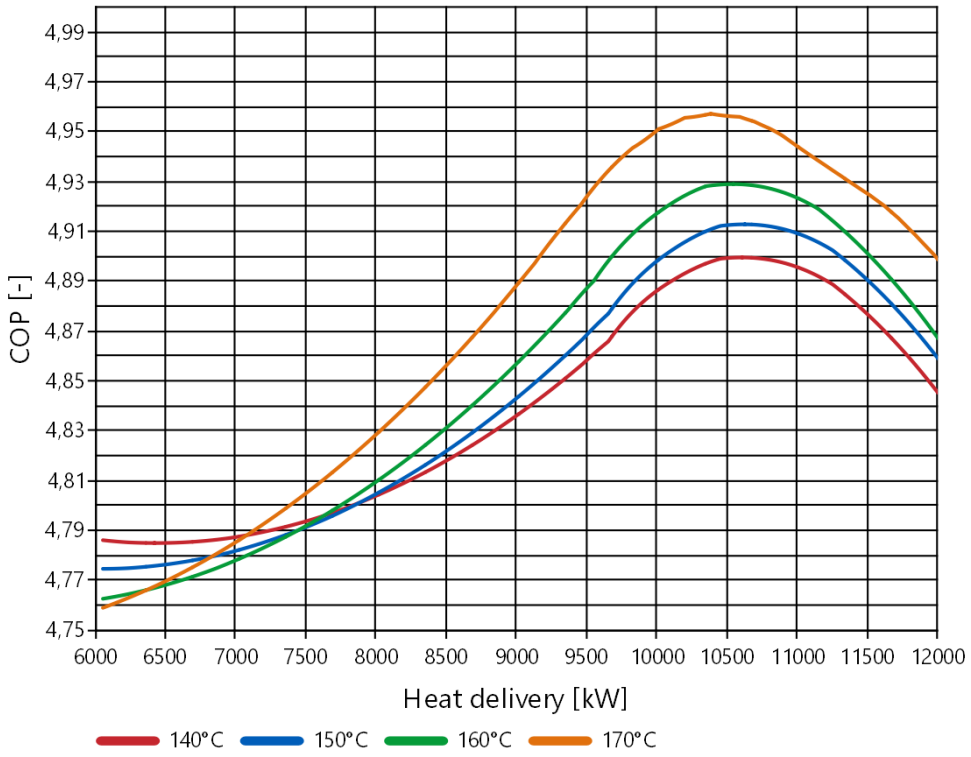

Figure 50: COP values for different heat pump loads and varying HTF condenser inlet temperatures.

6.1.3.2 Heat Exchanger Heat Transfer Coefficients

Figure 51 shows the heat transfer coefficients, h, obtained for the HTF in the evaporator and condenser. The heat transfer coefficient depends greatly on the Reynolds number, which in turn is affected by the mass flow rates of the HTF. Higher mass flow rates result in higher Reynolds numbers and improved heat transfer coefficients.

The heat transfer coefficient therefore reduces at lower heat transfer rates, but also at reduced HTF condenser inlet temperatures as this also reduces the mass flow rate, as seen in Figure 52. As a result, this causes a great difference between the coefficient values for 170°C and 140°C and is the main reason why COP is generally improved at higher inlet temperatures. This also leads to reduced COP at lower heat transfer rates.

The heat transfer area in the condenser and evaporator was increased with about 100% compared to the calculated area for design conditions in the concept evaluations in chapter 5.3.2.2. However, the calculated heat transfer coefficients for the HTF were significantly reduced compared to the film heat transfer coefficient used for liquids in the concept evaluations. Because of this the calculated overall heat transfer coefficient (U-value) for the condenser

and evaporator at design conditions were 1538 W/m^{2}K and 1482 W/m^{2}K, respectively, which is a U-value reduction of 32% and 41% compared to the average U-values for evaporation and condensation in Table 9.

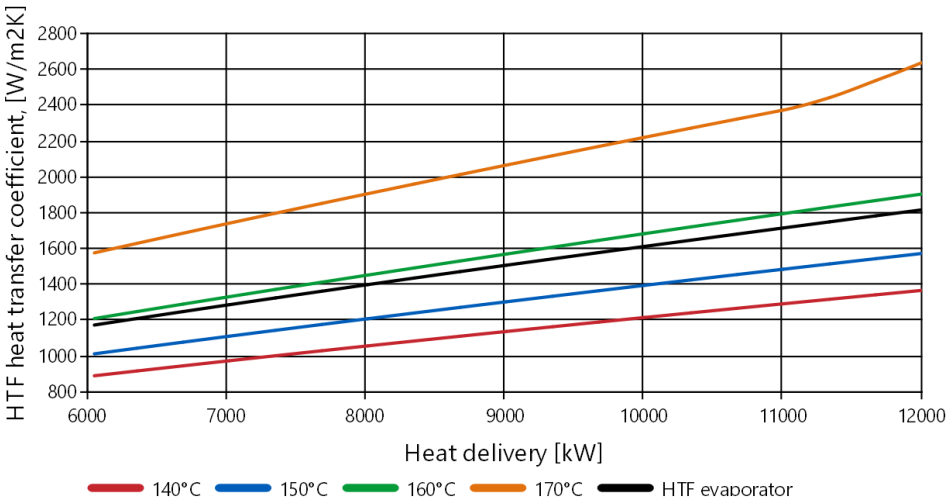

Figure 51: HTF heat transfer coefficients for the evaporator and various condenser inlet temperatures as a function of heat transfer rate.

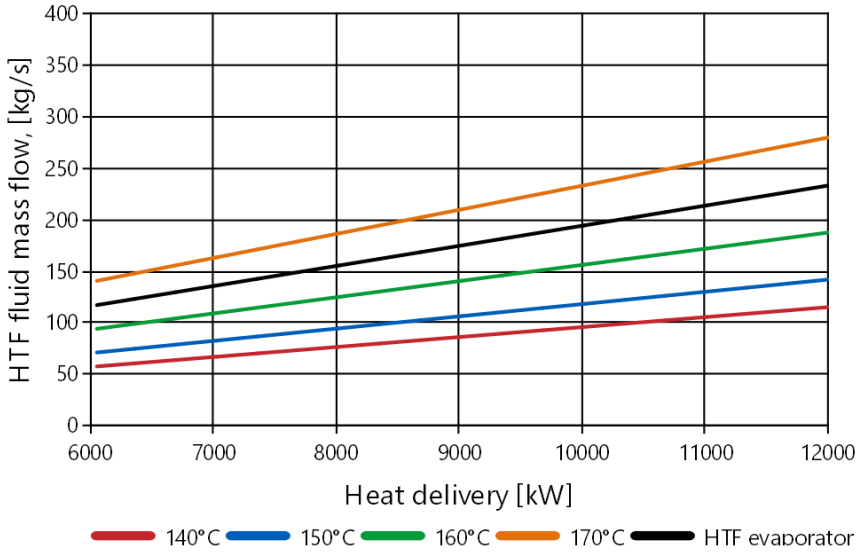

Figure 52: HTF mass flow rates for the evaporator and various condenser inlet temperatures as a function of heat transfer rate.

Because constant values for the heat transfer coefficients for the working fluid were used in the evaporator and condenser, the U-value is not reduced to the same extent as the h-value when the mass flow rate is reduced. As the heat delivery from the heat pump is reduced, the heat exchangers effectively become oversized and the heat transfer area more than compensates for the drop in U-value. This leads to reduced approach temperatures between the working fluid and HTF, which in turn reduces the effective temperature lift required by the heat pump. This is shown in Figure 53, which shows the inlet temperature of the steam entering the condenser and its pressure. As the inlet temperature is reduced, the pressure also reduces since this is the saturated vapor pressure. This leads to reduced compressor work and improves COP.

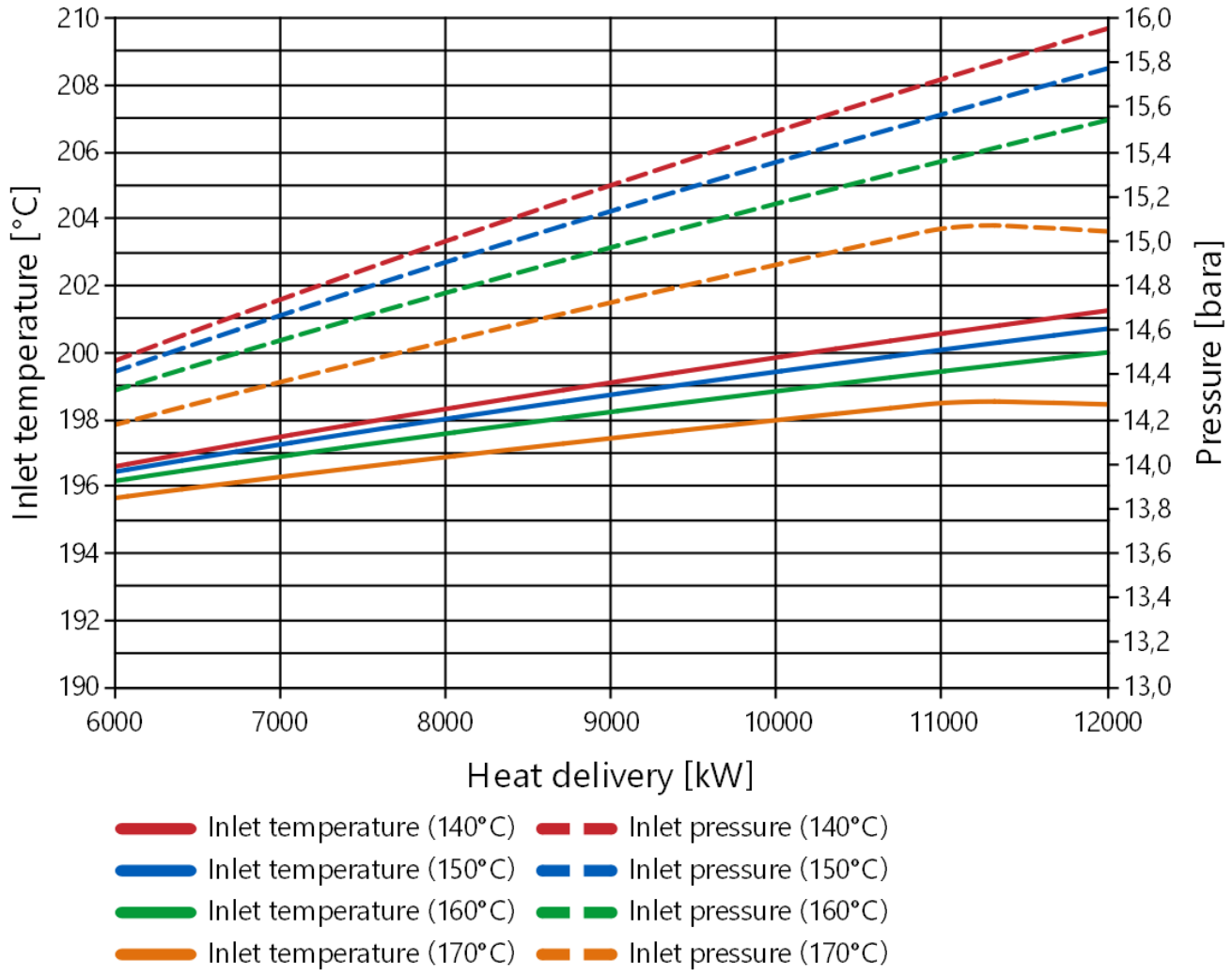

Figure 53: Working fluid condenser inlet temperature and pressure for varying HTF condenser inlet temperatures.

6.1.3.3 Turbo Compressor

Figure 54 shows how the compressor power consumption changes with varying heat loads. The power consumption for each compression stage ranges from around 350-450 kW at 50% heat load to about 700-900 kW at 100 % load, resulting in a total power consumption from around 1250 kW to 2500 kW. The results show that relationship between the power consumption and the heat delivery is relatively linear.

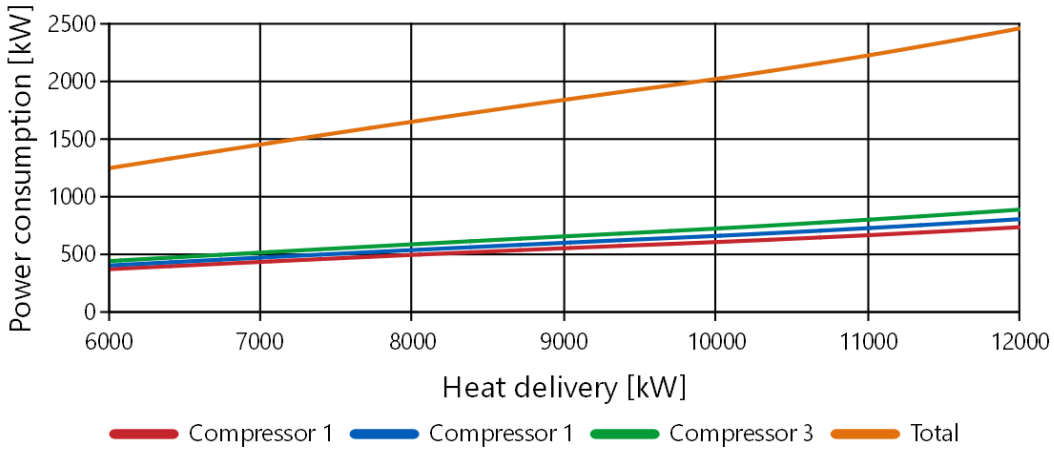

Figure 54: Compressor power consumption for HTF condenser inlet temperature 160°C.

An explanation to this can be found in Figure 55, which shows how the isentropic efficiency and pressure ratio changes with varying compressor speed. At design conditions, i.e. 90 000 rpm the pressure ratio is 1.79, and the isentropic efficiency is 0.75. As the heat load is reduced, the compressor speed is also reduced and the isentropic efficiency decreases, to around 0.65. This would normally result in significantly increased compressor specific work. However, as discussed in the previous section, a reduction in heat load also leads to a reduced condensation pressure. For the same reasons as for the condenser, it also leads to increased evaporation pressure. The result of this is that the pressure ratio for the compressors is reduced from 1.79 to 1.67 and partly compensates for the reduction in isentropic efficiency.

An explanation to why the highest COP values were obtained outside design conditions is how the isentropic efficiency changes when the heat load is reduced. Close to the design conditions the changes are small, and at 86 000 rpm, which corresponds to a heat load of around 85% (10 250 kW), the isentropic efficiency is still 0.74. The combination of a high isentropic efficiency, but slightly reduced pressure ratio is the reason why the best COP values were observed for heat loads in the 10 000 kW area.

In order to more accurately describe the performance at part loads, it would be beneficial to use a film heat transfer relation for the evaporation and condensation process instead of constant values. This would most likely increase the approach temperature between the hot and cold fluid in the heat exchangers and correspondingly increase compressor power consumption at part loads, leading to an even further reduction of COP at part load / off design conditions.

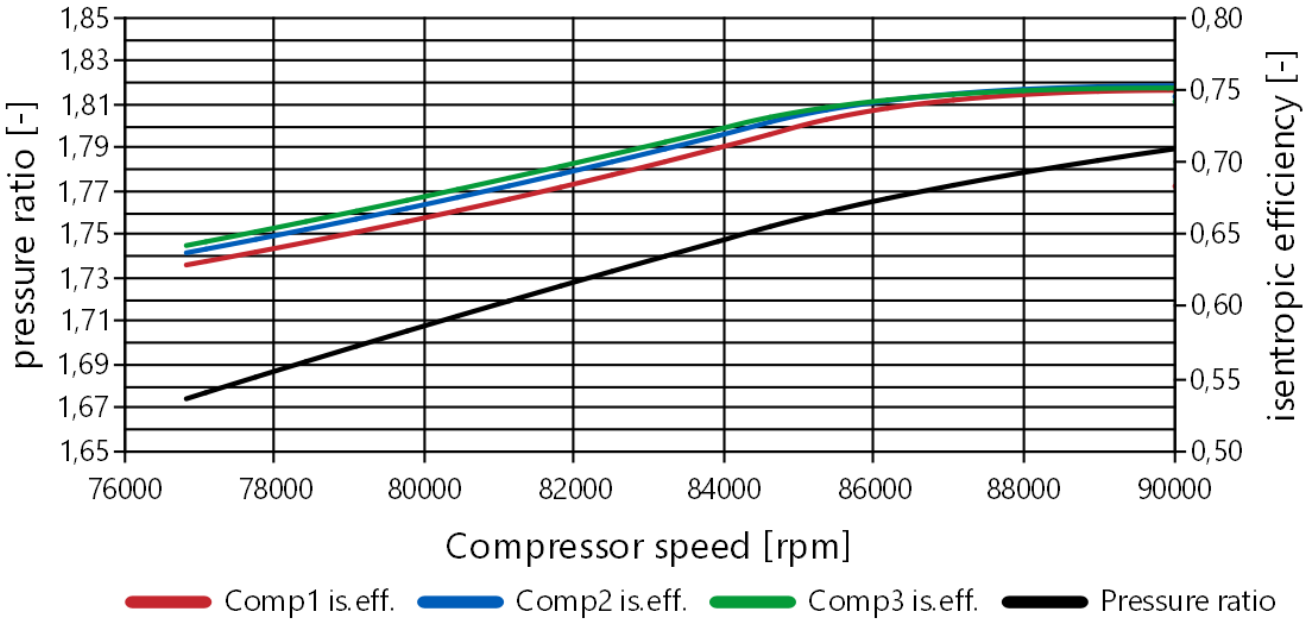

Figure 55: Isentropic efficiency and pressure ratio at varying compressor speeds for HTF condenser inlet temperature of 160°C.

Comparing the behaviour of the turbo compressors in relation to the compressor map in Figure 48 it is clear that as the speed is reduced, the operation moves closer to the assumed surge line. At 78 000 rpm the pressure ratio is 1.67 and the isentropic efficiency is about 0.65. Placing this point on the map would result in a point to the left of the surge line. Although it is not possible to conclude on the potential for surge issues at this point, it is an indication that the compressors could run into stall or surge issues when operating at 50% load. This would effectively limit the operational range of the heat pump. An option to enhance operational range and performance at part loads is to use multiple compressors in a parallel arrangement for load distribution.

6.1.3.4 Heat Exchanger Pressure Drop

The resulting frictional pressure drop for the HTF in the evaporator and for different HTF inlet temperatures in the condenser is shown in Figure 56. The pressure drop in the condenser at design conditions is about 140 mbar.

A reduction in heat load leads to reduced pressure drop due to lower mass flow rates. Correspondingly, if the HTF condenser inlet temperature is increased to 170°C the pressure drop is more than doubled at maximum load conditions. For the evaporator the pressure drop at design conditions is 210 mbar. With the length of the plates being around 0.8 m, this corresponds to a pressure drop of about 0.15-0.25 bar/m plate length.

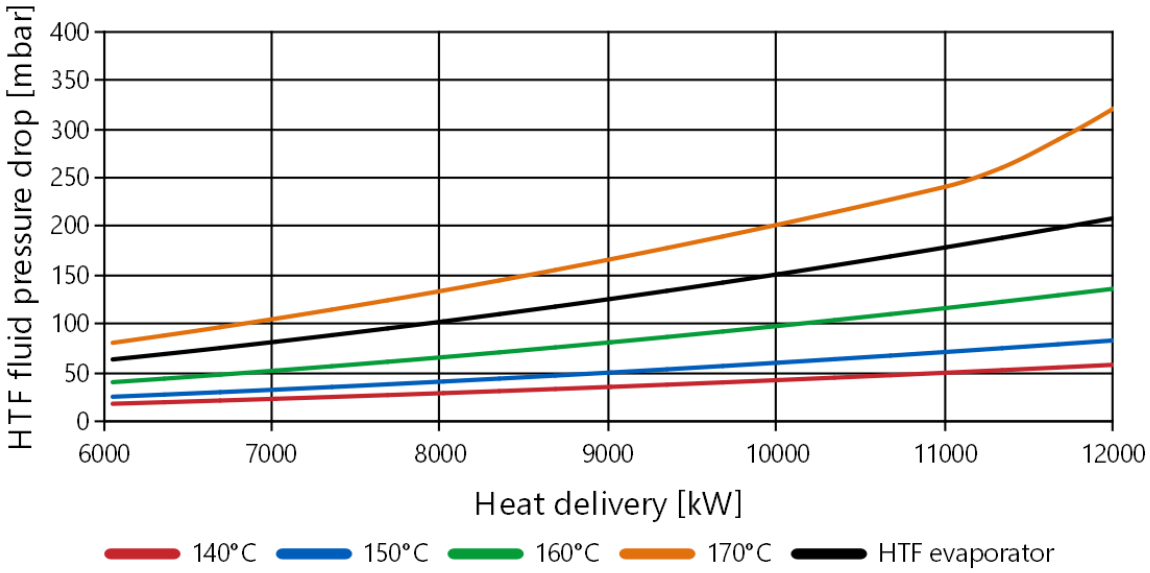

Figure 56: HTF pressure drop in the evaporator and the condenser.

6.1.3.5 De-superheating

The de-superheating mass flow rates are given in Figure 57, for design conditions. At maximum heat load, the values are similar to those obtained in the concept evaluations, given in Table 10. At 50% load, the mass flow rates reduce correspondingly with about 50%. The liquid injector therefore needs to handle a turndown ratio, i.e. the maximum flow / minimum flow of 2, which is achievable by most de-superheating systems.

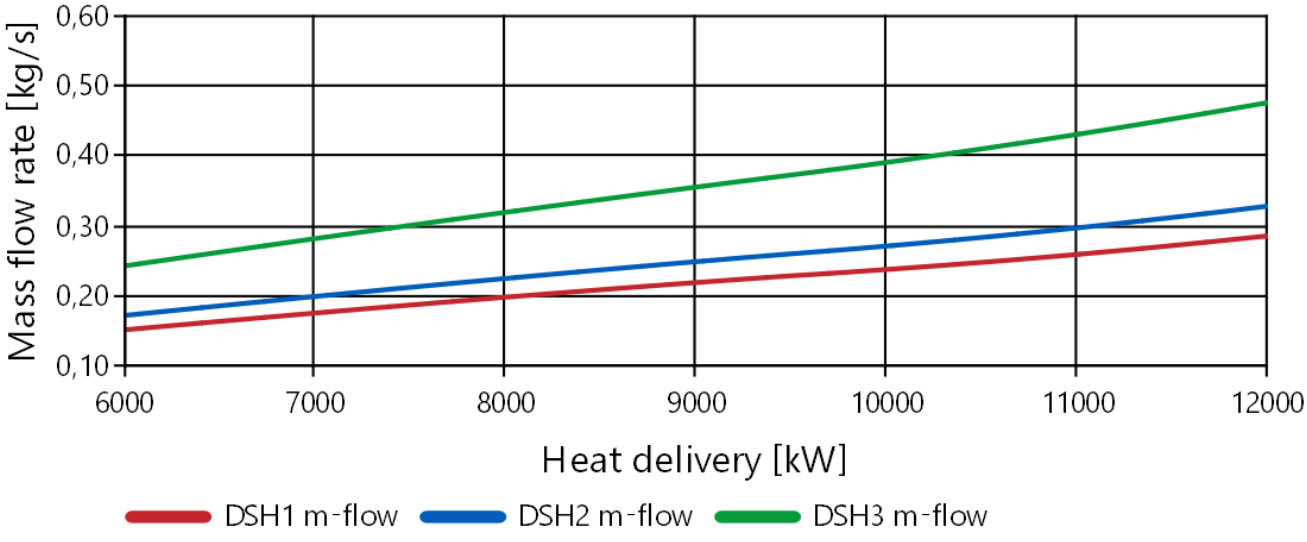

Figure 57: De-superheating mass flow rates.

6.1.3.6 Summary of results

The temperatures and pressures for all cases at maximum heat load are shown in Figure 58 and Figure 59, respectively. The data labels represent the case with HTF condenser inlet temperature of 160°C. Table 26 summarizes the main parameters of the heat pump at design conditions.

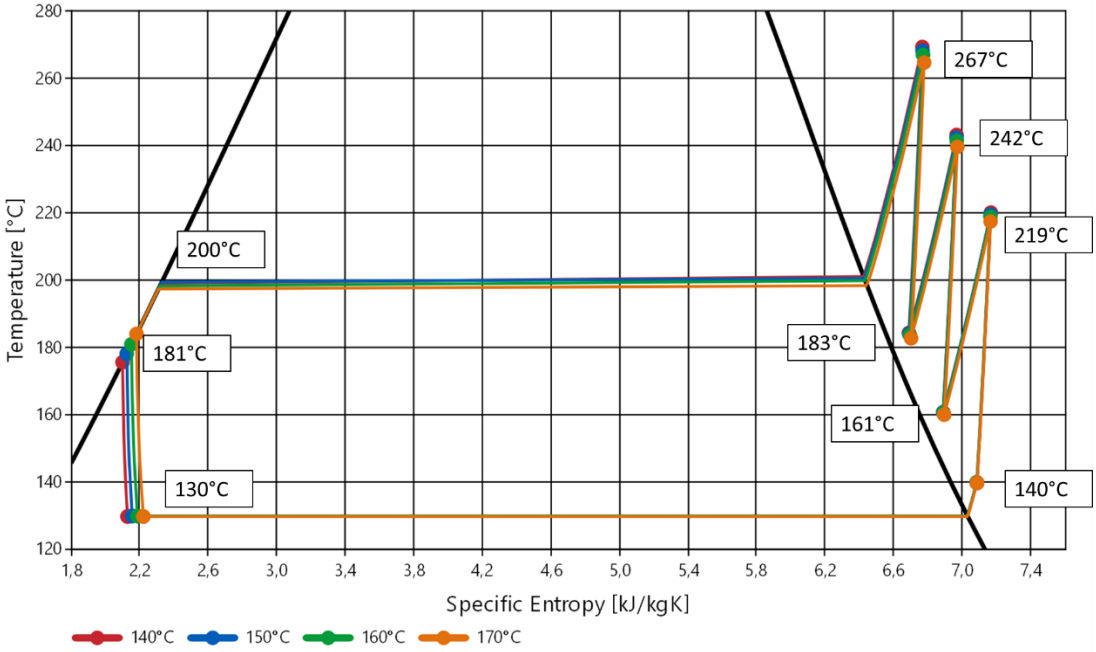

Figure 58: Temperature-entropy diagram of the heat pump cycle at 12 full load (12 MW heat rate) for varying HTF condenser inlet temperatures

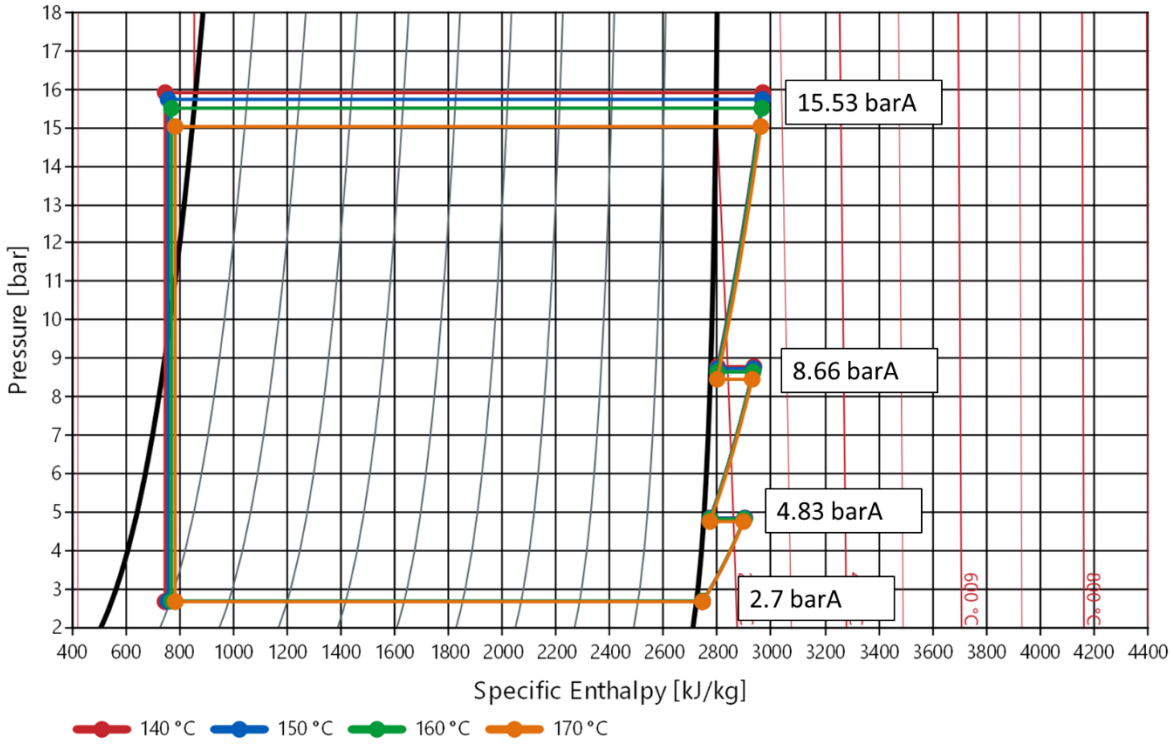

Figure 59: Pressure-enthalpy diagram of the heat pump cycle at 12 full load (12 MW heat rate) for varying HTF condenser inlet temperatures

Table 26: Summary of main parameters at design conditions (Thermal load: 12 MW, HTF condenser inlet temperature: 160°C)

Parameter	Value
Condenser:	
HTF mass flow [kg/s]	190
Working fluid mass flow [kg/s]	5.925
Total heat transfer area [m^2]	470
Evaporator:	
HTF mass flow [kg/s]	236
Working fluid mass flow [kg/s]	4.83
Total heat transfer area [m^2]	468
Heat transfer from PTC [kW]	9534
1st stage Compressor:	
Power [kW]	749
Volumetric flow rate, inlet [m3/h]	11990
2nd stage Compressor:	
Power [kW]	818
Volumetric flow rate, inlet [m3/h]	7340
3rd stage Compressor:	
Power [kW]	900
Volumetric flow rate, inlet [m3/h]	4496
Total compressor power [kW]	2468
De-superheating:	
1st stage water injection flow rate [kg/s]	0.29
2nd stage water injection flow rate [kg/s]	0.33
3rd stage water injection flow rate [kg/s]	0.48
Total injection flow rate [kg/s]	1.10

6.2 Reversed Brayton Cycle Heat Pump Modelica Simulations

6.2.1 System Description

The reversed Brayton sCO_2 heat pump system was modelled numerically with the software Dymola 2021 using the TIL component library implemented in the Modelica language.

The heat exchangers are modelled using the "Tube and tube" heat exchanger component with a counterflow arrangement. The ports on the HTF sides are connected to respective fluid sources and sinks according to the defined boundary conditions.

The compressor and expander component models are connected to the heat exchanger ports to form a closed cycle.

The component parameters have been adjusted to match design point operation conditions and PI-controllers are used to maintain specific system parameter values at off-design operation.

The model specifications are given in Table 27, while the graphical representation of the system is presented in Figure 60.

Table 27: Model specifications

Component	Model specification
Turbo compressor	Gasparovic turbo compressor model Design pressure ratio: 2.3717 Design speed: 90 000 rpm Max. stage efficiency: 1.803 Design inlet temperature: 150°C Design inlet pressure: 150 bara Design mass flow rate: 97.6686 kg/s
Gas cooler	Tube and tube heat exchanger. based on PCHE model by Ren et al. Tube length 8.518 m, 141784 tubes for each fluid. Total heat transfer area: 8879 m^2 Wall material: Inconel 617 Wall thickness 1 mm Heat transfer coefficient, h_CO_2: 970 W/m^2K Heat transfer coefficient, h_HTF: calculated based on available correlation for single phase fluids in the TIL tube and tube heat exchanger component Pressure drop HTF: Calculated based on available correlation for single phase fluids in the TIL tube and tube heat exchanger component
Gas heater	Tube and tube heat exchanger based on model by Ren et al. Tube length 1.26 m, 210714 tubes for each fluid. Total heat transfer area: 1911 m^2 Wall material: Inconel 617 Wall thickness 1 mm Heat transfer coefficient, h_CO_2: 798 W/m^2K Heat transfer coefficient, h_HTF: calculated based on available correlation for single phase fluids in the TIL tube and tube heat exchanger component. Pressure drop HTF: Calculated based on available correlation for single phase fluids in the TIL tube and tube heat exchanger component.
Expander	Efficiency based expander. Isentropic efficiency 75%. Fillfactor 1. Design speed: 90 000 rpm Intake volume: 1.273e-4 m^3

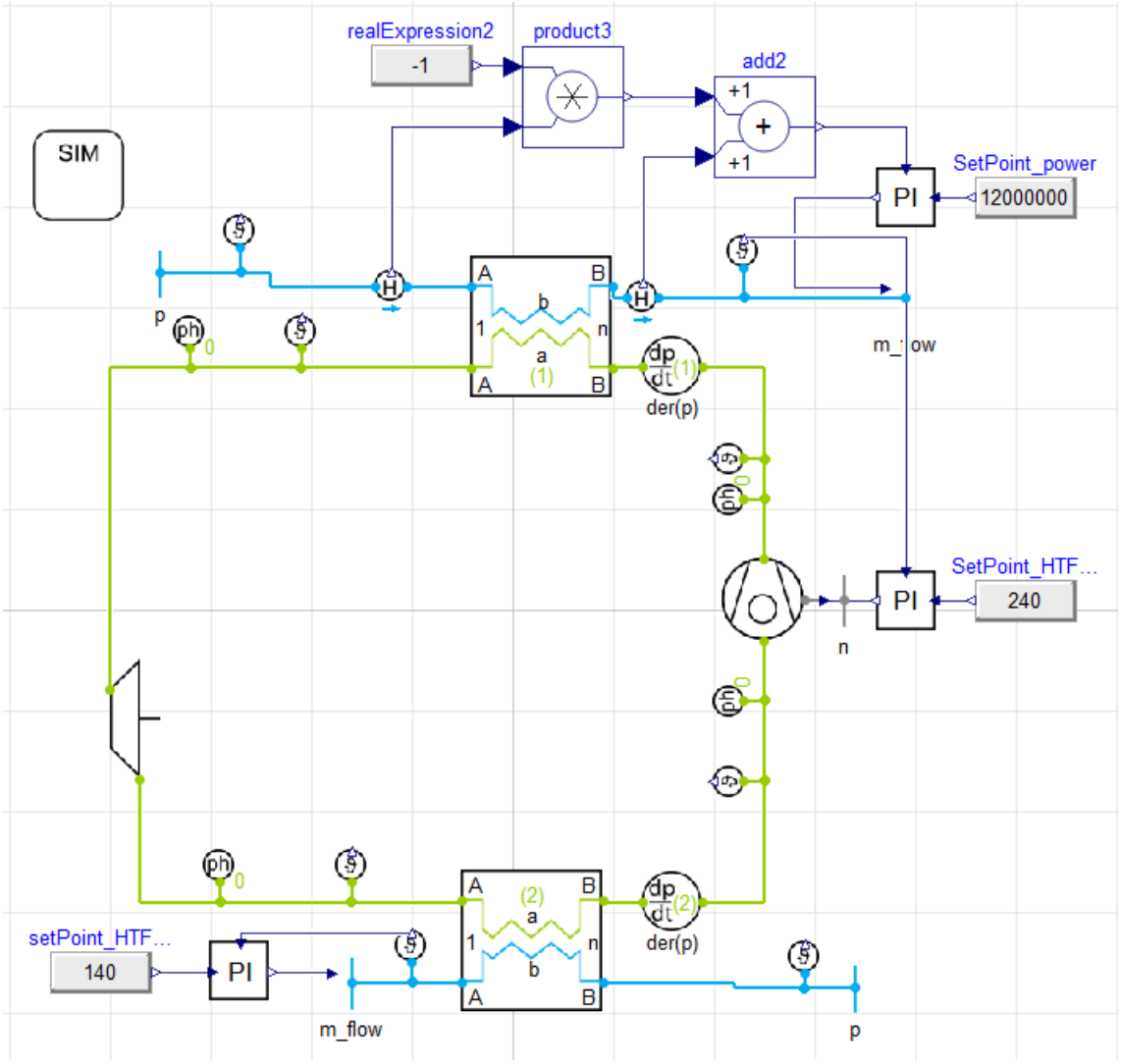

Figure 60: Heat pump system setup in Dymola 2021.

6.2.2 Component Model Description

6.2.2.1 Compressor

The compressor was modelled with the Gasparovic turbo compressor model described in section 6.1.1.1. A single stage was used, and the design parameters are summarized in the table above. The parameter max. stage efficiency was adjusted until the correct temperature was produced at the specified outlet pressure according to an isentropic efficiency of 70%. The speed of the compressor was controlled during simulations of a PI controller to keep the sink HTF outlet temperature at 240 °C.

6.2.2.2 Expander

The expander was modelled with an efficiency-based expander with parameters specified in the table above. The intake volume was adjusted during design to give the correct sCO_2 mass flow in the cycle. This value was fixed for further off-design simulations. To simulate a system where the expander and compressor share a common shaft, the expander speed was adjusted to be the same as the compressor speed for each simulation case.

6.2.2.3 Heat Exchangers

The heat exchangers were modelled with the tube and tube heat exchanger components. A number of tubes must be specified for each fluid side along with tube length, cross section circumference and cross section area. These values were calculated from the PCHE model presented by Ren et al. [47] For simplicity, the same number of tubes were used for both fluid sides in the heat exchanger. The wall geometry was specified by calculating the total area

of the tubes for one fluid side. The same thermal conductivity as used by Ren et al. [47] was used for the wall material.

The computer model of the heat exchanger uses a number of smaller heat exchanger cells in series where each cell is modelled with a thermal resistance between the hot and cold sides where the properties are constant within each cell. In order to capture the temperature profiles inside the heat exchanger, a sufficiently high number of cells is needed.

6.2.2.3.1 Gas Cooler

The number of tubes was calculated by specifying a Reynolds number of 10000. This also gave an estimated length to provide the heat transfer area need to deliver the specified heat rate with 10°C temperature difference between the heat exchanger sides. The length of the tubes was adjusted through iterations in the Modelica model until the correct heat transfer was achieved with the cycle design specifications on the fluid inlet values.

In the case simulations, the HTF mass flow was controlled with a PI controller to give a specific output heat rate.

6.2.2.3.2 Gas Heater

A similar procedure to the one used to specify the parameters for the gas cooler was used to specify those for the gas heater. A PI controller was used to control the HTF mass flow to give the specific HTF outlet temperature in the case simulations.

6.2.3 Simulation Case Description

The parameters defining the system component models were specified according to design point operation as described earlier. At the design point the HTF fluid inlet temperature on the sink side was 160°C. To simulate the system at expected off-design operation, cases with HTF fluid inlet temperature of 140°C, 150°C, 160°C and 170°C were simulated.

Cases with off-design system loads were also simulated. At design the heat pump system delivers 12 MW at the heat sink. Off-design cases with 6 MW and 8 MW sink heat delivery were simulated for each of the 4 HTF inlet temperature values.

For each simulation case, the system was simulated to steady state.

6.2.4 Results – and Discussions

6.2.4.1 Full Load

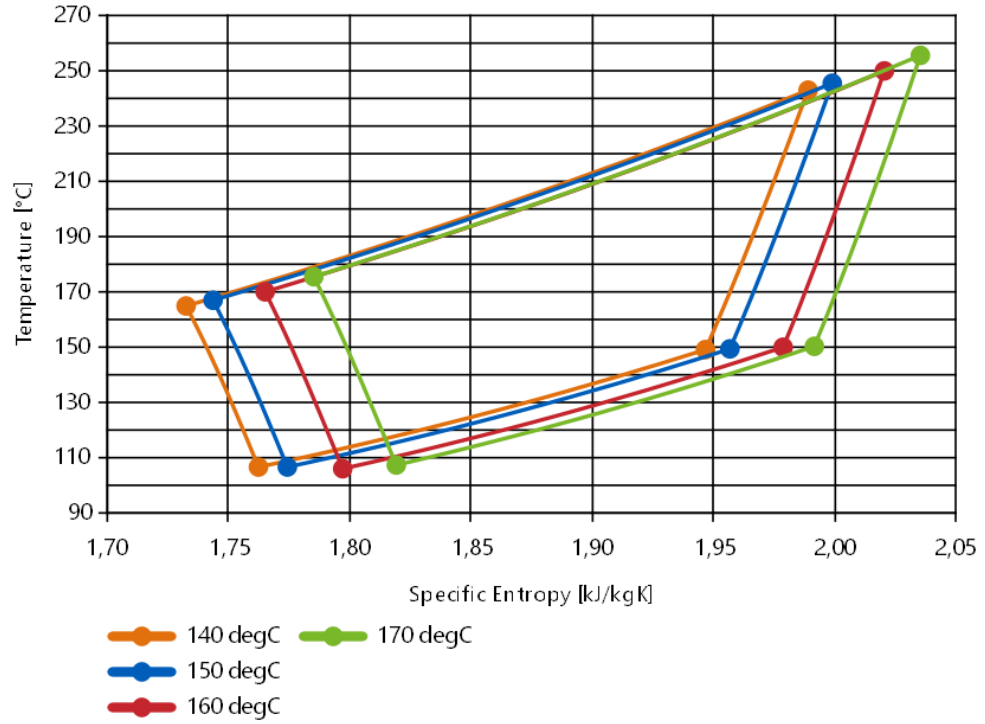

Figure 61: Temperature-entropy diagrams for different HTF inlet temperatures at full load.

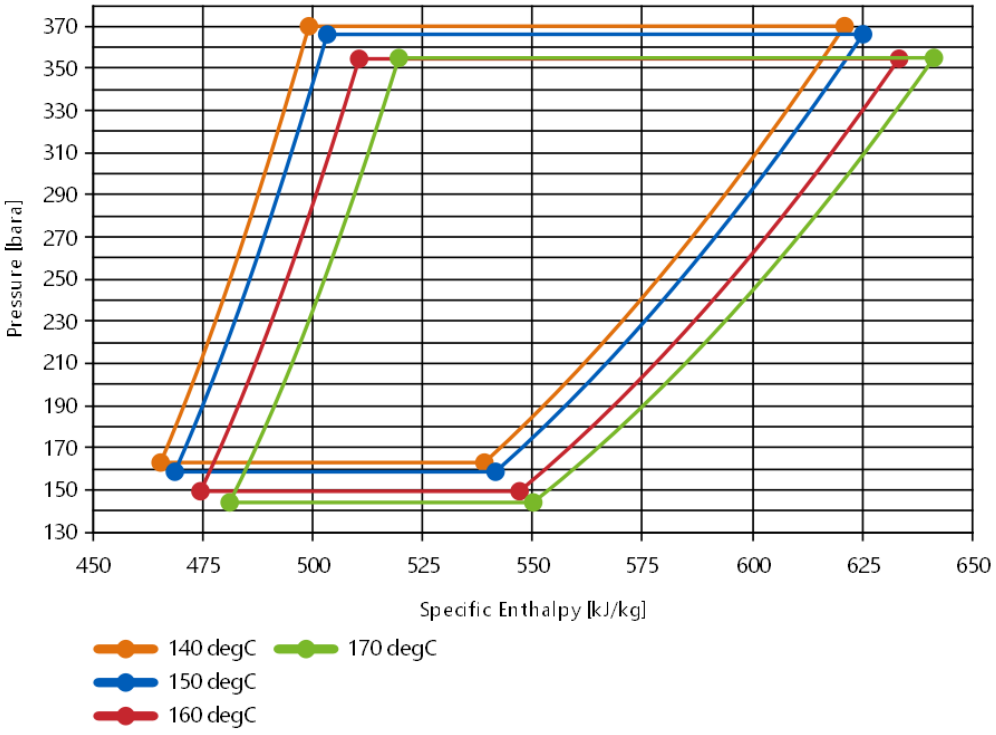

Figure 62: Pressure-enthalpy diagrams for cases with different HTF inlet temperatures at full load.

The temperature-entropy (T-s) and pressure-enthalpy (p-h) diagrams for the heat pump cycles at full load for different HTF inlet temperatures are shown in Figure 61 and Figure 62, respectively.

From the T-s diagram, it can be seen that the temperature glides at the heat sinks are very similar for all cases although there seems to be a slight decrease in the range of the temperature glide with decreasing HTF inlet temperature from the design value (160 °C). This indicates that the mass flow remains nearly the same as HTF inlet temperature is changed. The mass flow is somewhat restricted by the fact that the expander intake volume is fixed and the rotation speed is coupled to the compressor rotation speed. The mass flow varies only from 97.77 kg/s to 98.66 kg/s among the four cases, as seen in Table 28.

The temperature difference between the working medium and HTF, between gas cooler inlet and outlet increases with decreasing inlet HTF temperature which means greater total entropy generation for the same heat delivery.

Although the compressor operation is removed further from the design point with decreasing HTF inlet temperature from 160 °C, the compressor work during the compression is reduced which is reflected in the shorter horizontal distance along the compression line in the p-h diagram. Since the heat delivery is equal for all cases, the cases with lower HTF inlet temperatures have higher COPs. In the case with HTF inlet temperature of 170°C, the compression starts at a lower pressure and ends at the same pressure compared to the case with 160°C and involves a larger compression work to reach the higher temperature, which is necessary to drive the heat transfer in the gas cooler.

There is similarly a larger expansion work in the expander, but with a smaller enthalpy difference compared to the 160°C case as the compression and expansion involves irreversible losses. This results in a lower COP for the 170°C case. The numerical values related to these parameters are presented in Table 28. The lower HTF temperatures enable lower temperature in the working medium which is reflected in the lower compressor outlet temperature and results in a higher Lorenz COP (as calculated from the working fluid temperatures, i.e. not using the external HTF boundary temperatures so that the effect of heat exchanger efficiency is removed). Figure 63 shows the COP values for the cycle along with the Lorenz COP calculated from the temperatures at the inlet and outlet of the heat exchangers in each case. A comparison of the curves indicates that the thermodynamic penalty of higher temperature lifts can explain the general trend in the reduction of COP with increasing HTF inlet temperatures. However, as the HTF inlet temperature is reduced from the design point, the increase in COP is smaller than that indicated by the Lorenz COP. This indicates that the off-design operation results in a reduced efficiency which partially cancel the benefit of increased Lorenz COP. In a similar manner, the reduced Lorenz COP and reduced efficiency at off-design operation compound to give a larger decrease than the one expected from the Lorenz COP alone as the HTF inlet temperature is increased above the design condition.

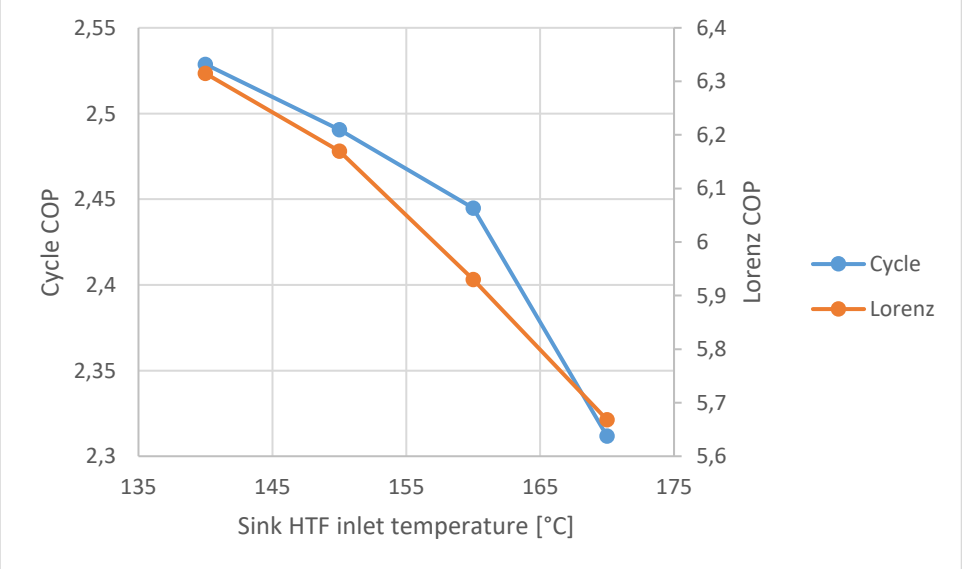

Figure 63: COP for the cycle and Lorenz COP calculated from the cycle temperatures.

Calculated from the temperatures at the HTF boundaries, the Lorenz efficiency at design point is 9.64, giving a Lorenz efficiency of 25.4%.

The inlet and outlet temperatures of working medium in the gas cooler remains nearly constant for the investigated operation modes at full load.

Table 28: Summary of the main parameters of the full-scale ship250 reversed Brayton heat pump with a thermal capacity of 12 MW.

	Gas cooler: HTF inlet temperature [°C]			
Parameter	**140**	**150**	**160**	**170**
Cycle:				
Working fluid mass flow [kg/s]	98.554	98.516	97.765	98.659
Highest pressure [barA]	370.544	366.685	355.068	355.479
Highest temperature [°C]	242.981	245.478	249.948	255.655
Gas cooler:				
HTF mass flow [kg/s]	55.584	61.248	68.335	77.456
HTF pressure drop [kPa]	11.202	11.639	14.465	16.482
Gas heater:				
HTF mass flow [kg/s]	180.096	178.257	146.046	169.027
HTF pressure drop [kPa]	6.187	6.121	6.036	5.796
Heat transfer from PTC [kW]	7254.84	7180.74	7091.81	6809.06
Compressor:				
Power [kW]	8069.22	8229.54	8434.45	8985.11
Volumetric flow rate, inlet [m3/h]	1365.26	1411.096	1507.90	1590.77
Expander:				
Power [kW]	3323.81	3411.44	3526.27	3794.16
Volumetric flow rate, inlet [m3/h]	656.760	667.603	688.102	710.539

6.2.4.2 Reduced Load

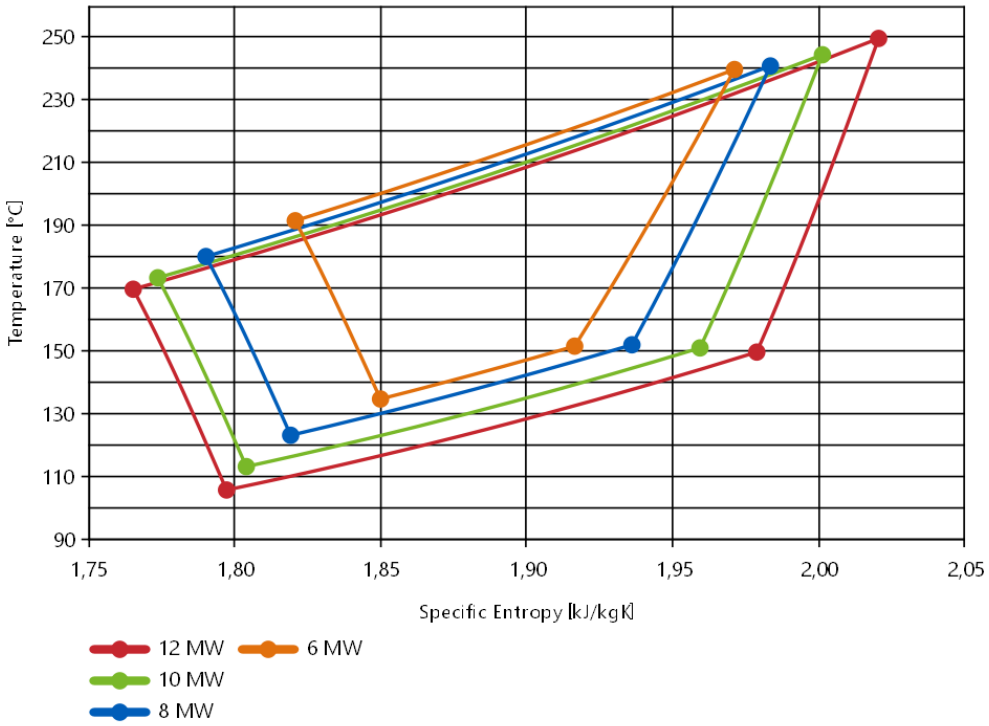

Figure 64:Temperature-entropy diagrams for cases with different heat loads and 160°C HTF inlet temperature.

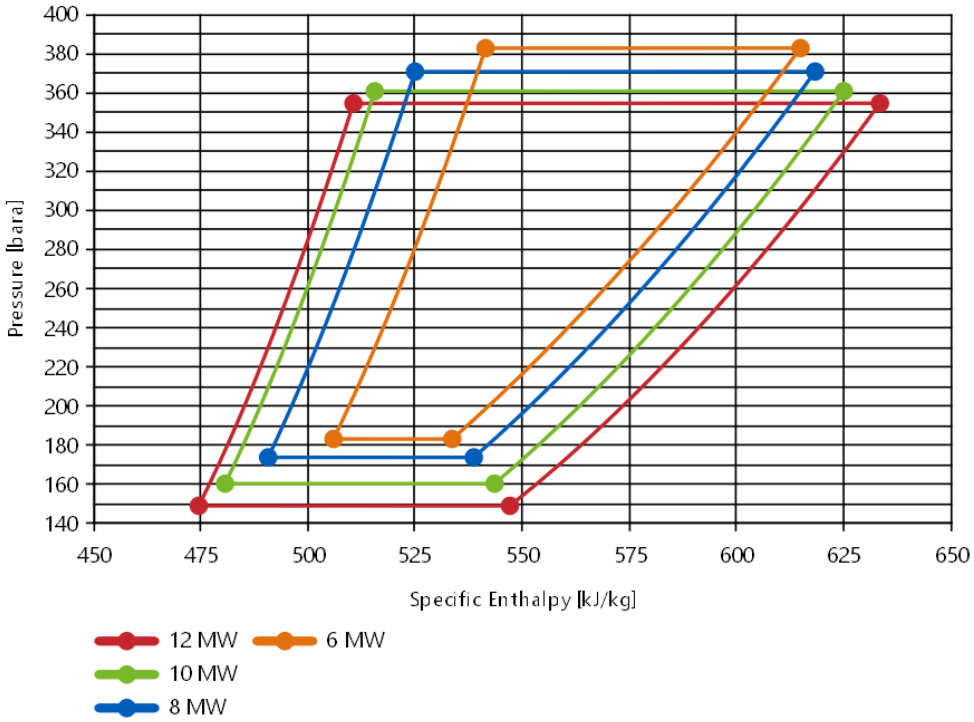

Figure 65:Pressure-enthalpy diagrams for cases with different heat loads and 160°C HTF inlet temperature.

Figure 64 and Figure 65 represent the T-s and p-h diagrams, respectively, for the heat pump cycles with HTF inlet temperature of 160 °C for varying heat output. From these diagrams it can be seen that the heat sink temperature glide range decreases proportionally more than the enthalpy change of compression as the heat load is decreased, which in turn gives a lower COP. This is reflected in the general trend of decreasing COP with reduced load as shown in Figure 66.

The increased compressor inlet pressure seen with decreasing load leads to a compressor operation further from the design point. The first p-h diagram shows that the cycle with HTF inlet temperature 170°C has a compressor inlet pressure below the design pressure. The relative offsets of the different cases could explain why the isentropic efficiency is highest for the 170°C case on partial load, decreasing with decreasing HTF inlet temperature, as the compressor remains closest to design operation when the load percentage is decreased beyond a certain point. The load at where this happens is indicated by the crossing of the curves labelled "160°C" and "170°C" in Figure 67 (which is an interpolation in the figure so the value is not exact) which shows the isentropic efficiency of the compressor for the different cases.

While the seeming "reversal" of the arrangement of curves between Figure 66 and Figure 67 in the upper load range is possibly due to the fact that the Lorenz efficiency dominates the COP at these loads as was elaborate on in the analysis of the full load operation. The crossing of the curves in Figure 66 as the load is reduced could indicate that off-design operation dominates the COP in the lower load range.

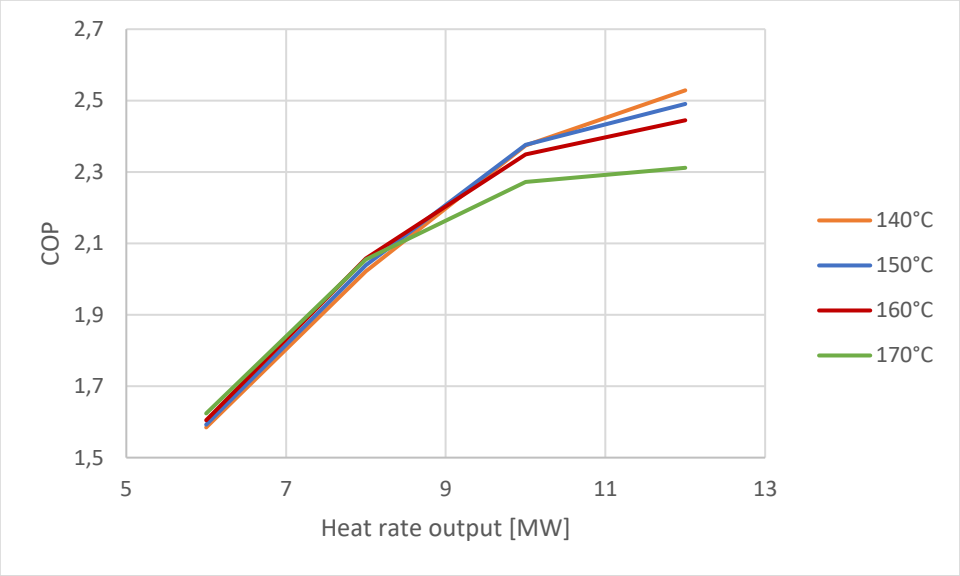

Figure 66: COP as function of heat rate output for the different HTF inlet temperatures.

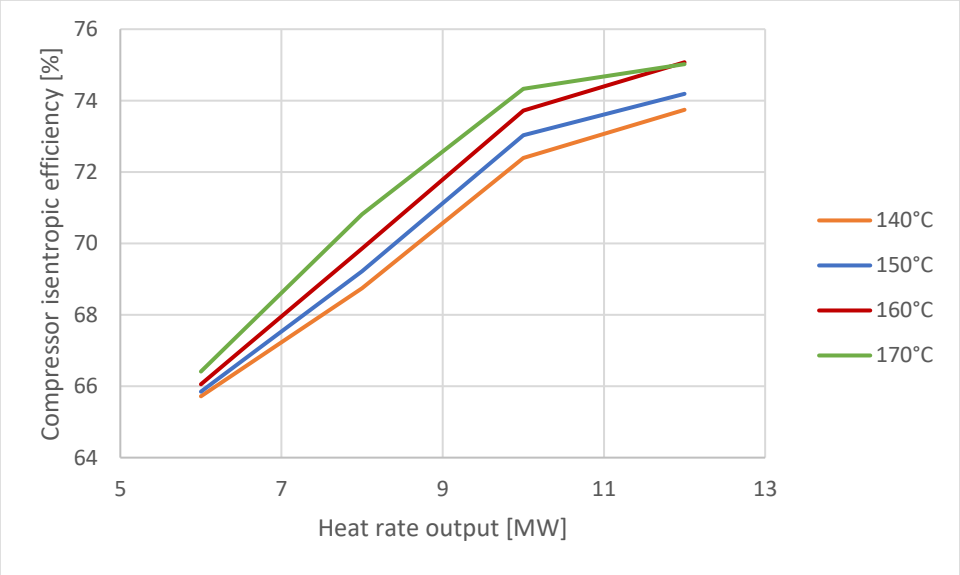

Figure 67: Isentropic efficiency of the compressor as function of heat rate output for the different HTF inlet temperatures.

For the cases with lower load, it seems like the working medium could have benefited from running with a lower mass flow and a larger temperature glide range, as the reduced temperature glide is a large reason for the reduced COP. During the simulations, the expander rotation speed was coupled to the rotation speed of the compressor in

a nearly 1:1 ratio. With a fixed intake volume from the setup at design condition, this put a constraint on the volume flow through the expander and therefore largely constrained the mass flow in the cycle. A system where the expander speed is adjusted to e.g. control the outlet temperature of the working medium from the gas cooler, the cycle could possibly perform better in the range of reduced load.

The elevated cycle pressures associated with the off-design operation could be a reason for concern with respect to system safety and component integrity. The compressor outlet pressure could therefore be an important parameter to control. This would also shift the compressor operation closer to design pressure conditions for the off-design cases, but the pressure ratio and mass flow could possibly be pushed further from the design point.

For all cases, the compressor inlet temperature remained nearly the same, although this was not a condition that was controlled directly.

7 Conclusions

This report presents an evaluation of initial heat pump concepts and integration principles for SHIP200. Two main concepts are developed; a high-temperature concept based on water (R718) for short-term heat delivery up to 200°C and a reversed Brayton heat pump concept based on CO_2 (R-744) for long-term heat delivery up to 250°C.

The market overview shows that there is a great demand for heat supply in the temperature range of 100-200°C in many industrial sectors. A few heat pumps can reach temperatures in the range of 120°C-165°C. However, these are either at laboratory or pre-commercialization stage.

Water is a natural working fluid with many advantageous properties, and is one of few suitable natural fluids that can be utilized in a vapor compression refrigeration cycle with heat delivery up to 200°C. The use of turbo compressors can offer great capacities in terms of flow rates with a compact footprint and can therefore contribute to significantly reduced investment costs. However, the pressure ratio is limited and for the steam heat pump, multiple compression steps are necessary to reach the expected temperature lift in SHIP200. It is estimated that the turbo compressor is the component in the steam heat pump with the lowest TRL, due to temperature limitations. The other main components are already at higher TRL.

Supercritical CO_2 is, like water, a natural working fluid. It offers many of the same advantageous properties, plus an exceptional volumetric refrigeration capacity. The reversed Brayton cycle heat pump operates with the working media gas phase only, and heat is therefore transferred at gliding temperatures. Large temperature lifts can therefore be achieved with small pressure ratios compared to a vapor compression refrigeration cycle, and with the use of sCO_2 very compact systems can be designed.

The components that can be operated at the required pressure conditions for an sCO_2 heat pump for SHIP200 are not yet commercially available. Research and development on sCO_2 components are ongoing, mainly for purposes of Brayton power cycle development, and could possibly enable a reversed Brayton heat pump system for temperature delivery at 240°C - 250°C in the future.

Printed circuit heat exchangers have been suggested as suitable for sCO_2 applications while some improvement may be needed to be operated under the high pressures. Turbomachinery for sCO_2 is being researched where turbo compressors have been suggested for the compression process in the power range considered in this work.

Concept evaluations of both the steam heat pump and the reversed Brayton cycle heat pump were made. SHIP200 boundary conditions were assumed. The capacity reflected a large-scale industrial system of 12 MW_{th}. Sensitivity analyses in terms of HTF inlet temperature to the condenser/gas cooler in order to reflect charging/discharging of the combined heat and storage was performed.

The concept evaluations for the steam heat pump showed that subcooling and de-superheating after all compression stages resulted in the best performance, achieving a COP of 5 at design conditions. Evaluations of an open-cycle steam heat pump showed that excellent COP values can be achieved. However, this depends on the steam supply pressure. With a pressure ratio equal to a closed-cycle heat pump, the performance is relatively similar. Cost estimation showed a specific investment cost in the range of 267 €/kW, which is competitive. It is expected that the investment cost for a system with all components included is higher, and that smaller scale systems will have a higher investment cost.

The concept evaluations for the reversed Brayton heat pump showed that the optimal low- and high-pressure of the cycle was 150 barA and 356 barA, respectively, which resulted in a COP of 2.44. For large temperature lifts, the use of an internal heat exchanger (IHX) can be advantageous to the performance if the temperature glide of the external system is small. However, the use of IHX was not found to be feasible for the evaluated conditions. It was shown that improved turbomachinery isentropic efficiency could possibly give a significant improvement to the COP.

Modelica simulations of both the steam heat pump and reversed Brayton cycle heat pump concepts were performed based on the results from the concept evaluations and included simulations of variable load conditions (50-100%). Both heat pump models used a Gasparovic model for the turbo compressor. The steam heat pump was modelled using plate and frame heat exchangers based on geometric properties from existing heat exchangers from Alfa Laval for the condenser and evaporator, while the reversed Brayton cycle used properties from printed circuit

heat exchangers modelled as using a tube and tube heat exchanger model. The reversed Brayton cycle used a constant isentropic efficiency expander for expansion.

The Modelica simulations of the steam heat pump resulted in COP values of 4.97 at design conditions and 4.75 at minimum load conditions. The COP values at part loads conditions were higher than expected due to high heat exchanger performance caused by limitations in the numerical model. In a real situation, the COP values at part loads are expected to be lower. Still, the required heat transfer area was more than twice of what was initially calculated in the concept evaluations. The evaluation of the compressor model indicated potential surge conditions at 50% load. Overall, the model performed as expected at design conditions, and the control strategy and integration of the heat pump worked quite well under all operational conditions. The model accuracy at part load conditions can be improved.

The Modelica simulations of the reversed Brayton resulted in the same COP as for the concept evaluations at design point, 2.44. Reducing the HTF gas cooler inlet temperature gave a slight increase (3.4%) in the COP. Off-design operation generally decreased the COP and the isentropic efficiency of the compressor. At 50% load, the COP had been reduced by 34%. Improved off-design operation could possibly be achieved by improving the system control strategy. Partial load operation could possibly benefit from reduced mass flow to achieve higher temperature glides, although this shifts compressor operation further from the design point. Control of the cycle pressures could be necessary for safety and could possibly improve the COP by making the compressor operate closer to design conditions. The model would benefit from using an expander with similar characteristics as the turbo compressor for improved control and accuracy.

8 Degree of Progress

Cost estimations of the reversed Brayton Cycle heat pump were not completed due to lack of cost data as the components have a very low commercial maturity. However, further revisions of the present deliverable are not expected, since deliverable D3.4 will present the evolution of the work in WP3 T3.1 as it progresses throughout the project.

Thus, this deliverable is considered complete.

9 Dissemination Level

This deliverable is public and therefore it will be available for download on the project's website and on demand.

10 References

[1] H. J. Bauder, “HOCHTEMPERATUR-WAERMEPUMPEN - MOEGLICHKEITEN DER ANWENDUNG UND IHRE GRENZEN.,” *Waerme*, vol. 86, no. 3, pp. 27–32, 1980.

[2] C. Arpagaus, F. Bless, M. Uhlmann, J. Schiffmann, and S. S. Bertsch, “High temperature heat pumps: Market overview, state of the art, research status, refrigerants, and application potentials,” *Energy*, vol. 152, pp. 985–1010, 2018, doi: 10.1016/j.energy.2018.03.166.

[3] C. Mateu-Royo, J. Navarro-Esbrí, A. Mota-Babiloni, M. Amat-Albuixech, and F. Molés, “State-of-the-art of high-temperature heat pumps for low-grade waste heat recovery,” *XI Natl. II Int. Eng. Thermodyn. Congr.*, no. June, pp. 217–228, 2019, [Online]. Available: https://www.researchgate.net/publication/333825430%0AState-of-the-art.

[4] O. Bamigbetan, T. M. Eikevik, P. Nekså, and M. Bantle, “Review of vapour compression heat pumps for high temperature heating using natural working fluids,” *Int. J. Refrig.*, vol. 80, pp. 197–211, 2017, doi: 10.1016/j.ijrefrig.2017.04.021.

[5] S. S. Foslie, “Possibilities for energy recovery by steam compression cycles.”

[6] IEA, *Annex 35: Application of Industrial Heat Pumps, Final Report, Part 1, Report No. HPP-AN35-1*. 2014.

[7] et al. Fleiter T, Elsland R, Rehfeldt M, Steinbach J, Reiter U, Catenazzi G, “Profile of heating and cooling demand in 2015,” 2017. Accessed: Jun. 02, 2021. [Online]. Available: https://heatroadmap.eu/wp-content/uploads/2018/11/HRE4_D3.1.pdf.

[8] F. Bless, C. Arpagaus, S. S. Bertsch, and J. Schiffmann, “Theoretical analysis of steam generation methods - Energy, CO2 emission, and cost analysis,” *Energy*, vol. 129, pp. 114–121, Jun. 2017, doi: 10.1016/j.energy.2017.04.088.

[9] “HeatBooster | Heat Pump Technology — Heaten.” https://www.heaten.com/technology (accessed Jun. 02, 2021).

[10] O. Bamigbetan, T. M. Eikevik, P. Nekså, M. Bantle, and C. Schlemminger, “Theoretical analysis of suitable fluids for high temperature heat pumps up to 125 °C heat delivery,” *Int. J. Refrig.*, vol. 92, 2018, doi: 10.1016/j.ijrefrig.2018.05.017.

[11] B. Zühlsdorf, F. Bühler, M. Bantle, and B. Elmegaard, “Analysis of technologies and potentials for heat pump-based process heat supply above 150 °C,” *Energy Convers. Manag. X*, vol. 2, p. 100011, 2019, doi: 10.1016/j.ecmx.2019.100011.

[12] V. Aga, E. Conte, R. Carroni, B. Burcker, and M. Ramond, “Supercritical CO2-Based Heat Pump Cycle for Electrical Energy Storage for Utility Scale Dispatchable Renewable Energy Power Plants,” 2016.

[13] M. Lauermann, “Feasibility study on high temperature heat pump with heat sink at 200°C. Identification of working fluid, technology readiness levels and system availability,” *FME HighEFF*, pp. 1–21, 2017, [Online]. Available: https://www.sintef.no/globalassets/project/higheff/deliverables-ra3/d3.2_2017.01-feasibility-study-on-high-temperature-heat-pump-to-200-degc.pdf.

[14] M. Chamoun, R. Rulliere, P. Haberschill, and J.-L. Peureux, “Purdue e-Pubs Experimental Investigation of a New High Temperature Heat Pump Using Water as Refrigerant for Industrial Heat Recovery Experimental investigation of a new high temperature heat pump using water as refrigerant for industrial heat recovery.” Accessed: May 31, 2021. [Online]. Available: http://docs.lib.purdue.edu/iracc/1165.

[15] H. Madsboell, M. Weel, and A. Kolstrup, “DEVELOPMENT OF A WATER VAPOR COMPRESSOR FOR HIGH TEMPERATURE HEAT PUMP APPLICATIONS.”

[16] M. Chamoun, R. Rulliere, P. Haberschill, and J. L. Peureux, “Experimental and numerical investigations of a new high temperature heat pump for industrial heat recovery using water as refrigerant,” *Int. J. Refrig.*, vol. 44, pp. 177–188, Aug. 2014, doi: 10.1016/j.ijrefrig.2014.04.019.

[17] M. Bantle, C. Schlemminger, I. Tolstorebrov, M. Ahrens, and K. Evenmo, “Performance evaluation of two

stage mechanical vapour recompression with turbo-compressors," 2018, doi: 10.18462/iir.gl.2018.1157.

[18] "Free2heat." https://www.sintef.no/en/projects/2019/free2heat/ (accessed Jun. 11, 2021).

[19] "Developing the world's 'hottest' heat pump ever." https://norwegianscitechnews.com/2021/04/developing-the-worlds-hottest-heat-pump-ever/ (accessed Jun. 11, 2021).

[20] M. Bantle, C. Schlemminger, and C. GABRIELII Marcel AHRENS, "Turbo-compressors for R-718: Experimental evaluation of a two-stage steam compression cycle," 2019, doi: 10.18462/iir.icr.2019.0973.

[21] "https://superchargersonline.com/." https://superchargersonline.com/2002/04/05/roots-type-superchargers-explained/ (accessed Jun. 10, 2021).

[22] "https://www.lghvacstory.com/." https://www.lghvacstory.com/compressors/ (accessed Jun. 10, 2021).

[23] "WORKING PRINCIPLE OF CENTRIFUGAL COMPRESSOR." https://www.hkdivedi.com/2019/10/working-principle-of-centrifugal.html (accessed Jul. 08, 2021).

[24] B. Zühlsdorf, C. Schlemminger, M. Bantle, K. Evenmo, and B. Elmegaard, "Design recommendations for R-718 heat pumps in high temperature applications," *Refrig. Sci. Technol.*, vol. 2018-June, no. c, pp. 1101–1110, 2018, doi: 10.18462/iir.gl.2018.1367.

[25] M. N. Šarevski and V. N. Šarevski, "Thermal characteristics of high-temperature R718 heat pumps with turbo compressor thermal vapor recompression," *Appl. Therm. Eng.*, vol. 117, pp. 355–365, May 2017, doi: 10.1016/j.applthermaleng.2017.02.035.

[26] R. Smith, *Chemical Process Design and Integration*. John Wiley & Sons, Ltd, 2005.

[27] S. R. Nordtvedt, B. R. Horntvedt, and J. J. Eikefjord, "HYBRID HEAT PUMP FOR WASTE HEAT RECOVERY IN Norwegian Food Industry," pp. 57–62, 2011, doi: http://dx.doi.org/10.14279/depositonce-4859.

[28] T. Kaida, I. Sakuraba, K. Hashimoto, and H. Hasegawa, "Experimental performance evaluation of heat pump-based steam supply system," in *IOP Conference Series: Materials Science and Engineering*, Jul. 2015, vol. 90, no. 1, p. 012076, doi: 10.1088/1757-899X/90/1/012076.

[29] "Alfa Laval AlfaNova HP400." www.alfalaval.com (accessed Jun. 13, 2021).

[30] "Alfa Laval AC1000DQ." www.alfalaval.com (accessed Jun. 13, 2021).

[31] G. Lee *et al.*, "Development of steam generation heat pump through refrigerant replacement approach," 2017.

[32] P. Stathopoulos, "The design process of the DLR Brayton cycle High Temperature Heat Pump (HTHP) Deep dive – IEA Annex 58." 2021.

[33] J. Hoppe, "MAN and ABB introduce unique Energy Storage Solution." pp. 3–5, 2018.

[34] Y. Zhang *et al.*, "Performance analysis of a large-scale helium Brayton cryo-refrigerator with static gas bearing turboexpander," *Energy Convers. Manag.*, vol. 90, pp. 207–217, Jan. 2015, doi: 10.1016/j.enconman.2014.10.068.

[35] G. Angelino and C. Invernizzi, "Prospects for real-gas reversed Brayton cycle heat pumps Perspectives des pompes chaleur fi, cycles inverse de Brayton fi gaz r6el," *Int. J. Refrig*, vol. 18, no. 4, pp. 272–280, 1995.

[36] M. J. Driscoll, "Supercritical CO 2 Plant Cost Assessment," 2004.

[37] Z. Liu, W. Luo, Q. Zhao, W. Zhao, and J. Xu, "Preliminary design and model assessment of a supercritical CO2 compressor," *Appl. Sci.*, vol. 8, no. 4, p. 595, Apr. 2018, doi: 10.3390/app8040595.

[38] M. T. White, G. Bianchi, L. Chai, S. A. Tassou, and A. I. Sayma, "Review of supercritical CO2 technologies and systems for power generation," *Applied Thermal Engineering*, vol. 185. Elsevier Ltd, p. 116447, Feb. 25, 2021, doi: 10.1016/j.applthermaleng.2020.116447.

[39] L. M. Rapp, "Experimental Testing of a 1MW sCO2 Turbocompressor. (Conference) | OSTI.GOV."

https://www.osti.gov/biblio/1643439 (accessed Jul. 01, 2021).

[40] L. Chai and S. A. Tassou, “A review of printed circuit heat exchangers for helium and supercritical CO2 Brayton cycles,” *Thermal Science and Engineering Progress*, vol. 18. Elsevier Ltd, p. 100543, Aug. 01, 2020, doi: 10.1016/j.tsep.2020.100543.

[41] A. M. Johnston, W. Levy, and S. O. Rumbold, “Application of Printed Circuit Heat Exchanger Technology within Heterogeneous Catalytic Reactors,” 2001.

[42] F. Finotti and E. Verpe, “Deliverable: D1.2 - List of specifications for all component’s subssystems and global SHIP200 & SHIP300 parameters,” 2020.

[43] C. Tanolin, “Deliverable: D1.3 - Test plan and validation methods for all components or subsystems and global SHIP200&SHIP 300,” 2020.

[44] V. K. Patel and B. D. Raja, “A comparative performance evaluation of the reversed Brayton cycle operated heat pump based on thermo-ecological criteria through many and multi objective approaches,” *Energy Convers. Manag.*, vol. 183, pp. 252–265, Mar. 2019, doi: 10.1016/j.enconman.2018.12.109.

[45] “Gasketed plate heat exchangers.” https://www.alfalaval.com/globalassets/documents/microsites/heating-and-cooling-hub/pd-leaflets---gasketed/alfa-laval-gasketed-plate-heat-exchangers.pdf (accessed Jun. 16, 2021).

[46] “Thermal Conductivity of Steel - Thermtest Inc. - Blog.” https://thermtest.com/thermal-conductivity-of-steel (accessed Jun. 16, 2021).

[47] Z. Ren, C. R. Zhao, P. X. Jiang, and H. L. Bo, “Investigation on local convection heat transfer of supercritical CO2 during cooling in horizontal semicircular channels of printed circuit heat exchanger,” *Appl. Therm. Eng.*, vol. 157, p. 113697, Jul. 2019, doi: 10.1016/j.applthermaleng.2019.04.107.

[48] K. G. Schmidt, *VDI Heat Atlas*. 2010.